SEPARATING THE EPS IN A BIOFILM: MODELS AND SIMULATIONS OF MOVEMENT OF THE EPS WITHIN.

by

Nathan James McClanahan

A dissertation submitted in partial fulfillment
of the requirements for the degree

of

Doctor of Philosophy

in

Mathematics

MONTANA STATE UNIVERSITY
Bozeman, Montana

August, 2016

DEDICATION

Dedicated to my wife and kids
Carrie, Amelia, and Aiden
Without them none of this would be possible.

ACKNOWLEDGEMENTS

There are many people I would like to acknowledge for their help and support with this dissertation. First, my advisor, Dr. Tianyu Zhang, for his help in everything related to this project. For providing guidance, support, and his patience while working through the work presented here. For the time spent reading, editing this dissertation, and providing insight into some of the finer details of writing a large research paper such as this. Dr. Ben Jackson for his help with numerous LaTeX problems as well as many helpful discussions related to biofilms and math in general. Dr. Gary G. Sackett for the support provided this summer allowing work on this project to be my primary focus for the entire summer. My kids, Amelia and Aiden, for always being able to brighten a day and bring a smile to my face no matter how difficult the rest of the day has been. Finally, my wife, Carrie, for her love, unending support, and patience. Her willingness to care for our kids giving me the opportunity to work the entire day and more when it was needed. Without her none of this would be possible.

TABLE OF CONTENTS

LIST OF TABLES

Table Page

LIST OF FIGURES

Figure Page

LIST OF FIGURES - CONTINUED

Figure Page

ABSTRACT

In this dissertation two models are investigated for describing movement of different components within a biofilm. The first model uses a single fluid three component formulation of the biofilm to model the movement within the biofilm in 1D. This is done using a system partial differential equations to model the expansion or contraction of the biofilm in order for the three components to reach an ideal concentration. The model is further refined to include separate velocities for each component as well as using zeroth order kinetics for the growth. In order to solve this system of partial differential equations a finite difference method with an upwind scheme was used to solve the system numerically.

The second model is an energy based approach done in both 1D and 2D. An energy, in the case the Flory-Huggins free energy density, is used to describe the interactions of different components within the biofilm. The Cahn-Hilliard equation with the Flory-Huggins free energy density is used to model the separation of the biofilm into two phases. A brief derivation of both the Flory-Huggins equation and the Cahn-Hilliard equation is given using a lattice model and thermodynamic properties. The Flory-Huggins equation is modified slightly for simplicity. A movement energy is also added to the Flory-Huggins equation in order to allow the polymers within the biofilm to move around the domain.

In the 1D case the numerical solution was found using finite differences with an upwind scheme similar to the first model. The 2D case is more difficult to solve due to the extra dimension. Due to this the projection method was used to solve part of the system of equations and finite difference using central difference instead of upwind is used to solve the rest.

CHAPTER ONE

INTRODUCTION

From the bottom of a river to the middle of a corn field to the drain pipe in a sink biofilms are found throughout nature and man made settings. While it is easy to look out a window and come to the conclusion that plant life must be the largest component of all biomass on the planet this may not necessarily be true. It has been estimated that the total amount of carbon contained in prokaryotes, which include bacteria, is between 60-100% of the total amount of carbon contained within all plant life [1]. While the common depiction of bacteria is as the planktonic cells that must be washed off hands to prevent them from spreading diseases it is not the most common place for bacteria to be. The most common place bacteria are found is attached to a surface as a part of a biofilm [2,3]. The International Union of Pure and Applied Chemists defines a biofilm as "an aggregate of micro-organisms in which cells that are frequently embedded within a self-produced matrix of extracellular polymeric substance (EPS) adhere to each other and/or to a surface. [4]"

A biofilm can be made up entirely of a single species but generally has a wide range of species of bacteria, fungi, algae, many other micro-organisms as well as debris and other particulate material. As the definition mentions biofilms are held in place and held together by a matrix of extracellular polymeric substances(EPS). The cells within a biofilm produce the EPS. EPS is a major part of biofilms. Understanding what it does and how it does those things is one of the many reasons to study biofilms.

Bacteria are like any other organism; they do things to survive. This is one of the main reasons that biofilms are formed. Bacteria in planktonic form are relatively easy to kill. There are numerous products on the market designed to do specifically

that. In the Flemming paper *The Perfect Slime* he discusses how the biofilim or more precisely the EPS matrix acts as a house [5]. Houses have a few roles but the major reason people generally live in houses is for protection and safety. The EPS matrix acts this same way. Studies have shown that bacteria within a biofilm have a superior ability to resist and survive the use of antimicrobial treatments [6, 7]. Studying how biofilms react to the biocides and finding better ways to kill them is a big reason to study them.

The EPS in a biofilm plays other important rolls. EPS helps protect the organisms living within the matrix as was mentioned. It also anchors the organism in place which means there must be a way for the organisms within the biofilm to get needed nutrient. The EPS matrix itself does this. It gives the organisms a way to collect and hold on to materials that may be needed. If a planktonic cell needs something to live the cell needs to come into contact with it at the right time. The cell itself is not able to hold onto extra nutrient. The EPS matrix allows for the sorption and storage of organic compounds useful to the organisms inside. Another property of the matrix is that it has a slightly different index of refraction compared to water. This allows light to enter a biofilm instead of being reflected [8]. This allows photosynthetic organisms to live within a biofilm at a deeper level. They don't need to live on the top in order to get light.

Most of the discussion in this dissertation assumes that biofilms are adhering to a solid-water interface, such as the base of a river or sides of a pipe, this is not always the case. Biofilms can also be found at other interfaces such as a water-oil interface or even a solid-air interface [9]. Because of this biofilms can be found almost anywhere there is moisture, nutrients, and a surface, which as just stated does not need to be a solid surface.

Due to this wide spread nature of biofilms they cost the U.S. billions of dollars every year. These loses come from damage to equipment, contamination of not just food and water but industrial products as well, and medical infections. Biofilms are a major hindrance to any industrial process that involves water such as cooling processes or delivery systems from oil lines to medical lines [10, 11]. There are many ways to combat these problems such as hygienic manufacturing plant layout, better materials, and correct use of detergents and physical cleaning methods [12]. Biofilms also play a major roll in medicine. It has been estimated that biofilms are linked to $65 - 85\%$ of chronic infections [13]. Biofilms also have many beneficial uses as well. Some of these include bioremediation, recovery of hard to mine minerals, and acting as a sealant through biomineralization [14–16].

For the last 25 years there has been an increased desire to model biofilms because of their wide spread nature, damage caused by them, and associated benefits of better understanding them [17–20]. There have been a number of different methods used. There are discrete based methods where the biofilm is modeled by a cellular automaton approach [21]. There are continuum based models [22]. There are also models that combine the two ideas depending on what is being modeled. For example, Picioreanu and van Loosdrecht used a discrete model for the polymer and bacteria combined with a differential approach to model the nutrient substrate [23].

Whether the model is discrete, a continuum, or a model somewhere in between there are many other aspects of the model to look at. Things such as the number of dimensions, the number of species modeled, and how the biofilm itself will be modeled. There are many ways to model the physical biofilm. These can include multifluid or single fluid models [24,25] and within both of these is the number of components each fluid has [25]. Using a single species or multiple species within the biofilm can also have an effect on the outcome [22]. Biofilm can be treated as elastic or viscoelastic

fluids depending on the timescale used [25]. However, the standard approach is to treat them as viscoelastic fluids as this has been supported by experimental results [26]

Some of the original work done on biofilm modeling assumed that biofilms were spatially homogeneous mainly due to lack of experimental data saying otherwise. This led to change only being allowed in the direction perpendicular to the surface on which the biofilm was growing [27]. While 1D models may not be capable of showing the amount of detail shown in 2D or 3D models they are simple enough to be understood quickly. They also are generally much faster to run numerical simulations on which makes them more attractive. The simplistic nature of 1D models does not necessarily detract from their usefulness either. There are places where a 1D model is useful. Situations where the physical dimensions are small enough that 2D and 3D are unnecessary such as pore or microfracture filling work [15]. While the 1D model is a good starting place there are a lot of applications and reasons for using a 2D model as well.

The 2D model does address some of the shortcomings of a 1D model. While early work assumed biofilms were spatially homogeneous this is not the case. Work using confocal laser scanning microscopy has shown that biofilms are not spatially homogeneous [22]. This means that while 2D and 3D models may be computationally more expensive they are useful for simulating these differences. While both single species and multispecies biofilms are spatially heterogeneous there may be factors such as temperature, acidity, or availability of nutrient that may cause different species to have different growth rates in different places within a biofilm [28,29]. This is just one example of the uses of multidimensional multispecies models. The multidimensional models also allow the use of meaningful shear forces or simulations of flow above the biofilm as there is now variation in both the direction perpendicular to the surface and in the direction of the flow.

This dissertation is organized into two models that were intended to answer questions about the EPS within a biofilm. The motivation behind this work came from a quote from Flemming in his paper discussing the varied ways to think of a biofilm [5] which was inspired by Stoodley et al. [30]. "High shear forces may improve matrix cohesion when all those EPS components are washed out which cannot withstand the shear, leaving the biofilm with those that resist–this inevitably results in stronger matrix cohesion."

In chapter 2 we use a three component model for the biofilm with a variable height. The bacteria is treated separately from the EPS and the EPS is treated in two components. The model used is based on mass balance. In this model we looked at how three forces interact to change the biofilm over time. The quantities of interest in this model are the height of the biofilm as well and the concentration of the three components. These forces are growth, erosion, and expansion/contraction. While there are more complex ways to model these effects the model uses first order differential equations with simple kinetics within those equations.

For chapter 2 two growth models were used. The first was just a standard exponential growth equation $\frac{\partial x}{\partial t} = ax$ as part of the larger mass balance equation. The other method implemented is a zeroth order kinetic model where the model says that the bacteria will grow at a max rate wherever there is nutrient to be consumed [31]. The location of nutrient is determined by a reaction-diffusion equation where the time component is ignored due to the difference in time scales. Solutions for both methods are presented within the chapter.

Erosion in this case is a simplified model of the effects of the shear forces due to flow across the top of the biofilm. The erosion used is a constant multiplied by concentration for each part of the biofilm, γx. The purpose of the erosion is to balance the growth and expansion within the biofilim so that eventually the biofilm would

reach a steady state for the height. There are different aspects of the erosion that are discussed some of which ran contrary to the initial idea of the model that the erosion could affect different components of the biofilm differently. One problem discussed is how the erosion in its initial form does not balance the growth and expansion. Fixing this problem mathematically is easy to do and will be discussed more in the chapter.

The final force modeled is the expansive force. This is used to model how the components of the biofilm will reach their ideal concentrations. If a component has a concentration higher than the ideal concentration the biofilm will expand to lower the concentration and the opposite if the concentration is lower than the ideal concentration. The biofilm will change in concentration and height as well due to the expansive forces pushing out when new material is added. The model combined these three forces to create change in the height and concentration of each component with respect to time.

The rest of the chapter is made up of numerical methods and the results from the simulations. Everything from change of variables, nondimensionalization, and methods used is covered. The results are then presented with explanations of what was wrong with the model. Finally, an second set of results is presented with more explanation of them and what was wrong again. These problems combined with the uncertainty of how or if they could be fixed led to a change of focus to the second model used.

The second model is based off of the work of Zhang et al [25,32]. While there are many equations to the model, most of which will be discussed in chapter 3 the main focus will be on the Cahn-Hilliard equation and the Flory-Huggins free energy density. The Cahn-Hilliard equation is an equation that models the process of phase separation which describes the way a binary fluid spontaneously separates into two pure states [33]. The phase separation is due to non-Fickian diffusion which is created by the

gradient of the chemical potential as opposed to Fickian diffusion which is driven by the gradient of composition [34]. The reason why the diffusion occurs is to minimize the energy of the system which is a result of the second law of thermodynamics. While the work presented here is based in biofilms and the origination of the Flory-Huggins free energy density is in polymer chemistry this combination of equations has uses in other areas as well. One example is the use of these two equations to model the unmixing in mineral formations when they are cooled after moving closer to the surface [35].

The second model used was implemented in both 1D and 2D. In the 1D case a finite difference scheme along with an upwind scheme was used to numerically solve the system of equations. In chapter 3 both the Flory-Huggins free energy density and Cahn-Hilliard equation are derived from thermodynamic principles. One of the main differences between the model presented here and the work of Zhang et al. is the addition of a term to simulate movement of the polymers within the biofilm. In the 1D model this is a volume fraction dependent movement term with an arbitrary function to prescribe the preferred region for polymer to occupy within the biofilm. The other difference is the change that was made to the form of the Flory-Huggins free energy density which is discussed in greater detail in chapter 3.

The quantities of interest in this model are different than the previous 1D model. In the energy based system there is not a height variable as we are now modeling volume fraction on a fixed domain. The fluid is also modeled as a binary fluid with the bacteria being encased within the polymer matrix, instead of a separate component, and a solvent which contains the nutrient. Another difference is that there is experimental data to help determine the parameters used in the model. This gave assurances that the results would at least be following previous publications up to the changes that are made to the model. These results along with the previously

mentioned derivations of the two main equations are found in more detail in chapter 3.

Once the background material is out of the way in chapter 3 the 2D model is essentially the same with a few changes to the numerics. The equations don't change from chapter 3 to chapter 4. In addition to the standard changes made to the numerics due to the increase in dimension some of the solution techniques are changed. In the 2D model some of the equations become more difficult to solve due to the derivatives being gradients and divergences. The addition of a second dimension led to the use of the projection method to solve the momentum and continuity equations. This will be discussed in more detail later. The upwind method that was used in the 1D model was also abandoned in favor of central differences. The other difference is in the results. Due to the extra dimension there are some unexpected results for the 2D model when compared to the 1D model.

CHAPTER TWO

A 1D MULTICOMPONENT CONTINUUM MODEL FOR MOVEMENT WITHIN A BIOFILM

In this chapter a velocity driven model for a single fluid with three components will be introduced. This model uses growth, erosion, and expansion to create a velocity to show how a biofilm can evolve with time. This model was the first attempt at creating a system of equations that would model the separation of EPS within the biofilm. The model presented here is a 1-dimensional model. The system of equations and results will be presented and a description of both will be given. Numerical methods will be discussed as well as some of the problems with how the growth and velocity of each component was modeled. These problems led to changing the model. The new results from the changed model had problems of their own. The biggest problem was that the model was too restrictive. Changes were not allowed to happen they were forced. This was the main issue which eventually led to moving on from this model.

2.1 The Mathematical Model in 1D

The biofilm in this model is a mixture of three components. The three major components of the biofilm are treated as concentrations. There are the bacteria cells which are represented by x in the model. A two component EPS is used in the model. These are represented by p_1 and p_2 in the model. The velocity v in this model is assumed to have a standard orientation with positive being up and negative being

down. The original model is as follows

$$\frac{dh}{dt} = v - \gamma_0 x - \gamma_1 p_1 - \gamma_2 p_2 \Big|_{z=h(t)}, \tag{2.1}$$

$$\frac{\partial v}{\partial z} = F(z), \tag{2.2}$$

$$F(z) = \beta_0(x - x^\star) + \beta_1(p_1 - p_1^\star) + \beta_2(p_2 - p_2^\star),$$

$$\frac{\partial x}{\partial t} + \frac{\partial (vx)}{\partial z} = cx, \tag{2.3}$$

$$\frac{\partial p_1}{\partial t} + \frac{\partial (vp_1)}{\partial z} = cx, \tag{2.4}$$

$$\frac{\partial p_2}{\partial t} + \frac{\partial (vp_2)}{\partial z} = cx. \tag{2.5}$$

This model has an equation to represent the changing height h of the biofilm (2.1), where t is the time variable and z is the dimensional spatial variable with the restriction $0 \leq z \leq h(t)$. This equation is a mass balance equation at the top of the biofilm which looks at the amount taken away by erosion and the amount added by growth and movement from within, which may not necessarily be positive. For this model the three terms with a γ are erosion terms. The original idea was that the larger the γ the faster that the corresponding component would be washed away. This will be discussed in more detail later. Next, the model has a movement equation (2.2) to model how the expansion or contraction of the components within the biofilm would influence the change in height of the biofilm. The equation takes each component and finds how far away it is from its ideal value, $x^\star$, $p_1^\star$, and $p_2^\star$, from here it will either expand or contract the biofilm to move it closer to the ideal values in a weighted sense. Each β combined with the corresponding difference between a concentration and its ideal value will determine which component has the most influence on how the biofilm expands or contracts. If β_1 is 100 times greater than either of the other two β's but $p_1 - p_1^\star = 0$ then β_1 has no influence on the outcome. A Dirichlet

boundary condition is used where $v(0,t) = 0$ for the lower boundary. This boundary condition is implemented in equation (2.2) is where the lower boundary condition on the velocity is implemented. Finally, the model has an equation to model the change in concentration for each of the three components mentioned before, equations (2.3)-(2.5). In equations (2.3)-(2.5) the c parameter is a growth constant. Initial attempt assumed that all three components grew at an equal rate that only depended on the amount of bacteria present in the biofilm, due to the nutrient being abundant.

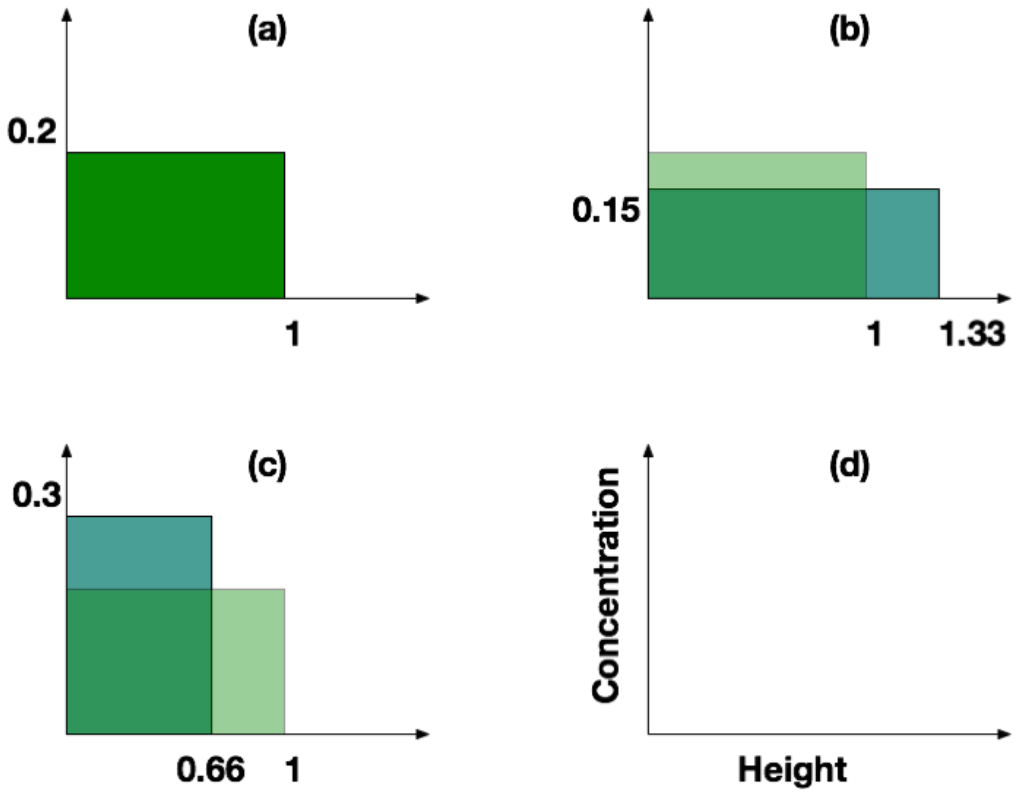

Figure 2.1: (a) The initial height of the biofilm is 1 and the initial concentration is a constant of 0.2. (b) The height has increased in order to lower the concentration. (c) The height is decreased in order to increase the concentration. (d) The labeled axis.

A short description of what the model does will be given before the more in depth description of the model that follows. This explanation matches with Figure 2.1 only if there is no growth and no erosion. The biofilm starts out with a height of one and a certain prescribed concentration of each component as in Figure 2.1(a). In Figure 2.1 the concentration is always a constant but this may not always be the case. Depending on the values used the model will do one of two things. It will either increase the height in order to decrease the concentration as in Figure 2.1(b) or it will decrease the height in order to increase the concentration as in Figure 2.1(c). In this figure the area of the shaded region is conserved due to no growth and no erosion.

2.1.1 Description of the Model

Looking at the model above it is modeling what happens to the biofilm in 1D. Each part of the model will be examined to ensure it has a physical interpretation that makes sense. The height equation (2.1) says the height will change depending on how the biofilm grows and how much is washed away. This agrees with a simple mass balance idea. There is an upward flux of material from an expansion of the biofilm. There is also a flow above the biofilm so it is possible that some material would be washed away due to this flow. The only other source of material into or out of the biofilm would be from the boundaries. This model is only looking at the three components listed in the model so it is not possible for bacteria cells or polymer to come into the biofilm from the bulk fluid above the biofilm. For the bottom it was assumed that there is no flux through the bottom layer so this means that neither the cells nor the polymer is able to leave through the ground. This makes sense from a physical perspective as well. There is no flow or shearing forces where the biofilm is attached so it would not make sense to have material leaving the biofilm through the bottom boundary.

Equation (2.2) describes how things move around within the biofilm. For this model upward was assumed to be positive. This equation says that the upward velocity of the biofilm would be determined by the individual components moving to reach an ideal concentration. This is a balance between expanding or contracting the biofilm to increase or decrease the total volume of the biofilm and the growth of each component due to equations (2.3)-(2.5) thereby changing the concentration of each component.

The last three equations (2.3)-(2.5) are all similar but the small variations within them will be examined. In general each equation models how each component will change over time. They say that the component can move around within the biofilm due to the velocity given by equation (2.2) and there will also be a growth of each component in the biofilm. Given a cursory glance these all seem to make sense from a physical perspective. Growth and expansion would change the concentration of the components of the biofilm. Taking a closer look at the model there could potentially be some problems develop under certain circumstances. It was assumed in the model that each component would grow at a rate proportional only to the amount of bacteria present within the biofilm. This model also initially used only one velocity which means all three components will move with the same velocity function. There were some problems with these two ideas which will be discussed later.

2.2 Change of Variables and Nondimensionalization

2.2.1 Change of Variables

Looking at the model above it can be seen that after solving the entire system there will most likely be a change in the height with respect to time, unless everything is dead and there is no flow. While not any more difficult to solve in the current form

it would lead to extra work while solving the system instead of a smaller amount of pre and post processing work. In its current form the model has a variable height which means that in order to solve the system across multiple time steps either the spatial grid size, Δz, or the number of spatial nodes would need to change each time step. There could be numerous problems with either of these options. If the number of spatial nodes is fixed when the height becomes large there could be decreased accuracy due to the size of Δz. If the height approaches zero there could be numerical issues with Δz becoming too small to be used. If Δz is fixed and the number of nodes is allowed to vary then the simulation make take too long if the height becomes too large or if the height approaches zero the number of nodes would approach zero again affecting the accuracy. Another problem would be if the height is in between nodes. The entire domain should be discretized but with a fixed Δz and variable height this is not guaranteed. The best way to handle the system as is would be to have a dynamic number of nodes and size of Δz giving a range for the acceptable size of Δz but this would be more difficult to do. An easier and quicker way is to skip all of this and change the variables.

The numerics are easier with a change of variables. While the change of variables fixes many of the issues discussed in the previous paragraph there model breaks down as time increases if either $\lim_{t\to\infty} h(t) = 0$ or $\lim_{t\to\infty} h(t) = \infty$. The problems mentioned above go away because under the change of variables $\xi = \frac{z}{h(t)}$ the domain changes from $z \in [0, h(t)]$ to $\xi \in [0, 1]$. The height under this change of variables is fixed at one. This allows for a fixed number of spatial nodes and a fixed size for the new spatial step size $\Delta\xi$. The pre-processing work that needs to be done will be discussed in the following sections but it only needs to be done once instead of doing it each time step in the computer simulation. This does introduce a small amount of post processing work as was mentioned above. Since the height is now fixed at one and

the results are in ξ space they may need to be translated back to z space at the end of the simulation.

The change of variables used are $t = t$ and $\xi = \frac{z}{h(t)}$ which leads to the following changes to the derivatives:

$$\frac{\partial}{\partial t} = \frac{\partial}{\partial t} + \frac{\partial \xi}{\partial t}\frac{\partial}{\partial \xi} = \frac{\partial}{\partial t} - \frac{\dot{h}z}{h^2(t)}\frac{\partial}{\partial \xi} = \frac{\partial}{\partial t} - \frac{\xi}{h}\dot{h}\frac{\partial}{\partial \xi} \tag{2.6}$$

$$\frac{\partial}{\partial z} = \frac{\partial \xi}{\partial z}\frac{\partial}{\partial \xi} = \frac{1}{h}\frac{\partial}{\partial \xi} \tag{2.7}$$

where $\dot{h} = \frac{dh}{dt}$. After the change of variables the new system is as follows.

$$\dot{h} = v - \gamma_0 x - \gamma_1 p_1 - \gamma_2 p_2\Big|_{\xi=1}, \tag{2.8}$$

$$\frac{1}{h}\frac{\partial v}{\partial \xi} = F(\xi), \tag{2.9}$$

$$F(\xi) = \beta_0(x - x^\star) + \beta_1(p_1 - p_1^\star) + \beta_2(p_2 - p_2^\star),$$

$$\frac{\partial x}{\partial t} - \frac{\xi}{h}\dot{h}\frac{\partial x}{\partial \xi} + \frac{1}{h}\frac{\partial (vx)}{\partial \xi} = cx, \tag{2.10}$$

$$\frac{\partial p_1}{\partial t} - \frac{\xi}{h}\dot{h}\frac{\partial p_1}{\partial \xi} + \frac{1}{h}\frac{\partial (vp_1)}{\partial \xi} = cx, \tag{2.11}$$

$$\frac{\partial p_2}{\partial t} - \frac{\xi}{h}\dot{h}\frac{\partial p_2}{\partial \xi} + \frac{1}{h}\frac{\partial (vp_2)}{\partial \xi} = cx. \tag{2.12}$$

The height equation (2.8) is the same as it was before. This is due to the height not depending on ξ which leads to $\frac{\partial h}{\partial \xi} = 0$ and equation (2.6) reduces to just $\frac{\partial}{\partial t}$.

2.2.2 Nondimensionalization

Equations (2.8)-(2.12) are nondimensionalized by using a characteristic time scale t_0, length scale h_0 and characteristic concentration scales for each component.

The dimensionless variables are given in (2.13).

$$\widetilde{t} = \frac{t}{t_0}, \qquad \widetilde{h} = \frac{h}{h_0}, \qquad \widetilde{x} = \frac{x}{x_0}, \qquad \widetilde{p_1} = \frac{p_1}{p_{1,0}}, \tag{2.13}$$

$$\widetilde{p_2} = \frac{p_2}{P_{2,0}} \qquad \widetilde{v} = \frac{vt_0}{h_0}, \qquad \widetilde{c} = \frac{c}{c_0}$$

where c_0 is the characteristic nutrient concentration. The length scale is determined by the scale of our simulation and the time scale is based on the growth rate of the biofilm. These lead to the following dimensionless parameters

$$\widetilde{\gamma}_0 = \gamma_0 x_0 \frac{t_0}{h_0}, \qquad \widetilde{\gamma}_1 = \gamma_1 p_{1,0} \frac{t_0}{h_0}, \qquad \widetilde{\gamma}_2 = \gamma_2 p_{2,0} \frac{t_0}{h_0} \tag{2.14}$$

$$\widetilde{\beta}_0 = \beta_0 x_0 t_0, \qquad \widetilde{\beta}_1 = \beta_1 x_0 t_0, \qquad \widetilde{\beta}_2 = \beta_2 x_0 t_0$$

Dropping the $\widetilde{\cdot}$ from the equations for simplicity the new system of equations looks almost exactly like the set of equations (2.8)-(2.12), keeping in mind that all the variables are now dimensionless

$$\dot{h} = v - \gamma_0 x - \gamma_1 p_1 - \gamma_2 p_2 \Big|_{\xi=1}, \tag{2.15}$$

$$\frac{1}{h}\frac{\partial v}{\partial \xi} = F(\xi), \tag{2.16}$$

$$F(\xi) = \beta_0(x - x^\star) + \beta_1(p_1 - p_1^\star) + \beta_2(p_2 - p_2^\star),$$

$$\frac{\partial x}{\partial t} - \frac{\xi}{h}\dot{h}\frac{\partial x}{\partial \xi} + \frac{1}{h}\frac{\partial (vx)}{\partial \xi} = t_0 c_0 c x, \tag{2.17}$$

$$\frac{\partial p_1}{\partial t} - \frac{\xi}{h}\dot{h}\frac{\partial p_1}{\partial \xi} + \frac{1}{h}\frac{\partial (vp_1)}{\partial \xi} = t_0 c_0 c x, \tag{2.18}$$

$$\frac{\partial p_2}{\partial t} - \frac{\xi}{h}\dot{h}\frac{\partial p_2}{\partial \xi} + \frac{1}{h}\frac{\partial (vp_2)}{\partial \xi} = t_0 c_0 c x. \tag{2.19}$$

2.3 Numerical Methods

Since (2.16) is integrable the trapezoid method [36] was used to solve for v first. After this the velocity was used to update the height of the biofilm, again using the trapezoid method. To do this the v^{n+1}, x^n, p_1^n, and p_2^n values were used in (2.15), where the superscript refers to the time step with n being the current time. To solve the last three equations an upwind method was used [37]. The $\dot{h}$ and v^{n+1} terms were used for the upwinding. Looking at the sign of these two determined whether a forward or backwards difference was used for the corresponding term. Equation (2.17) was solved first so that x^{n+1} could be used on the right hand side of (2.18) and (2.19). The resulting system of equations form a tridiagonal system that can be solved by a number of methods. The Thomas Algorithm was chosen as the numerical method to solve the system. Since the system was small there was not a significant gain in speed due to the Thomas Algorithm.

2.3.1 The Thomas Algorithm

The Thomas Algorithm is a form of Gaussian elimination that is used to solve tridiagonal systems [37]. It is a simplified version of Gaussian elimination. Because of this it may not be stable. There are certain conditions that if met will make the method stable such as the matrix being diagonally dominant or symmetric positive definite. While it may not be possible to show that the matrix is diagonally dominant in general for the current problem it can be shown that for the particular choices of parameters used that it is a diagonally dominant matrix. The Thomas algorithm was used for this problem because of speed. The method takes $\mathcal{O}(n)$ operations [38], where n is the number of rows in the matrix, as opposed to standard Gaussian elimination which takes $\mathcal{O}(n^3)$ operations [38, 39]. For example adding two vectors of length n

takes $\mathcal{O}(n)$ operations. Using Gaussian elimination to put the matrix in a reduced form and then solving by back substitution takes $\mathcal{O}(n^3)$ operations because there are $n(n+1)/2$ divisions, $(2n^3+3n^2-5n)/6$ multiplications, and $(2n^3+3n^2-5n)/6$ subtractions required, which is approximately $4n^3/6$ or $2n^3/3$ operations [39].

Looking at a small example where $j = 1 \cdots 4$ the system that is being solved is

$$\begin{bmatrix} b_1 & c_1 & 0 & 0 \\ a_2 & b_2 & c_2 & 0 \\ 0 & a_3 & b_3 & c_3 \\ 0 & 0 & a_4 & b_4 \end{bmatrix} \begin{bmatrix} x_1^{n+1} \\ x_2^{n+1} \\ x_3^{n+1} \\ x_4^{n+1} \end{bmatrix} = \frac{1}{\Delta t} \begin{bmatrix} d_1^n \\ d_2^n \\ d_3^n \\ d_4^n \end{bmatrix} \tag{2.20}$$

Using a fixed time size, Δt, and spatial step size, $\Delta\xi$, a general discretized form of (2.17) would be

$$\begin{aligned} \frac{x_j^{n+1}-x_j^n}{\Delta t} &+ \frac{1+\text{sign}(-\dot{h})}{2}\frac{-\xi\dot{h}}{h^{n+1}}\frac{x_j^{n+1}-x_{j-1}^{n+1}}{\Delta\xi} \\ &+ \frac{1+\text{sign}(v_j^{n+1})}{2}\frac{1}{h^{n+1}}\frac{v_j^{n+1}x_j^{n+1}-v_{j-1}^{n+1}x_{j-1}^{n+1}}{\Delta\xi} \\ &+ \frac{1-\text{sign}(-\dot{h})}{2}\frac{-\xi\dot{h}}{h^{n+1}}\frac{x_{j+1}^{n+1}-x_j^{n+1}}{\Delta\xi} \\ &+ \frac{1-\text{sign}(v_j^{n+1})}{2}\frac{1}{h^{n+1}}\frac{v_{j+1}^{n+1}x_{j+1}^{n+1}-v_j^{n+1}x_j^{n+1}}{\Delta\xi} \\ &= t_0 c_0 c x_j^{n+1}. \end{aligned} \tag{2.21}$$

Where $x_j^n \cong x(\xi_j, t_n)$ and $v_j^n \cong v(\xi_j, t_n)$. The assumption that both $\dot{h}$ and v^{n+1} are positive mean that the coefficients for all x_{j+1}^{n+1} terms will be zero. There could be a mix of terms if either $\dot{h}$ or v^{n+1} is negative due to a change in the upwind scheme. If one of these is negative a forward difference is used instead of a backward difference. To solve equation (2.17) the right hand side of equation (2.21) is moved over to the

left and the coefficient are grouped with the corresponding terms. The discretized forms of equations (2.18) and (2.19) would both be similar with the x on the left hand side being changed to p_1 and p_2 respectively. Also, the growth term would stay on the right hand side with the newly solved for x^{n+1} being used. Using equations (2.20) and (2.21) the coefficients for the second row end up being

$$a_2 = \frac{-v_1}{h^{n+1}\Delta\xi} + \frac{\xi_2\dot{h}}{h^{n+1}\Delta\xi}$$
$$b_2 = \frac{1}{\Delta t} - t_0 c_0 c + \frac{\xi_2^{n+1}}{h^{n+1}\Delta\xi} - \frac{\xi_2\dot{h}}{h^{n+1}\Delta\xi}$$
$$c_2 = 0$$
$$d_2 = \frac{x_j^n}{\Delta t}$$

The first and last rows of the matrix involve using the boundary conditions which is why they are not used here.

The Thomas Algorithm involves modifying the coefficients of a system of tridiagonal equations. The equation $a_j x_{j-1} + b_j x_j + c_j x_{j+1} = d_j$ will be used for reference with $a_1 = 0$ and $c_n = 0$. For this problem the matrix (2.20) will be used. The c_j and d_j coefficients are modified and prime notation will be used to denote the new coefficients. The first step is to modify c_j and d_j in the following way

$$c_i^{'} = \begin{cases} \dfrac{c_i}{b_i} & : i = 1 \\ \dfrac{c_i}{b_i - a_i c_{i-1}^{'}} & : i = 2, 3, ..., n-1 \end{cases} \qquad d_i^{'} = \begin{cases} \dfrac{d_i}{b_i} & : i = 1 \\ \dfrac{d_i - a_i d_{i-1}^{'}}{d_i - a_i c_{i-1}^{'}} & : i = 2, 3, ..., n \end{cases}$$

From here the solution is found through back substitution. This is done with the

Table 2.1: A list of parameters used for the simulations for chapter 2

Symbol	Parameter	Value	Units
t_0	Characteristic time scale.	1×10^3	s
h_0	Characteristic length scale	1×10^{-3}	m
β	Expansion coefficient.	1×10^{-3}	$m^3kg^{-1}s^{-1}$
γ	Erosion coefficient.	1×10^{-8}	$m^4kg^{-1}s^{-1}$
c	Growth coefficient.	1.5×10^{-6}	s^{-1}

equations

$$x_n = d'_n$$
$$x_i = d'_i - c'_i x_{i+1} \quad : i = n-1, n-2, ..., 1$$

2.4 Results

In this one dimensional model the evolution of the biofilm was studied without explicitly modeling any external forces such as shear or turbulent flow. Instead, the model simulates these forces with the erosion terms in equation (2.1). All of the numerical results presented are for $\Delta t = 0.01$ and $\Delta \xi = 0.01$ unless noted otherwise. Unless otherwise noted the parameters in Table 2.1 were used for all simulations.

2.4.1 Zero Growth and Zero Erosion

This particular simulation was run to see the effects of the velocity on the biofilm. In order to isolate these effects $\gamma_0 = \gamma_1 = \gamma_2 = 0$ and $c = 0$ were used. This results in zero growth of the three components and zero erosion; or conservation of matter for the three components. The results in Figure 2.2(a) were obtained using $x^\star = p_1^\star = 0.2$ and $p_2^\star = 0.3$ with the ideal concentrations having units of kg/m^3. Notice that the concentration for each component does not converge to its ideal concentration. What does happen is that the final weighted average concentration of all three components is equal to the weighted average of the ideal concentration, using the corresponding

β value as the weight. In this case the average of the ideal concentrations is 0.2333 and the average value of the final values for the three components is 0.2334. While Figure 2.2(a) has $\beta_0 = \beta_1 = \beta_2$ similar results were observed with non-equal β values, such as in Figure 2.2(b).

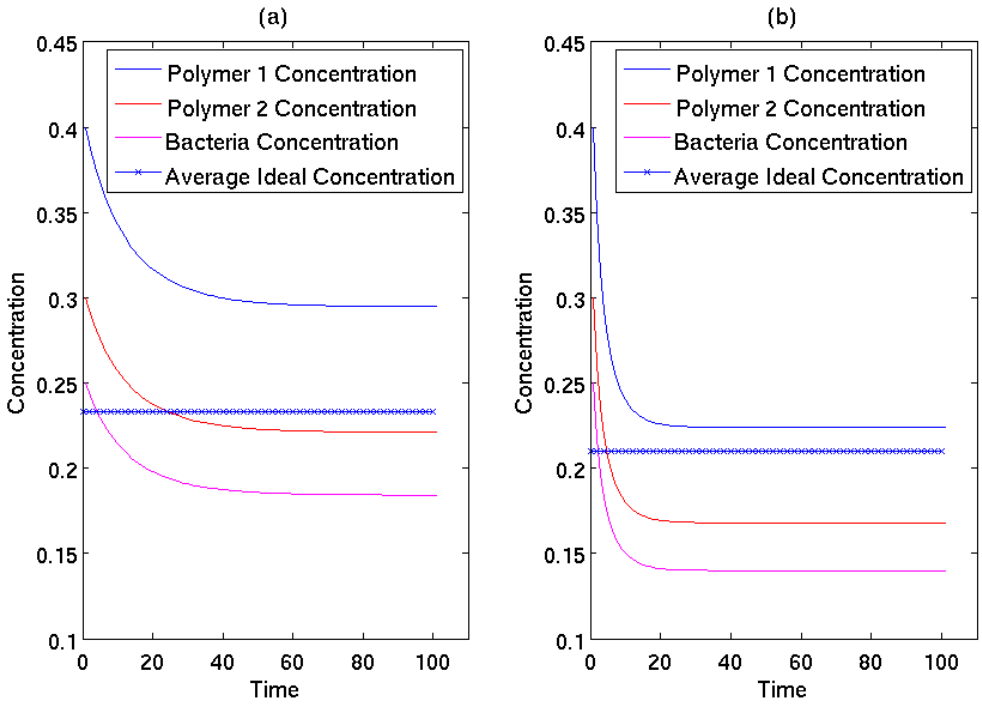

Figure 2.2: (a)The average of the final values for all three components is equal to the average of the ideal concentrations. (b) In this plot the average is a weighted average as the β values are no longer equal. For this plot β_1 is eight times greater than β_0 and β_2.

While it looks like the amount of each component in the biofilm is decreasing Figure 2.2 shows concentration not amount. There is conservation in this simulation which can be seen in Figure 2.3(a). The change in Figure 2.2 is due to using a concentration instead of a mass. This change in concentration is due to an increase in height. Looking at equation (2.2) and using the values from above we can see that $\frac{\partial v}{\partial \xi}$ is positive. This will lead to a positive velocity. Now, in (2.1) the γ values

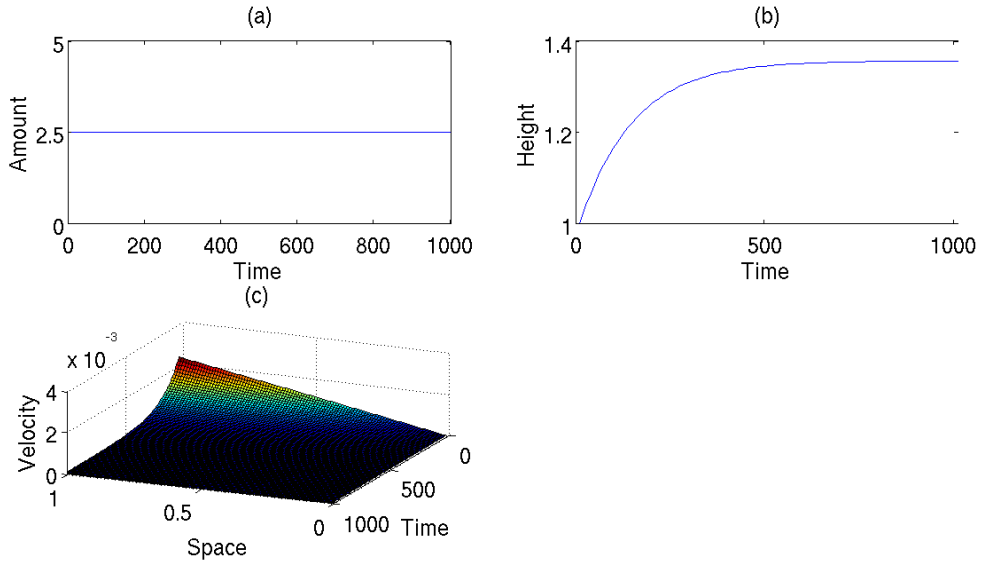

Figure 2.3: (a) A representation of the amount, not concentration, of bacteria. It is flat showing that there is a conservation of material. (b) The height changing over time. (c) The velocity that drives the change in height.

are all zero and $v > 0$. This means the height will increase. This is the driving force behind the lowering of the concentration of the three components of the biofilm. There is a dilution of the biofilm in this case. If the initial values were below the average ideal concentration the differences for the current concentration and the ideal concentration would be negative. This would mean the velocity would be negative which would lead to a decrease in the height of the biofilm due to contraction. This in turn would cause the concentration of the components to increase.

2.4.2 Growth and Erosion

When growth and erosion are added to the model the expectation is that they will reach an equilibrium where the amount being added through growth with balance out the amount being taken away through erosion. In equations (2.15)-(2.19) the erosion was determined by the amount of x, p_1, and p_2 at the top of the biofilm. If all the

polymers had separated such that p_1 was at the top and p_2 was all at the bottom it would not be possible for p_2 to erode away.

2.4.2.1 Only Erosion If growth is ignored it would be expected to see the erosion wash everything away in the model. Figure 2.4(a) shows that the erosion will do this in the absence of growth to balance it out. It can also be seen from Figure 2.4(b),(c) that increasing one of the erosion coefficients, γ, will cause the material to erode faster. It can been seen from equation (2.15) that the amount eroded is proportional only to the amount of each component at the top of the biofilm. Since the erosion terms are contained only in equation (2.15) there is no way for the erosion to directly affect the interior of the biofilm. Also, a change in one of the γ values changes how all parts of the biofilm erode. If, for example, p_1 and p_2 start with the same profile at $t = 0$ then the profile of p_1 will be the same as the profile for p_2 for all time. This is true even if γ_1 is changed and γ_2 is left the same. The reason for this has two parts. First, as was mentioned above the erosion only affects what is at the top so if p_1 and p_2 have the same profile they will have the same concentration at the top. Second, since equation (2.15) takes all three components into account to change the height, the current model does not differentiate between x, p_1, and p_2 in the erosion. It requires separate erosion equations for each component to accomplish this.

2.4.2.2 Only Growth For equations (2.17)-(2.19) it is assumed that the biofilm was saturated with nutrient. This will lead to exponential growth of the bacteria. The right hand side of equations (2.18) and (2.19) both contain an x which will lead to exponential growth of the polymers p_1 and p_2 because of the exponential growth of x. This can be seen in Figure 2.5. For the results in Figure 2.5 the expansion

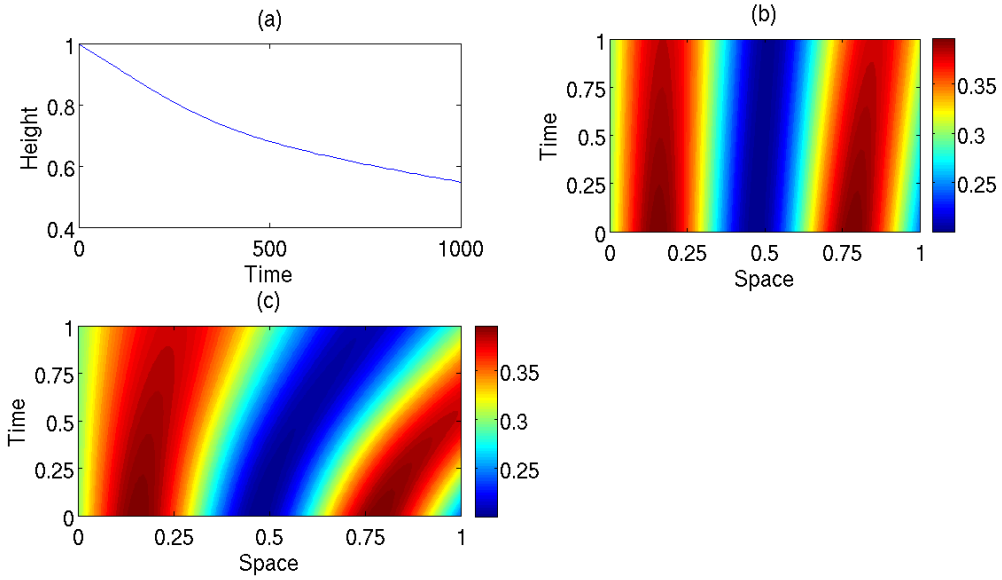

Figure 2.4: (a) The height decays when there is no growth present. (b) A space versus time view of the evolution of the polymers when all three gamma values are $\gamma = 10^{-7}$. (c) A space versus time view of the evolution of the polymers when $\gamma_0 = \gamma_2 = 10^{-7}$ and $\gamma_1 = 10^{-6}$.

coefficients, β, and erosion coefficients, γ, are all zero. The only change in the biofilm is due to growth of the three components.

2.4.2.3 Both Growth and Erosion As was said before when both growth and erosion are used in the model the hope is that they will balance each other and the height will reach or at least approach a constant value other than zero. The results for this model can be seen in Figure 2.6(a) and (b). In this case the results are a mix of good and bad. The concentration of bacteria does reach a steady state. The height however does not reach a steady state, it grows exponentially. For perspective on what these results show if everything is converted back into seconds and meters from their non-dimensional values in Figure 2.6 the height of the biofilm would be similar to the diameter of Saturn. It will have reached this thickness in about 11.5 days.

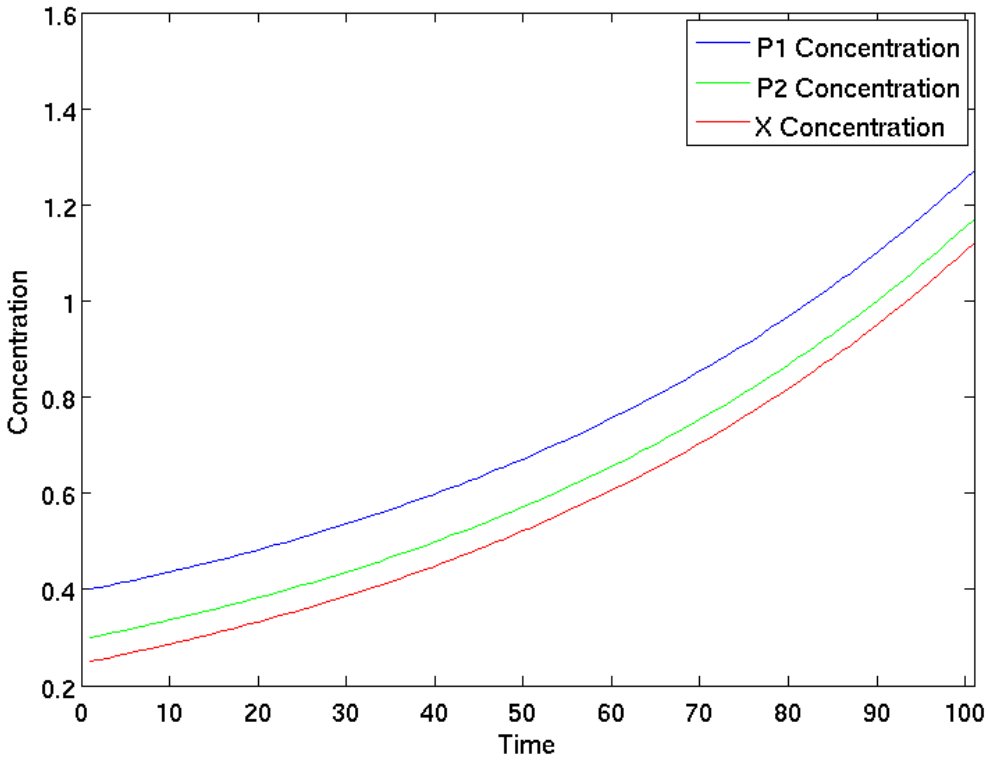

Figure 2.5: The concentration of the three components of the biofilm. All three are constant in space and since $\frac{\partial h}{\partial t} = 0$ the growth here corresponds to growth in the amounts as well as growth in the concentration.

Since these results are clearly wrong we need to figure out what is wrong with the model that produced them. The problem lies in equation (2.15). In its current form the model has an upward velocity and erosion that need to balance to reach steady state. Using equation (2.16) to find the velocity requires an integral over the entire domain. The erosion is only dependent on the amount of bacteria and polymer at the top of the biofilm. The growth of each component re-enforces both the velocity and erosion but for the same reason as was just mentioned it creates a larger change in the velocity than the erosion. This means that the erosion will never be large enough to cause the system to reach steady state.

This means the erosion term must be changed to somehow make it larger. One attempt was to change the γ values but the result of this is the same as in Figure 2.6(a) and (b). In the short term the erosion may be strong enough to lower the height of the biofilm. Eventually due to the growth and equation (2.16) the height will start to increase. Once the height begins to increase it will follow a similar curve as Figure 2.6(b). What is needed is a term that will change with time so that as the height increases the erosion increases. The obvious choice would be to multiply the erosion terms by h. This ended up not being a large enough change. In order to guarantee convergence to a steady state for the height an h^2 is needed [27]. This leads to equation (2.22) replacing equation (2.1) in the model.

$$\frac{\partial h}{\partial t} = v - h^2(\gamma_0 x + \gamma_1 p_1 + \gamma_2 p_2), \tag{2.22}$$

This change produces the a change in the units of the γ values as well. The new units for γ are $\mathrm{m^2 kg^{-1} s^{-1}}$. While this change does not have a large affect on the profile of x in Figure 2.6(c) it does significantly change the long term behavior of the height, as can be seen in Figure 2.6(d). While Figures 2.6(a) and (c) look different the final time is different. When plotted on the same set of axis the plots are very similar. Figure (2.6)(a) reaches its limiting value faster but that is the only difference.

2.5 The Problem with these Results

While the results look nice and match the model there are problems with them. A biofilm does not move as a single cohesive unit. If the entire biofilm moved as a single unit there would be the same interface between the biofilm and the bulk fluid for all time. Since the results follow from the model the errors must be in the model. Previously, in the description of the model reference was made to two

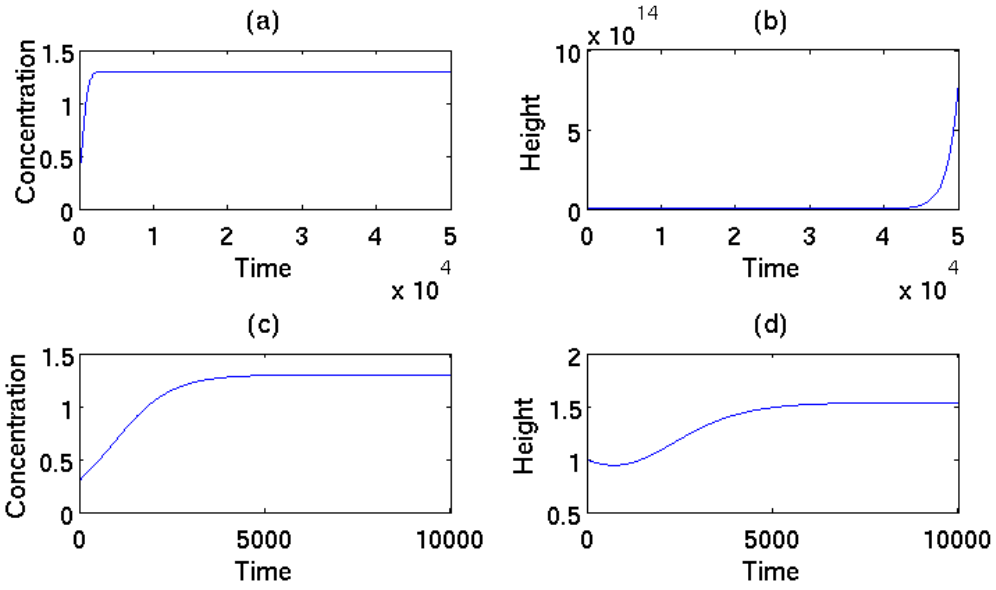

Figure 2.6: These concentration profiles are constant in space. (a)The concentration of the bacteria when the height equation (2.1) is used. Both growth and erosion are non-zero. (b) The height of the biofilm resulting from (2.1). This is clearly incorrect. (c) The concentration of the bacteria from when the height equation (2.22) is used. (d) The height of the biofilm resulting from (2.22).

possible problems that would be discussed later. These were that the model only used a single velocity for all three components of the biofilm and that the growth of all three components was proportional only the the concentration of bacteria in the biofilm.

2.5.1 The Velocity Problem

The problem with a single velocity term in the model was that it caused all three components to move in the same direction with the same velocity. As was shown in the previous section the model will cause components of the biofilm to move away from their ideal concentration if another component is mathematically dominant and moving in the opposite direction, as can be seen in Figures 2.7(a) and (b). While

there should be interaction between the components of the biofilm, one component should not dominate the behavior of everything else in the biofilm. If p_1 has a higher ideal concentration and p_2 has a lower ideal concentration both should be allowed to move closer to those values without one component dominating the behavior of the other components. The model was supposed to model how different components moved around within the biofilm. In this regard the model failed.

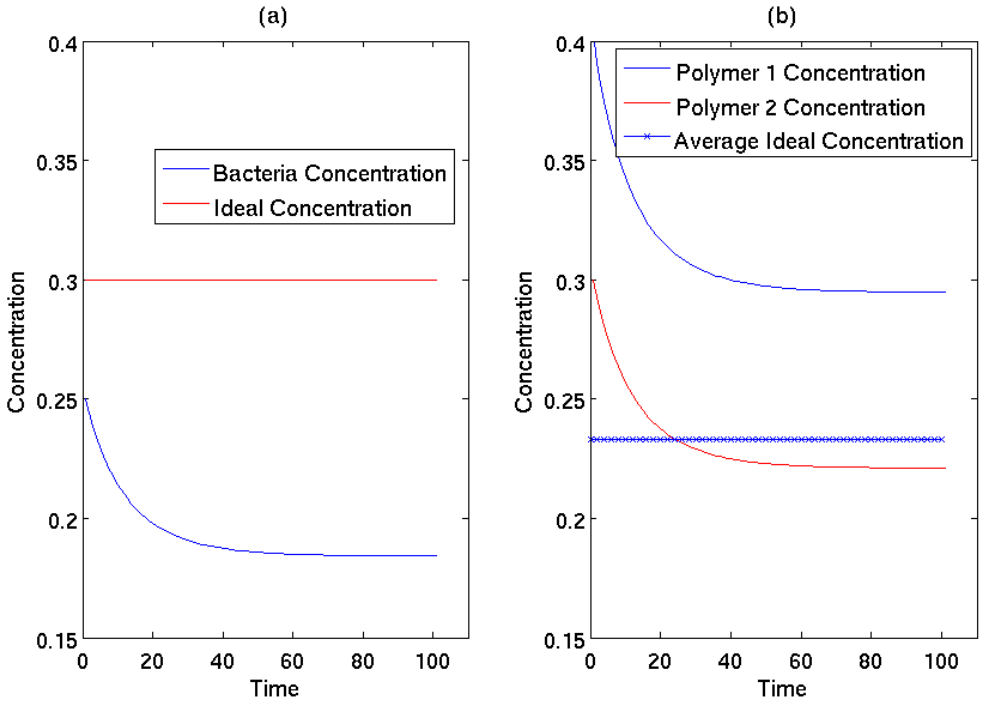

Figure 2.7: (a)The results, illustrating one of the problems with the model, showing the concentration of the bacteria moving in the wrong direction. (b) A plot showing why plot (a) moves away from the ideal concentration. The components p_1 and p_2 are the dominant terms for the current choice of parameters.

The first change made to the model to fix this problem was to change the single velocity to a separate velocity term for each component of the biofilm. The initial attempt was to take the right hand side of equation (2.2) and use each term of this to be the right hand side of a new velocity equation for each component. This gives

a total of four velocity equations. There is still the velocity from equation (2.2) that will change the height of the biofilm but there are now three new velocity equations for each component of the biofilm.

$$\begin{aligned}
&\frac{1}{h}\frac{\partial v}{\partial \xi} = F(\xi),\\
&F(\xi) = \beta_0(x - x^\star) + \beta_1(p_1 - p_1^\star) + \beta_2(p_2 - p_2^\star),\\
&\frac{1}{h}\frac{\partial v_i}{\partial \xi} = \beta_i(f_i - f_i^\star),
\end{aligned} \tag{2.23}$$

where $i = x, p_1, p_2$ and f represents x, p_1, and p_2 with $f^\star$ being the ideal concentration for the corresponding component of the biofilm. The new equations maintain the effect that movement within the biofilm would have on the height while allowing each component to move around within the biofilm. The new equations do a better job of handling the way in which a biofilm may change. A biofilm is not an undulating mass where everything moves in unison and the model now reflects that.

2.5.2 The Growth Problem

In the model there is a growth term of cx for equations (2.3)-(2.5). This results in exponential growth for each component as can be seen in Figure 2.5. While this is a standard initial attempt it ignores availability of nutrient. The model needed to more accurately reflect how biofilms grew and what might happen to them if there were not enough nutrients for the biofilm to grow in certain areas.

To make the model more realistic, the growth term is changed to a nutrient limited growth. The growth was set up to be dependent on diffusion of nutrient, which is represented as s in the equations below, into the biofilm. All three components growth depends on both the amount of bacteria and the amount and location of the nutrient within the biofilm. Since the polymers do not produce themselves it does not

make sense to have their growth dependent on themselves. There could be a negative feedback to slow down the growth rate of the polymers if there is too much but that is not used in this model.

The other thing that did not match physically was that all three components growth term had the same coefficient. The model needed to be able to model a scenario where one polymer took more energy or material to make. Changing the model so each growth coefficient was different allowed this to happen. This allowed polymer p_1 to be produced at twice the rate of polymer p_2 if it needed to be. Equations (2.4) and (2.5) did not allow this. They had each type of polymer growing at the same rate. Combining this new growth, explained below, with the new velocity led to the following equations to replace (2.3)-(2.5)

$$\frac{\partial x}{\partial t} + \frac{\partial (v_x x)}{\partial z} = g_x(s), \tag{2.24}$$

$$\frac{\partial p_1}{\partial t} + \frac{\partial (v_{p_1} p_1)}{\partial z} = g_{p_1}(s), \tag{2.25}$$

$$\frac{\partial p_2}{\partial t} + \frac{\partial (v_{p_2} p_2)}{\partial z} = g_{p_2}(s) \tag{2.26}$$

where $g_{1,2,3}(s)$ are functions that model the specific growth rate for each component. Depending on what type of kinetics are used the form of each g function will change. Zeroth order, first order, and Michaelis-Menten kinetics are all standard to use depending on various properties of the biofilm being investigated [40]. For this set of equations only zeroth order kinetics will be considered. The amount of substrate within the biofilm is modeled with a reaction-diffusion equation as follows [31]

$$D\frac{\partial^2 s}{\partial z^2} = \begin{cases} k & : s > 0 \\ 0 & : s = 0 \end{cases} \tag{2.27}$$

where k is the reaction rate coefficient with units of $1/s$ and a value of $k = 0.1$ and D is the diffusion coefficient with units of m^2/s and a value of $D = 2.3e^{-7}$. The diffusion happens on a timescale of seconds, using the characteristic values and diffusion coefficient the timescale for diffusion is 10 seconds. For biofilm growth the timescale is 1 hour. Since the diffusion happens on a much faster timescale than growth $\frac{\partial s}{\partial t}$ is ignored from the standard diffusion equation and does not show up in equation (2.27). The dimensionless diffusion coefficient $\widetilde{D}$ is defined as $\widetilde{D} = \frac{D}{kh^2}$. The $\widetilde{}$ is dropped for simplicity. This results in the growth function for $i = x, p_1, p_2$ being

$$g_i(s) = \begin{cases} c_i x & : s > 0 \\ 0 & : s = 0 \end{cases} \tag{2.28}$$

From this point everything was handled in the same way as was described in the numerics section 2.3 with the additional terms and using the Thomas Algorithm for the diffusion in (2.27) since it is a tri-diagonal system of equations.

In order to solve the equations using $g(s)$ as the growth s needs to be known. This was found by solving the following system of equations:

$$\begin{aligned} &D\frac{d^2s}{d\xi^2} = 1, && \xi_0 \leq \xi \leq 1, \\ &\frac{ds}{d\xi}(\xi_0) = 0, && s(\xi_0) = 0, && s(1) = 1 \end{aligned}$$

which results in the substrate profile being defined as a function of ξ

$$s(\xi) = \frac{k}{2D}\xi^2 + \frac{-k + \sqrt{2k}}{D}\xi + 1 - \frac{k}{2D} + \frac{k - \sqrt{2k}}{D} \tag{2.29}$$

where ξ_0 is variable that determines where the substrate profile intersects the ξ axis and where the substrate profile slope is zero.

2.6 Results 2

For the modified equations the parameters used were the same as the first set of equations. The main point of emphasis for these results was how the two different polymers moved around within the biofilm. The bacteria concentration stays constant in both space and time to make sure that there would always be bacteria for the growth in the top layer of the biofilm.

2.6.1 Using tanh(ξ) as the Ideal Concentration

To see if the changes to the model had the anticipated effect on the results zero growth and zero erosion were used to check the changes to (2.23)-(2.26). The results in Figure 2.8 were obtained using the functions

$$p_1^\star = 0.1\tanh(20(\xi - 0.5)) + 0.15, \tag{2.30}$$

$$p_2^\star = -0.1\tanh(20(\xi - 0.5)) + 0.15. \tag{2.31}$$

As can be seen from Figure 2.8 the constant initial condition evolved to match the ideal function almost exactly. The amount was conserved in this non-dimensional case. The initial amount for each type of polymer was $p_1(0) = p_2(0) = 0.15$ and the final amount was within 10^{-5} of $p_1(t_f) = p_2(t_f) = 0.15$. In this case conservation is due to the bacteria being at its ideal concentration and the average value of the polymers are at the ideal value which gives $\frac{\partial v}{\partial \xi} = 0$. This means that $v(\xi, t) = 0$ due to $v = constant$ and $v(0, t) = 0$ is one of the boundary conditions. This in turn means that $\frac{\partial h}{\partial t} = 0$ because there is no erosion in this case.

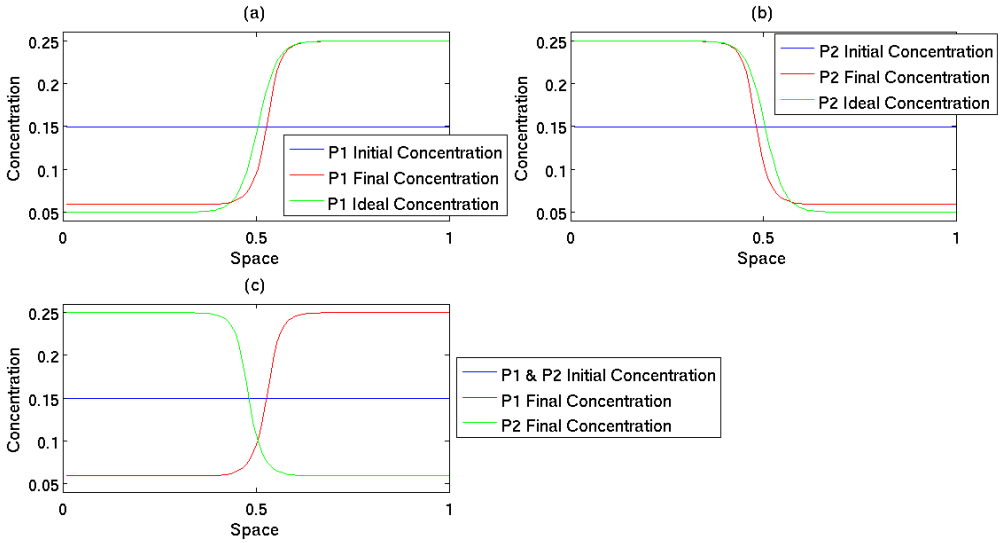

Figure 2.8: These three graphs show the values of initial and final concentrations using equations (2.30) and (2.31) as the ideal concentration. Graph (a) is for p_1 and (b) is for p_2. The last plot, (c), combines the two.

2.6.2 Growth and Erosion

The change to growth was an attempt to make the model more realistic. One thing that was done to capture more realistic results was to use a larger diffusion coefficient. Initially a coefficient of $D = 2.3 \times 10^{-9} m^2/s$ was used. Experimental data has shown that a larger diffusion coefficient may be appropriate to model the flow of substrate in the bulk fluid above the biofilm. In order to better match previous papers and to be able to see the changes going on in the biofilm D is treated as an apparent diffusion coefficient. It has been artificially increased by two orders of magnitude in order to account for convective mixing that occurs in the bulk fluid adjacent to the biofilm. The fluid flow above in essence pushes substrate into the biofilm and to model this a diffusion coefficient of $D = 2.3 \times 10^{-7} m^2/s$ was used instead. The results of this change are in Figures 2.9 and 2.10. In Figure 2.9 there is only growth in the biofilm to show the changes that result from equation (2.27). Equation (2.27) makes

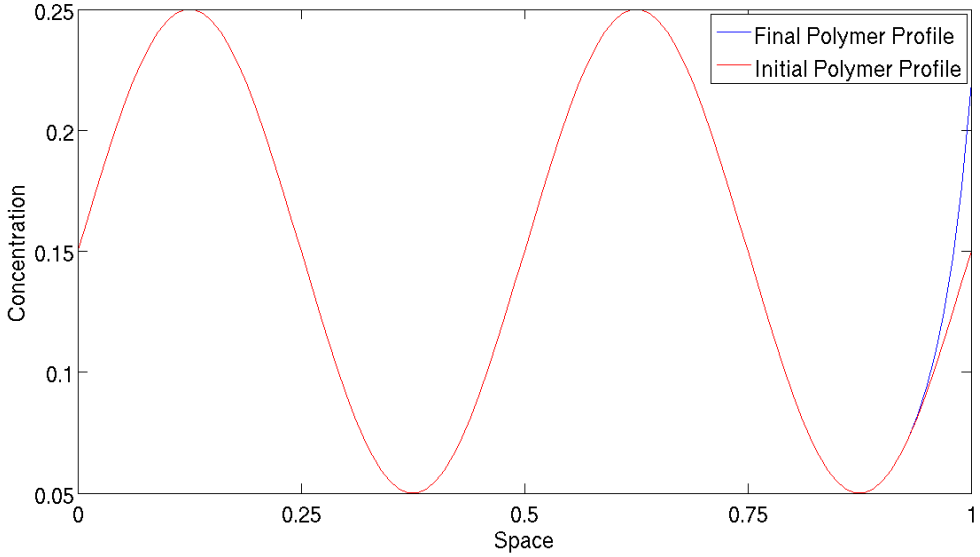

Figure 2.9: This plot is to show that the growth does have an affect on the biofilm in the region where substrate is allowed to diffuse as would be expected in the absence of both erosion and expansion within the biofilm. Here the production of polymer is determined using equations (2.24)-(2.27).

it so that the growth only happens in the region at the top of the biofilm where the substrate is able to diffuse into. This can be seen in Figure 2.9. There is a small region to the right of the graph where the growth happens. This can also be seen by comparing Figures 2.10(a) and (b). The effect of growth on the height can be seen in Figure 2.10(d). While the difference is not large the biofilm is slightly thicker in the case where there is growth versus when there is no growth.

Finally, the next set of results look at the entire changed model. Equations (2.15)-(2.19) have been changed to be of the form of equations (2.23)-(2.26) with (2.22) staying the same. Looking at the results in Figure 2.10(a) it can be seen that the growth is still working the exact same as was just discussed. The main difference in Figures 2.10 and 2.9 is that the concentration of each component can now change. This leads to the concentration of the polymer in Figure 2.10(a) moving towards a

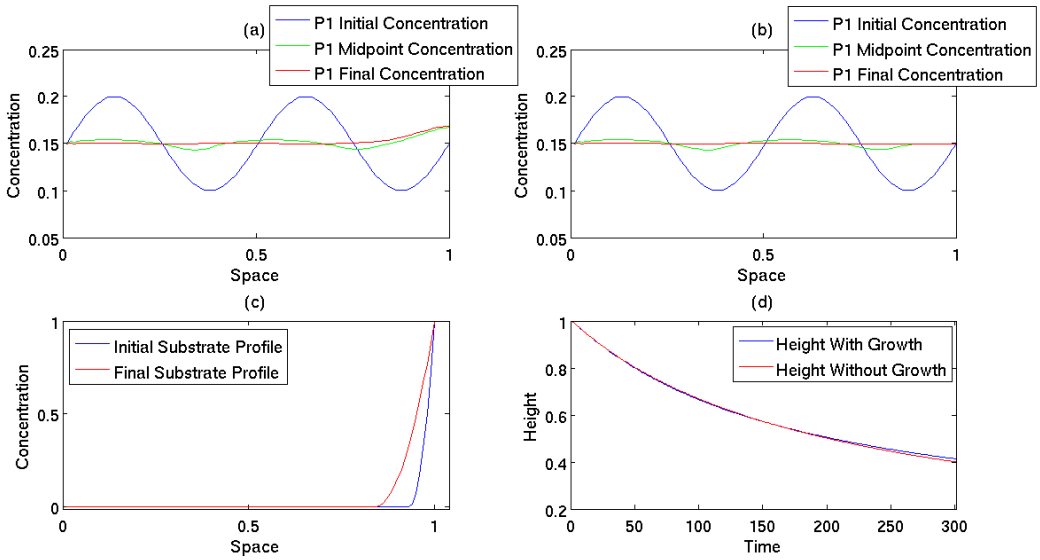

Figure 2.10: (a) This shows how the polymer profile would evolve with erosion, growth, and expansion all playing a role. The growth can be seen at the right side of the plot. The movement within the biofilm is captured with the profile changing from a sine wave to a flat line. The erosion is difficult to see in this plot. (b) For comparison to part (a) there is no growth in this plot. All the other parameters are exactly the same as part (a). (c) This is the substrate profile governed by equation (2.27). This is to show that the polymer in part (a) is only being produced where there is substrate. (d) The height of the biofilm with erosion and both with and without growth. It shows that growth will affect the height.

constant value. The exception to this being the area of growth where the erosion is balancing the growth. The effect of the erosion can be seen in Figures 2.10(c) and (d). In Figure 2.10(c) the effect of erosion is seen by how far the substrate diffuses into the biofilm. Since there is no change in any of the parameters the only way to explain a change in diffusion depth is a change in height due to erosion which can be seen in Figure 2.10(d). Since these are all plots with a max height fixed at one due to a change in variables a smaller real height would correspond to a larger percent of the biofilm having substrate diffuse to it.

2.7 More Problems

There were some problems with the modified model as well. Some of them were apparent from the first set of results in Section 2.6 and should have been seen from the time the equations were written down. Others took a while to figure out what was wrong. These problems ranged from the results being too good to the model being too specific in places and not able to capture enough of what was going on in other places.

From the first glance the results in Section 2.6 were suspicious because the results were perfect. Each component was converging to the exact value that had been set as the ideal concentration. This can be seen in Figures 2.8 and 2.11. The reason this happened was the velocity term for each component had been completely separated. This was done to allow them to move around with less interference from each other but the result was that there was zero interaction between them and they were able to move to their prescribed concentration exactly. There are numerous forces acting within a biofilm to provide structure and stability to it including: hydrogen bonds, weak electrostatic and ionic forces, van der Waal forces, and the polymers within a biofilm are tangled with each other [41, 42]. While all models must make simplifying assumptions, to completely ignore all of these forces results in the problem described here.

This change also allowed the end result for each component to be specified before solving the system. This can be seen in the difference between Figures 2.8 and 2.11. The results are completely different but the only thing that was changed in the model was the ideal value curve, $p_1^\star$. In each case the final result is converging to the ideal function as $t \to \infty$. Though not included here many other continuous functions have

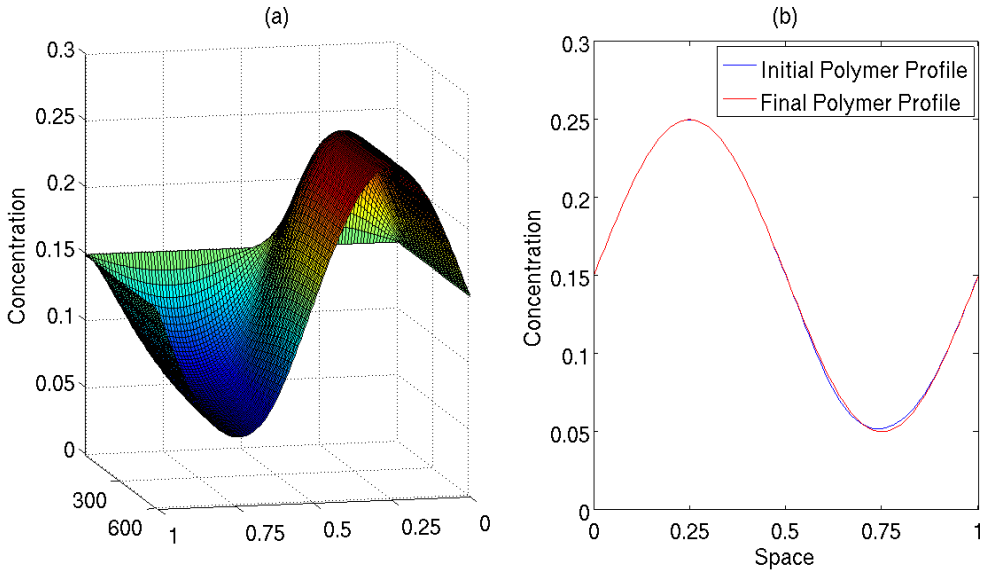

Figure 2.11: The result here shows that it is possible to change the initial concentration into almost any final concentration that is desired.

been used as the ideal value and the final result has shown convergence to these values.

Another problem was that a lot of the choices were arbitrary and were too specific about certain parts of the model. There is discussion on the idea being worked on but not any actual experimental data to use to approximate any of the parameters [5]. The ideal concentration used was too specific. Functions such as those in equations (2.30) and (2.31) were used for the ideal concentration curves. This not only gave a concentration but a location as to where each of those polymers were going to be. This was a combination of an arbitrary choice and being too specific. There is nothing in the model that says p_2 should be at the bottom of the domain other than that equation. There was no physical reason that p_2 could not have been directly in the middle of the domain and p_1 could have been on either side of it.

To fix most of these problems more needs to be added to the model. There still would have been problems with the velocity equations as each component needs

its own velocity but there still needs to be some sort of interaction with the other components. This would have led to more arbitrary choices and perhaps making more parts of the model too specific. Because of all these reasons an energy based model was chosen as the next step. It would allow the use physics instead of arbitrary choices to drive the evolution of the biofilm.

2.8 Conclusion

The 1D velocity driven model was meant to be a simple model to provide insight into how the biofilm would change due to the three forces of growth, erosion, and expansion. While the results were not as expected either before or after the modifications to the model it did provide valuable insight into how to proceed. Some ideas for how to improve the model are provided.

CHAPTER THREE

THE 1D ENERGY BASED MODEL

In this chapter the work of Zhang, Cogan, and Wang [25, 32] will be examined and expanded upon. A derivation of the Cahn-Hilliard equation as well as the Flory-Huggins mixing free energy density equation will be derived. An energy based model has a few advantages over what was done previously. This model is based on physics and chemistry. An energy based model follows from the basic principles of physics and chemistry, a system is at equilibrium if its energy is minimized [34]. The exact energy that is being minimized will be discussed in the chapter. Changes made to the original model are discussed along with justification that some of these changes did not fundamentally alter the model. Results from both before the changes and after will be presented.

This model is a one dimension model which implies that nothing is changing in two of the spatial directions. While the changes in the biofilm only occur in the y variable there is a velocity with a non-zero x component seen in Figure 3.1. For consistency with the equations in previous publications it is assumed that the variable where change occurs is y and the model is constant in the x and z directions.

3.1 An Energy Based Model

Looking to the work of Zhang, Cogan, and Wang [25] the basis for the work discussed here is found. In this model a two component fluid is assumed. The network of polymer that houses the bacteria and the solvent which includes the substrate form the two components of this model. For this model ϕ_n will represent the volume fraction of the network and $\phi_s = 1 - \phi_n$ will be the volume fraction for the solvent.

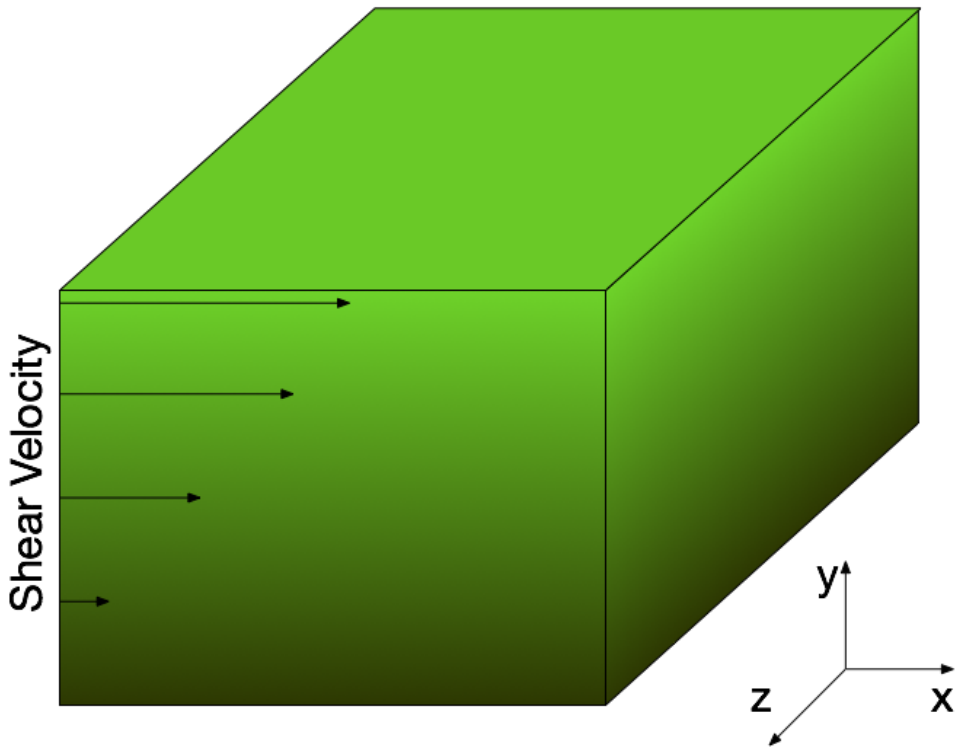

Figure 3.1: A cartoon of how the 1D model works. Velocity is in the x direction only and there is no change in the biofilm in the x or z direction.

The components are being viewed as volume fractions which leads to $0 \leq \phi_n < 1$. A volume fraction of $\phi_n = 0$ corresponds to pure solvent at that location. While the values of $\phi_n \geq 0.5$ are allowed they are unrealistic, as biofilms are mostly water and can be up to 98% water [42], but $\phi_n = 1$ is excluded because of it being physically impossible since biofilms are never dry .

For this work it is assumed that the biofilm-solvent mixture is incompressible, with a bulk fluid motion measured with a divergence-free averaged velocity using the network velocity, $\mathbf{v}_n$, and the solvent velocity, $\mathbf{v}_s$ [25]

$$\mathbf{v} = \phi_n \mathbf{v}_n + \phi_s \mathbf{v}_s \tag{3.1}$$

The fluid is convected by this velocity $\mathbf{v}$ but the polymer is also transported by an extra flux due to mixing of components within the fluid. The local flux has two parts; the flux convected by the average velocity $\mathbf{v}$ and the excessive flux from the mixing of the polymer and solvent [25]. This excessive flux from the mixing is assumed to be proportional to the gradient of the variation of the mixing free energy

$$\mathbf{f}_n = -\lambda_{ch} \nabla \frac{\delta f}{\delta \phi_n}, \tag{3.2}$$

with λ_{ch} being the proportionality parameter with units that match the mobility and f is the Flory-Huggins mixing free energy density [43]

$$f = kT \left[\frac{\gamma_1}{2} ||\nabla \phi_n||^2 + \gamma_2 \left(\frac{\phi_n}{N} \ln \phi_n + (1 - \phi_n) \ln (1 - \phi_n) + \chi \phi_n (1 - \phi_n) \right) \right] \tag{3.3}$$

where γ_1 measures the strength of the distortional energy, γ_2 is a measure of the strength of the bulk free energy in the extended Flory-Huggins mixing free energy density defined in equation (3.3), it is proportional to the reciprocal of the volume

occupied by the solvent molecule. The polymerization index of the polymer is given by N, k is the Boltzman constant, T is the temperature, and χ is the Flory-Huggins mixing parameter. The Flory-Huggins mixing parameter gives a measure of the interaction between polymers and the solvent as well as polymer-polymer interactions [44]. The Flory-Huggins mixing free energy density will be discussed more in the next section.

The transport of the polymer is modeled with the Cahn-Hilliard equation [33,45] using the averaged velocity throughout the model

$$\frac{\partial \phi_n}{\partial t} + \nabla \cdot (\phi_n \mathbf{v}) = \nabla \cdot \left(\lambda_{ch} \nabla \frac{\delta f}{\delta \phi} \right). \tag{3.4}$$

The assumption that the mobility was proportional to ϕ_n is used, which leads to $\lambda_{ch} = \lambda \phi_n$ in equation (3.4). In this equation λ_{ch} is the mobility parameter [25]. This change leads to the modified Cahn-Hilliard equation

$$\frac{\partial \phi_n}{\partial t} + \nabla \cdot (\phi_n \mathbf{v}) = \nabla \cdot \left(\lambda \phi_n \nabla \frac{\delta f}{\delta \phi} \right). \tag{3.5}$$

It has also been shown that the modified Cahn-Hilliard equation was more appropriate for modeling the transport of ϕ_n [25]. There will be more discussion on equations (3.4) and (3.5) in a following section.

The final equations governing the mixture are the continuity equation, momentum transport equation, and the transport equation for the nutrient

$$\nabla \cdot \mathbf{v} = 0, \tag{3.6}$$

$$\rho \frac{d\mathbf{v}}{dt} = \nabla \cdot (\tau_{extra}) - \left[\nabla p + \gamma_1 kT \nabla \cdot (\nabla \phi_n \nabla \phi_n) \right], \tag{3.7}$$

$$\frac{\partial}{\partial t} (\phi_s c) + \nabla \cdot (c \mathbf{v} \phi_s - D_s \phi_s \nabla c) = -g_c, \tag{3.8}$$

where ρ_n and ρ_s are the densities of the network and solvent, $\rho = \phi_n\rho_n + \phi_s\rho_s$ is the averaged density, and $\tau_{extra} = \phi_n\tau_{network} + \phi_s\tau_s$ is the total extra bulk stress for the mixture [25]. The reaction rate g_c is defined as

$$g_c = \phi_n A c \tag{3.9}$$

where A is the consumption rate of the substrate and c is the concentration of the nutrient substrate [24, 25]. The last piece to define is τ_{extra}. The stress tensor can be defined in various ways. Since biofilms have elastic or viscoelastic properties depending on the timescale used τ_{extra} should take these into account. To do this $\tau_{network}$ needs to be modified. The network contains the bacteria so the stress tensor should contain a part that takes the bacteria into account. The stress tensor is

$$\tau_{extra} = \phi_n \left(a\tau_n + \tau_{ns}\right) + \phi_s\tau_s \tag{3.10}$$

where a is a rate parameter and $\tau_s = 2\eta_s\mathbf{D}$ [25], with η_s being the solvent viscosity. The τ_n term in the stress tensor comes from a constitutive equation found by using the Johnson-Segalman viscoelastic model with the velocity being the average velocity $\mathbf{v}$ [46]. The τ_{ns} is defined as

$$\tau_{ns} = 2\eta_{ns}\mathbf{D} \tag{3.11}$$

with η_{ns} being the contribution of the bacteria to the viscosity of the network and $\mathbf{D} = \frac{1}{2}\left[\nabla\mathbf{v} + \nabla\mathbf{v}^T\right]$ is the rate of strain tensor [25]. In the simulations η_{ns} is treated as a constant. Before discussing the numerical methods and solutions for these equations a derivation for the two major pieces of the model will be given.

3.1.1 The Cahn-Hilliard Equation

The Cahn-Hilliard equation will derived following the work laid out by Lee et. al. in [34]. The Flory-Huggins free energy density will be derived by following the work of both Lee et. al. [34] and Dill and Bromberg [47].

3.1.1.1 The Helmholtz Free Energy for a Homogeneous System

As was mentioned above the goal is to minimize the energy of the system, but not just any energy. The energy to be minimized is the Helmholtz free energy. The reason for this is that in order for a simple and closed system to be at equilibrium its Helmholtz free energy must be minimized for a fixed temperature and volume [34]. The first steps are to look at the derivation of this energy using a lattice model and then show one derivation of the Cahn-Hilliard equation.

The Helmholtz free energy density per molecule, $F(T, x)$ where T is the temperature and x is the molar fraction, will be derived using a lattice model for a binary fluid where both component molecules are of equal size, each molecule occupies a single lattice site. The system will also be homogeneous in the sense that all the material will be in the same phase in this derivation. For example in this section think of taking a glass of water and adding a liquid dye into the glass. The heterogeneous case is handled in the next section. An example of a heterogeneous system would be a glass of ice water, where the liquid water and ice are the two phases. The molar Helmholtz free energy of mixing is

$$\Delta F_{mix} = \Delta E_{mix} - T\Delta S_{mix}. \tag{3.12}$$

The mixing entropy, ΔS_{mix}, will be derived first. Suppose there is a binary fluid at a constant temperature with N_A molecules of species A and N_B molecules

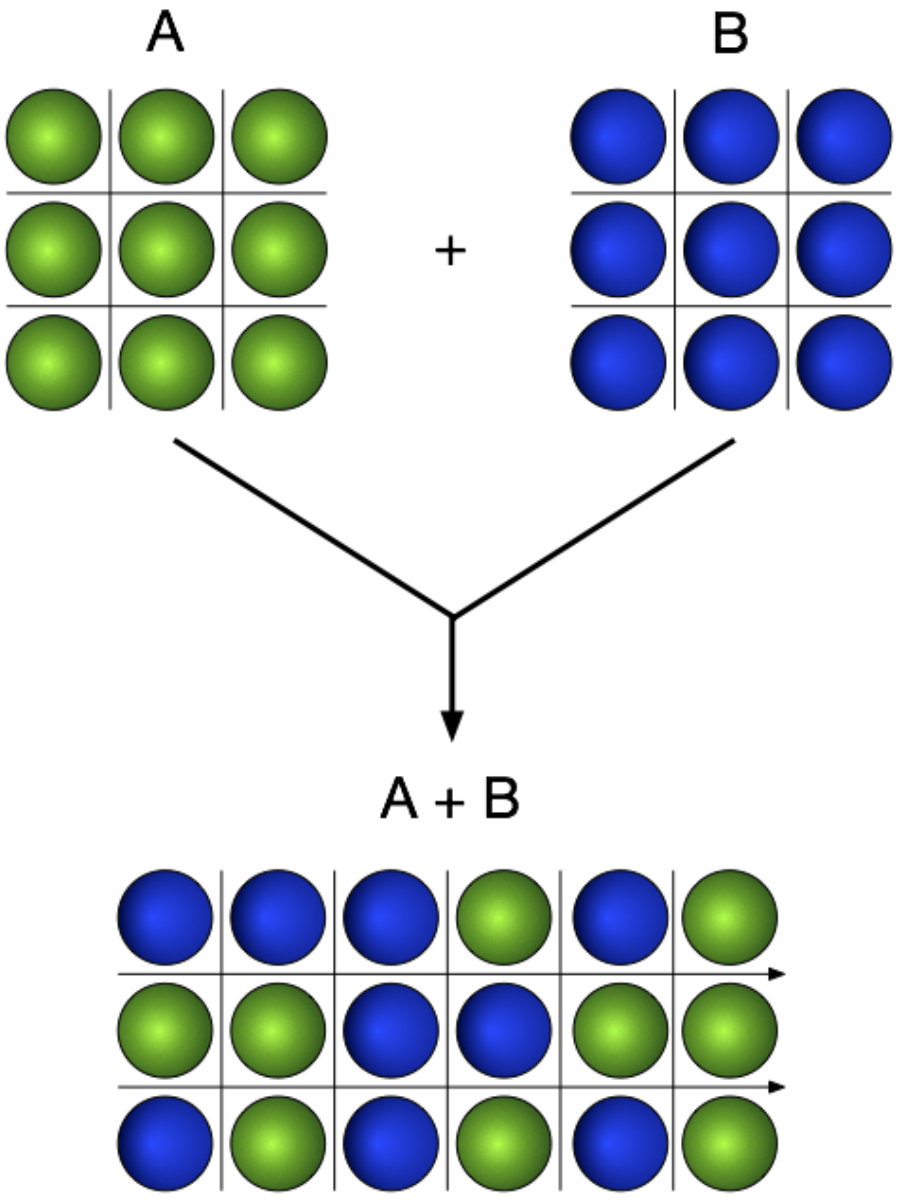

Figure 3.2: A cartoon of the lattice model of mixing. Starting with pure A and B they are mixed together and randomly fill the lattice.

of species B. Together there are $N = N_A + N_B$ molecules that occupy all possible lattice sites. A visual explanation of this mixing is seen in Figure 3.2. In this figure both $N_A = 9$ and $N_B = 9$. The mixing is assumed random in this derivation but only one possible configuration is given. This is only 1 of the W possible states. The multiplicity of states is given by a basic combination formula:

$$W = \frac{N!}{N_A! N_B!}. \tag{3.13}$$

The mixing entropy, ΔS_{mix}, comes from first using the Boltzmann Equation, $\Delta S = k \ln W$ with k being the Boltzmann constant [47]. Next, Sterling's approximation is applied, which states that $\ln N! \approx N \ln N - N$ when truncated after two terms [34, 47].

$$\begin{aligned}
\Delta S_{mix} \approx k \ln \frac{N!}{N_A! N_B!} &= k \left(N \ln N - N - N_A \ln N_A + N_A - N_B \ln N_B + N_B \right), \\
&= k \left(N_A \ln N + N_B \ln N - N_A \ln N_A - N_B \ln N_B \right), \\
&= -k \left(N_A \ln \frac{N_A}{N} + N_B \ln \frac{N_B}{N} \right), \\
&= -Nk \left(\frac{N_A}{N} \ln \frac{N_A}{N} + \frac{N_B}{N} \ln \frac{N_B}{N} \right). \\
\text{Which leads to} \frac{\Delta S_{mix}}{-kN} &= \left(p \ln p + (1-p) \ln(1-p) \right).
\end{aligned} \tag{3.14}$$

If N is Avagadro's number then $kN = R$ is the universal gas constant, $p = \frac{N_A}{N}$, and $1 - p = \frac{N_B}{N}$ are the molar fractions of N_A and N_B respectively.

The internal energy change due to mixing, ΔE_{mix} is derived with the same starting point. Consider a randomly mixed solution of N_A molecules of species A and N_B molecules of species B. The internal energy is the pairwise sum of inter-atomic potentials for each atom or molecule. For simplicity only the interactions between

nearest neighbors will be considered even though interactions between the molecules can happen over much larger distances. The only interactions considered are at the $A-A$, $B-B$, and $A-B$ bonds. Let w_{AA}, w_{BB}, and w_{AB} be the interaction potentials for each bond type. Now the total internal energy will be the number of each type of bond times the potential for each bond type. This will be expressed as

$$E = m_{AA}w_{AA} + m_{BB}w_{BB} + m_{AB}w_{AB} \tag{3.15}$$

where each m term is the number of the corresponding bond type. The number of each bond type can be found by using the total number of molecules of each type and the number of nearest neighbors. Let z be the number of nearest neighbors for each molecule. Then the total number of each bond type can be found given the total number of both A and B molecules. When counting the number of bond types m_{AA} will be counted twice because that bond has two A molecules in it and the number of bonds is being compared to the number of molecules. It is similar for m_{BB} bonds. The total number of A molecules N_A multiplied by the number of nearest neighbors z would be twice the number of m_{AA} bonds plus the total number of m_{AB} bonds. This calculation is being done for the entire lattice so there is no worry about multiple counting of a single molecule like there would be if this was done molecule by molecule and then the results added up at the end. This leads to the following two equations that relate the number of each type of molecule to the number of each type of bond:

$$N_A z = 2m_{AA} + m_{AB}, \qquad N_B z = 2m_{BB} + m_{AB}.$$

Solving each equation for m_{AA} and m_{BB} respectively and substituting into equation

(3.15) gives the total interaction energy for the system as follows

$$E = \left[\frac{N_A z}{2} w_{AA} + \frac{N_B z}{2} w_{BB}\right] + \left[w_{AB} - \frac{w_{AA} + w_{BB}}{2}\right] m_{AB} \tag{3.16}$$

where the only unknown quantity is the number of $A-B$ bonds, m_{AB}. The first term in equation (3.16) is the interaction energy for an unmixed state. The $\frac{N_A z}{2} w_{AA}$ term is the interaction energy for the A molecules in a pure state and similar for $\frac{N_B z}{2} w_{BB}$. This means the second term contained in the second set of square brackets must be the change in internal energy due to mixing, ΔE_{mix}. This is the last piece needed for equation (3.12).

To evaluate m_{AB} the mean-field approximation will be used. The mean-field approximation assumes that the molecules will be distributed randomly and as uniformly as possible. This means it is assumed that the molecules are randomly distributed with probability to occupy a specific lattice location equal to the fraction of lattice points occupied by the corresponding species of molecule [47]. In this case that probability is the molar fraction. For each lattice point the probability that it is occupied by a species A molecule is p and the probability for a molecule of species B is $1-p$. Take a single A molecule, there are z nearest neighbors. The average number of $A-B$ bonds formed by this specific A molecule is the probability that one of the nearest neighbors is occupied by a B molecule multiplied by the number of nearest neighbors. We repeat this process for each A molecule and find m_{AB} to be

$$m_{AB} = \frac{z N_A N_B}{N} = zNp(1-p). \tag{3.17}$$

Substituting equation (3.17) into equation (3.16) we have

$$\Delta E_{mix} = \left[w_{AB} - \frac{w_{AA} + w_{BB}}{2} \right] zNp(1-p) = \chi_{AB} p(1-p), \tag{3.18}$$

where (3.19)

$$\chi_{AB} = \left[w_{AB} - \frac{w_{AA} + w_{BB}}{2} \right] zN. \tag{3.20}$$

Finally, the molar Helmholtz free energy of mixing , ΔF_{mix}, is

$$\Delta F_{mix} = \chi_{AB}\, p(1-p) + kNT \left(p \ln p + (1-p) \ln(1-p) \right). \tag{3.21}$$

Here χ_{AB} is an exchange parameter that measures the energy cost of starting with pure states of A and B and moving one molecule of B into the pure A and one molecule of A into the pure B [47]. There were two main assumptions made to arrive at equation (3.21). It was assumed that the two species of molecules were the same size. Because of this assumption the volume fraction is the same as the molar fraction and equation (3.21) is valid for volume fractions as well. Because of this let $p = \phi$ unless otherwise stated for simplicity. The other assumption was that the mean field approximation is valid. This would be a problem if for some reason the $A-B$ bonds are preferred over the $A-A$ or $B-B$ bonds or vice versa.

3.1.1.2 The Variational Derivative Before going forward with the derivation the variational derivative or functional derivative needs to be examined. In calculus of variations functionals are usually expressed as an integral of a function, its arguments, and the functions derivatives [48]. Let the functional $G[y]$ be defined as [49]

$$G[y] = \int L[x, y(x), y'(x)]\, dx. \tag{3.22}$$

The change in $G[y]$ can be expressed as

$$\delta G = \int \frac{\delta G}{\delta y} h(\mathbf{x})\, d\mathbf{x} \tag{3.23}$$

where $h(\mathbf{x})$ is an arbitrary function with compact support [49] and its coefficient $\frac{\delta G}{\delta y}$ is called the functional, or variational, derivative. The variational derivative is defined as [50]

$$\int \frac{\delta G}{\delta y} h(x)\, dx = \lim_{\varepsilon \to 0} \frac{G[y + \varepsilon h] - G[y]}{\varepsilon}, \tag{3.24}$$

$$= \left[\frac{d}{d\varepsilon} G\left[y + \varepsilon h\right] \right]_{\varepsilon = 0}. \tag{3.25}$$

The functional derivative will now be found using the functional in equation (3.22) and applying the definition given in equation (3.25).

$$\begin{aligned}
\int \frac{\delta G}{\delta y} h(\mathbf{x})\, d\mathbf{x} &= \left[\frac{d}{d\varepsilon} \int L[\mathbf{x}, y(\mathbf{x}) + \varepsilon h(\mathbf{x}), \nabla y(\mathbf{x}) + \varepsilon \nabla h(\mathbf{x})]\, d\mathbf{x} \right]_{\varepsilon = 0}, \\
&= \int \frac{\partial L}{\partial y} h + \frac{\partial L}{\partial \nabla y} \cdot \nabla h\, d\mathbf{x}, \\
&= \int \frac{\partial L}{\partial y} h - \left(\nabla \cdot \frac{\partial L}{\partial \nabla y} \right) h\, d\mathbf{x}, \\
&= \int \left(\frac{\partial L}{\partial y} - \nabla \cdot \frac{\partial L}{\partial \nabla y} \right) h\, d\mathbf{x}
\end{aligned} \tag{3.26}$$

This means that the variational derivative for the functional in equation (3.22) is

$$\frac{\delta G}{\delta y} = \frac{\partial L}{\partial y} - \nabla \cdot \frac{\partial L}{\partial \nabla y} \tag{3.27}$$

3.1.1.3 The Free Energy of the Heterogeneous System As was mentioned above the volume fraction is the same as the molar fraction in the lattice model. This is true but the volume fraction is also used for a continuous model not just the discrete lattice model. Taking the entire volume of the biofilm a single differential element can be represented as an entire lattice as in Figure 3.3. To get the total energy a sum needs to be performed on all the molecules within the biofilm. In the limit the sum becomes the integral in equation (3.28). In their work Cahn and Hilliard also assumed that the system is isotropic which means the free energy is invariant under reflections and rotations [45]. This assumption will be carried forward in the following derivation.

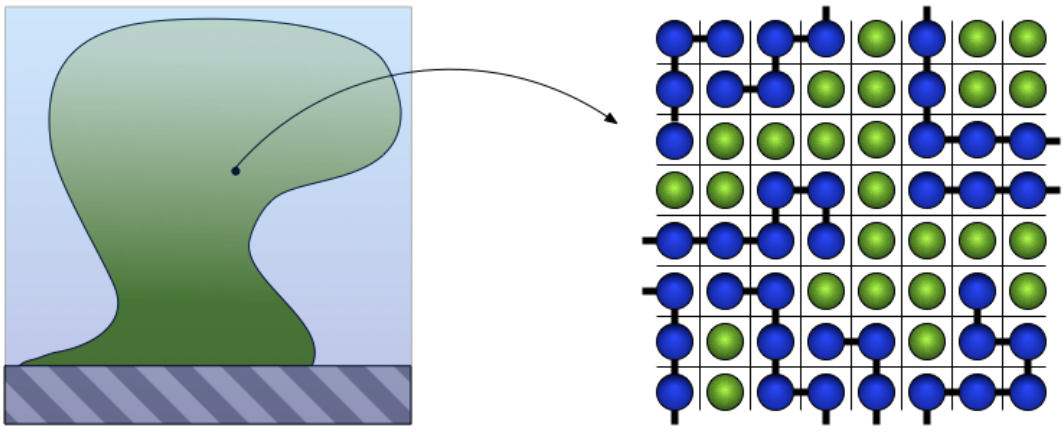

Figure 3.3: A cartoon of how the lattice and continuum models are related.

Next, the equation for the free energy of a nonuniform system with variations in the spatial composition will be examined. Let $\frac{\Delta F_{mix}}{N} = F(\phi)$, which is the Helmholtz free energy density per molecule, then the total free energy of a system at time t with

nonuniform composition is defined as

$$E(t) = N_V \int_\Omega \left[F(\phi) + \frac{\epsilon^2}{2} ||\nabla \phi||^2 \right] d\mathbf{x} \tag{3.28}$$

where N_V is the number of molecules per unit volume, $||\cdot||$ denotes the l_2 norm of a vector in $\mathbb{R}^n$, and F is the Helmholtz free energy density per molecule [34]. From here the Cahn-Hilliard equation is derived by first introducing the chemical potential μ as the variational derivative of equation (3.28) using equation (3.27).

$$\begin{aligned} \mu = \frac{\delta E}{\delta \phi} &= \frac{\partial \left(F(\phi) + \frac{\epsilon^2}{2} ||\nabla \phi||^2 \right)}{\partial \phi} - \nabla \cdot \frac{\partial \left(F(\phi) + \frac{\epsilon^2}{2} ||\nabla \phi||^2 \right)}{\partial \nabla \phi} \\ &= F'(\phi) - \nabla \cdot \epsilon^2 \nabla \phi, \\ &= F'(\phi) - \epsilon^2 \Delta \phi. \end{aligned} \tag{3.29}$$

The flux of component A in the binary fluid is defined as $J = -M \nabla \mu$ from Fick's law of diffusion. Fick's Law states that the flux of particles is proportional to the concentration gradient, where the minus sign means the the flow is from high to low concentrations [47]. Looking back to equation (3.2) and letting $M = \lambda_{ch}$ it can be seen that this flux is really the excessive flux as it was defined in section 3.1. The Cahn-Hilliard equation is found by using this flux in a continuity equation [34]

$$\frac{\partial \phi}{\partial t} = -\nabla \cdot J \tag{3.30}$$

with boundary conditions

$$\nabla \phi \cdot \mathbf{n} = 0, \qquad J \cdot \mathbf{n} = 0, \tag{3.31}$$

where $\mathbf{n}$ is the unit normal vector for the domain Ω. Where the first boundary

condition is the no flux boundary condition on the volume fraction and the second is that there is zero net flux through the boundary due to the mixing of polymer and solvent. When compared to equation (3.4) the Cahn-Hilliard equation derived here is not the same. The difference is due to equation (3.4) taking an external velocity into account, this is the $\nabla \cdot (\phi_n \mathbf{v})$ term. The external velocity could be thought of as the flow of a river over the biofilm at the bottom or a similar set up in a lab. Equation (3.30) is the Cahn-Hilliard equation for only mixing like the example used earlier with a glass of water with dye added.

As was mentioned earlier in order for the system to be at equilibrium it needs to have a minimized Helmholtz free energy. If it is not at equilibrium the energy should always be decreasing in order to try and reach a lower energy. To show that the energy is decreasing for all time it needs to be shown that the time derivative of the energy is at least non-positive for all time. Differentiating equation (3.28) with respect to time while ignoring the constant N_V and making use of the boundary conditions (3.31) leads to the following:

$$\begin{aligned}
\frac{d}{dt}E(t) &= \int_D \left[F'(\phi)\frac{\partial \phi}{\partial t} + \epsilon^2 \nabla\phi \cdot \nabla \frac{\partial \phi}{\partial t} \right] d\mathbf{x}, \\
&= \int_D F'(\phi)\frac{\partial \phi}{\partial t} - \epsilon^2 \frac{\partial \phi}{\partial t}\Delta\phi \, d\mathbf{x} + \int_{\partial D} \epsilon^2 \frac{\partial \phi}{\partial t} \left(\nabla\phi \cdot \mathbf{n}\right) d\mathbf{s}, \\
&= \int_D \mu \frac{\partial \phi}{\partial t} \, d\mathbf{x}, \\
&= \int_D \mu \left(\nabla \cdot M\nabla\mu\right) d\mathbf{x}, \\
&= -\int_D M\nabla\mu \cdot (\nabla\mu) \, d\mathbf{x} + \int_{\partial D} M\mu \left(\nabla\mu \cdot \mathbf{n}\right) d\mathbf{s}, \\
&= -\int_D M|\nabla\mu|^2 \, d\mathbf{x}. \qquad (3.32)
\end{aligned}$$

The integrand of equation (3.32) is positive which means the result of equation (3.32) will be negative. This guarantees that the energy will never increase. Due to the no flux boundary conditions there should be conservation of matter. There is conservation of matter which can be seen by computing the time derivative of the total amount of material, $\int_D \phi \, d\mathbf{x}$, using the boundary conditions from equation (3.31).

$$\frac{d}{dt}\int_D \phi \, d\mathbf{x} = \int_D \frac{\partial \phi}{\partial t} \, d\mathbf{x} = \int_{\partial D} M \nabla \mu \cdot \mathbf{n} \, d\mathbf{s} = 0 \tag{3.33}$$

3.2 The Flory-Huggins Free Energy

The previous section assumed that the molecules being mixed were of the same size. This assumption led to equation (3.13) and contributed to the derivation of equation (3.18). Polymers are chains which can contain hundreds or thousands of molecules, called monomers. Each individual polymer is then hundreds or thousands times larger than a single solvent molecule [47]. This does affect the physical properties of a solution. The mixing is different and the model must change slightly for the difference between a polymer/solvent solution and a solution of two similar sized molecules. This work was first done by PJ Flory who won the 1974 Nobel prize in Chemistry for his work on polymer science [51]. The derivation is largely the same as the previous section with slight changes to the lattice model due to the polymers being connected chains that have the possible positions of later monomers determined by the location of previous monomers in the lattice.

Another difference is that volume fraction and molar fraction are no longer interchangeable. For this derivation volume fraction must be used due to differences in the chemical properties of polymers and the equations used to model them. More discussion on this can be found in [47] pages 593-596. The basic idea can be seen from

a simple example of a solution of 10000 molecules. Assume there is a solution with $n_p = 10$ polymers each with $N = 999$ monomers where each monomer is the size of one solvent molecule and $n_s = 9990$ solvent molecules. Due to each monomer being the same size as a molecule of solvent there are $M = n_n N + n_s = 19980$ lattice points needed for this example. The molar fraction of the polymer and solvent respectively would be $\frac{1}{1000}$ and $\frac{999}{1000}$. The molar fractions are quite different. The volume fractions are both $\frac{1}{2}$ since the volume fraction of the solvent is $\phi_s = \frac{n_s}{M} = \frac{9990}{19980}$ and the volume fraction of the polymers is $\phi_n = \frac{n_n N}{M} = \frac{9990}{19980}$. Using the numbers for molar fraction in equation (3.21) there would be nearly zero change from a state of pure solvent to one with the polymers added in. The polymer makes up half of the volume of the solution even though it is only 0.1% of the molecules. It has a much larger impact on the chemical and physical properties of the solution and the math reflects this by using volume fraction instead of molar fraction in this case.

3.2.1 The Number of States with Polymers

Having polymers in the fluid make for a more difficult derivation of the number of states. It is no longer a simple mixing problem where any molecule can be put in any lattice point. Since the polymers can be thought of as strings of monomers the location of each monomer is dependent on the location of all the previous monomers to some degree. It is not possible to place one monomer and then place the next monomer in the polymer on the opposite side of the lattice. The next monomer must be located in one of the nearest neighbor locations to the previous monomer. In order to find the number of states function W used in the derivation the lattice must be carefully filled as opposed to using a random distribution.

The example above used some numbers to show the differences when polymers are part of the solution but more formal definitions are needed in order to derive the

updated formulas. Assume there is a lattice with M sites and each site has z nearest neighbors. There are n_s solvent molecules and n_p polymers each with N monomers. Each monomer is the same size as a solvent molecule and they both occupy a single lattice site. This means in order to completely fill the lattice the number of solvent molecules and polymers are related by

$$M = n_s + Nn_p. \tag{3.34}$$

The volume fractions for each molecule are defined as

$$\phi_n = \frac{Nn_p}{M}, \qquad \phi_s = \frac{n_s}{M}. \tag{3.35}$$

Now the lattice needs to be filled. To fill the lattice a growth method will be used for the polymers. First, place a single monomer, call it monomer 1, in any of the M lattice sites. From here there are z choices to place the next monomer, called monomer 2. In order to place the third monomer there are now $z - 1$ lattice sites available since one of the z nearest neighbors is occupied by monomer 1. This will be true for the rest of the monomer in the polymer chain. Now, repeat this process until an entire polymer is placed within the lattice. The total number of conformations within the lattice for this single polymer is defined as [47]

$$v_1 = Mz(z-1)^{N-2} \approx M(z-1)^{N-1}. \tag{3.36}$$

This equation is a good approximation but for large polymers it is missing some information. A large polymer could wrap back around onto itself even in a lattice model. Assume a standard 2D square grid. If a polymer has five monomers it is possible placing the next monomers in four adjacent sites could result in the fifth

monomer being able to be placed in the location of the first monomer. In order to model larger polymers lattice sites need to be excluded once they are filled with monomers. This equation does not do that. To account for this P.J. Flory's model will be followed. He made the approximation that this excluded volume was proportional to the total number of lattice sites already occupied as if the monomers were randomly distributed [47]. While this is not a perfect counting it is better than ignoring it completely. There are other more advanced theories for describing polymers in solutions such as the Flory-Krigbaum theory but those are not needed here [52]. Using this approximation the number of sites available for monomer 2 is changed from z to $z\frac{M-1}{M}$. Applying this to all the monomers the new equation for number of conformations is

$$\begin{aligned} v_1 &= M\left[z\frac{M-1}{M}\right]\left[(z-1)\frac{M-2}{M}\right]\cdots\left[(z-1)\frac{M-N+1}{M}\right] \\ &\approx \left(\frac{z-1}{M}\right)^{N-1}\frac{M!}{(M-N)!} \end{aligned} \tag{3.37}$$

In order to guarantee that all the polymers will fit in the lattice the polymers need to be built up simultaneously. The first monomer for all n_p polymers needs to be placed first and then place the second monomer in each polymer. This is repeated until all the polymers are in the lattice.

Mathematically the first monomer of the first polymer has M possible locations, the first monomer of the second polymer has $M-1$ possible locations, and so on until all the first monomers are placed. This means the number of arrangements for the first monomer of all the polymers can be expressed as

$$v_{first} = M(M-1)(M-2)\cdots(M-n_p+1) = \frac{M!}{(M-n_p)!} \tag{3.38}$$

Next, place the second monomer from each polymer in the lattice. For the second monomer of the first polymer there are $M - n_p$ sites left in the lattice and the second monomer in the last polymer has $M - 2n_p + 1$ lattice sites available. Each of the subsequent monomers must be in one of the nearest neighbor sites relative to the first monomer so there is an extra $z-1$ term for each monomer. Repeat this process for all the remaining monomers and using equation (3.37) the total number of arrangements for the rest of the monomers is [47]

$$v_{subsequent} = \left(\frac{z-1}{M}\right)^{n_p(N-1)} \frac{(M-n_p)!}{(M-Nn_p)!}. \tag{3.39}$$

Finally, multiply equations (3.38) and (3.39) and divide by $n_p!$, since the polymers are indistinguishable from one another, to get the total number of arrangements.

$$W(n_p, n_s) = \left(\frac{z-1}{M}\right)^{n_p(N-1)} \frac{M!}{(M-Nn_p)!n_p!} = \left(\frac{z-1}{M}\right)^{n_p(N-1)} \frac{M!}{n_s!n_p!} \tag{3.40}$$

The $\frac{M!}{n_s!n_p!}$ is the same as equation (3.13). Under the assumptions laid out above the addition of the polymers to the solution only add on the piece related to the nearest neighbors. With the number of possible states defined the approach is the same. A sample of a final part of a lattice can be seen in Figure 3.4.

3.2.2 The Mixing Entropy with Polymers

The mixing entropy is

$$\frac{\Delta S_{mix}}{k} = \ln\left(\frac{W(n_p, n_s)}{W(0, n_s)W(n_p, 0)}\right) \tag{3.41}$$

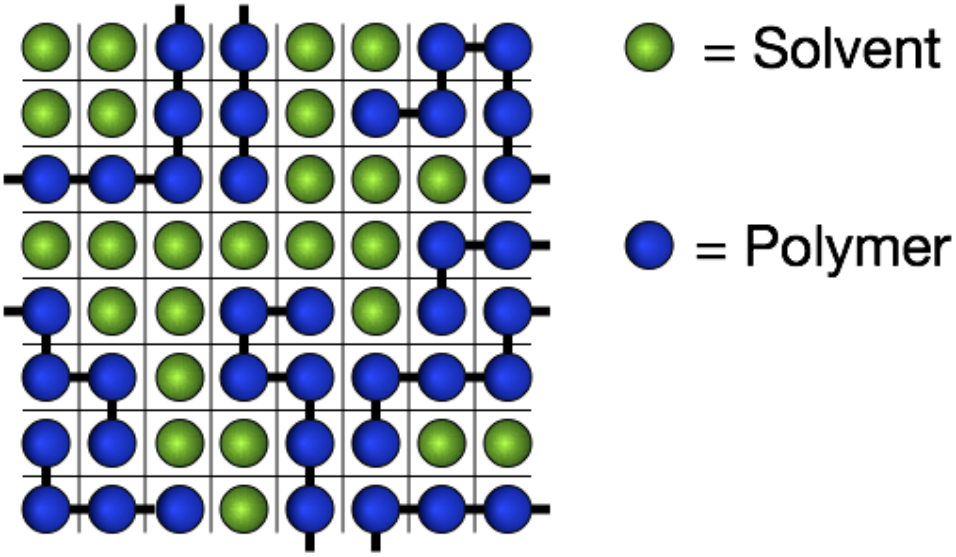

Figure 3.4: The end result of the process of filling a lattice with polymers and solvent molecules.

and the derivation continues the same as in Section 3.1.1.1 with laws of logarithms and Sterling's approximation. This leads to

$$\frac{\Delta S_{mix}}{-Mk} = \phi_s \ln \phi_s + \frac{\phi_n}{N} \ln \phi_n. \tag{3.42}$$

Where ϕ_s denotes the solvent volume fraction and ϕ_n denotes the polymer network volume fraction. The fluid is a binary fluid so $1 = \phi_s + \phi_n$ which gives the first part of the Flory-Huggins free energy density,

$$\frac{\Delta S_{mix}}{-Mk} = (1 - \phi_n) \ln (1 - \phi_n) + \frac{\phi_n}{N} \ln \phi_n. \tag{3.43}$$

The internal energy is done in the exact same way as Section 3.1.1.1 as well. Starting with the interaction energy being

$$E = m_{ss}w_{ss} + m_{nn}w_{nn} + m_{sn}w_{sn} \tag{3.44}$$

Replacing the subscript A and B in equations (3.15)-(3.18) with s for solvent and n for the polymer network respectively we can follow the exact equations and process as before. This leads to a free energy of [47],

$$F(\phi_n) = \frac{\Delta F}{MkT} = \frac{\phi_n}{N}\ln\phi_n + (1-\phi_n)\ln(1-\phi_n) + \chi_{ch}\phi_n(1-\phi_n). \tag{3.45}$$

Finally, we follow from equation (3.28) through equation (3.31) and arrive at a Cahn-Hilliard equation

$$\frac{\partial\phi_n}{\partial t} = \nabla\cdot\left[\lambda_{ch}\nabla\frac{\delta f}{\delta\phi_n}\right]. \tag{3.46}$$

3.3 System of Equations

There are two changes that were made to equations (3.45) and (3.46). First, the Cahn-Hilliard equation in equation (3.46) can be changed slightly as mentioned earlier to give the modified Cahn-Hilliard equation with an external velocity term

$$\frac{\partial\phi_n}{\partial t} + \nabla\cdot(\phi_n\mathbf{v}) = \nabla\cdot\left[\lambda\phi_n\nabla\frac{\delta f}{\delta\phi_n}\right]$$

The modified Cahn-Hilliard equation is different from the Cahn-Hilliard equation in that it has a polymer volume fraction dependent mobility as was mentioned before [33, 45, 53, 54]. The spatial domain is $I = [0, 1]$ with boundary ∂I and the boundary

conditions unless otherwise noted are

$$\mathbf{v}|_{\partial I} = \mathbf{v}_0, \qquad \left[\phi_n \mathbf{n} \cdot \nabla \frac{\delta f}{\delta \phi_n}\right]_{\partial I} = 0, \qquad [\mathbf{n} \cdot \nabla \phi_n]_{\partial I} = 0 \tag{3.47}$$

where, again, $\mathbf{n}$ is the unit normal vector to the boundary of the domain. These boundary conditions are the no slip boundary condition on the average velocity, the no-penetration boundary condition for the excessive polymer network velocity, and the no flux boundary condition on the polymer network volume fraction [25]. The boundary condition for the velocity from equation (3.47) where $\mathbf{v}|_{y=0} = [0, 0, 0]^T$ and $\mathbf{v}|_{y=1} = [10^{-3}, 0, 0]^T$ combined with a divergence free velocity, $\nabla \cdot \mathbf{v} = 0$, leads to zero velocity in the y direction for ϕ_n. This is seen in Figure 3.1 with the velocity field only being in the x direction and fading to zero as y approaches zero. It also shows that there is no change in the biofilm in the x or z direction as the only direction the gradient changes is in the y direction.

Second, the free energy due to thermodynamics is described by equation (3.45). For simplicity it can be replaced by a fourth degree polynomial such as [34]

$$g(\phi_n) = a(\phi_n - b)^2(\phi_n - c)^2. \tag{3.48}$$

For the model used in the following sections $a = \chi$, $b = 0$, and $c = \phi_{max}$ were used in equation (3.48). Equation (3.48) simplifies the numerics in the model compared to equation (3.21). Numerically any value for $\phi_n \in [0, 1]$ can be used in equation (3.49) while care needs to be taken with equation (3.3) as it has $\ln \phi_n$ and $\ln (1 - \phi_n)$ that can be problematic numerically near the end points of the interval at $\phi_n = 0$ or

$\phi_n = 1$. The energy functional used here is defined by [34, 43, 55]

$$f(\phi_n) = kT\left[\frac{\gamma_1}{2}||\nabla\phi_n||^2 + \gamma_2\left(\chi\phi_n^2\left(\phi_{max} - \phi_n\right)^2\right)\right]. \tag{3.49}$$

The ϕ_{max} is a parameter originally meant to help test the numerical results but was kept with the intent to use it to change ideal volume fractions for the case where there were two polymers; similar to what was done in chapter 2. The graphs of equations (3.21) and (3.49) are similar as can be seen in Figure 3.5.

The variation of f needed for equation (3.5) is

$$\frac{\delta f}{\delta\phi_n} = -kT\left[\gamma_1\Delta\phi_n - \gamma_2\chi\left(2\phi_{max}^2\phi_n - 6\phi_{max}\phi_n^2 + 4\phi_n^3\right)\right] \tag{3.50}$$

More on this will be discussed later. Section (3.6) will show that results from both cases agree.

3.3.1 Nondimensionalization.

The system of equations will be nondimensionalized using a characteristic time-scale, t_0, and length-scale, h. The values are specified in a table below in the results section. The nondimensionalized variables are as follows:

$$\widetilde{t} = \frac{t}{t_0}, \quad \widetilde{\mathbf{x}} = \frac{\mathbf{x}}{h}, \quad \widetilde{\mathbf{v}} = \frac{\mathbf{v}t_0}{h}, \quad \widetilde{p} = \frac{pt_0^2}{\rho_0 h^2}, \quad \widetilde{\tau}_n = \frac{\tau_n t_0^2}{\rho_0 h^2}, \quad \widetilde{c} = \frac{c}{c_0} \tag{3.51}$$

with c_0 being a characteristic substrate concentration. Using these variables the following nondimensional parameters are found [25]

$$\Lambda = \frac{\lambda p_0}{t_0}, \quad \Gamma_1 = \frac{\gamma_1 kTt_0^2}{\rho_0 h^4}, \quad \Gamma_2 = \frac{\gamma_2 kTt_0^2}{\rho_0 h^2}, \quad Re_s = \frac{\rho_0 h^2}{\eta_s t_0}, \quad Re_n = \frac{\rho_0 h^2}{\eta_n t_0},$$
$$Re_p = \frac{\rho_0 h^2}{\eta_[t_0}, \widetilde{D}_s = \frac{D_s t_0}{h^2}, \quad \Lambda_1 = \frac{\lambda_1}{t_0}, \quad \widetilde{\rho} = \phi_s \frac{\rho_s}{\rho_0} + \phi_n \frac{\rho_n}{\rho_0}, \quad \widetilde{A} = At_0, \quad \widetilde{\mu} = \mu t_0, \tag{3.52}$$

where ρ_0 is the averaged density; $Re_{s,n,p}$ are the Reynolds numbers for the solvent, the bacteria in the effective EPS polymer network, and the polymer network. The Λ, $\Gamma_{1,2}$, $\widetilde{D}_s$, and $\widetilde{\mu}$ are the dimensionless versions of the same named dimensional parameters. The Deborah number, Λ_1, is a number that is used to characterize the fluidity of materials [56]. In this case it is used in the dimensionless version of the differential equation to solve for τ_n from equation (3.10).

Similar to the previous chapter the $\widetilde{}$ will be dropped from the dimensionless variables and parameters. The average velocity from equation (3.1) is used throughout in these equations as well as the modified Cahn-Hilliard equation(3.5) for the polymer transport. The now dimensionless system of equations are as follows [25]

$$\begin{aligned}
&\nabla \cdot \mathbf{v} = 0, \\
&\rho \frac{d\mathbf{v}}{dt} = \nabla \cdot \left(\phi_n \left(a\tau_n + \tau_{ns}\right) \phi_s \tau_s\right) - \left[\nabla p + \Gamma_1 \nabla \cdot \left(\nabla \phi_n \nabla \phi_n\right)\right], \\
&\frac{\partial}{\partial t}\left(\phi_s c\right) + \nabla \cdot \left(c\mathbf{v}\phi_s - D_s \phi_s \nabla c\right) = -g_c, \\
&\frac{\partial \phi_n}{\partial t} + \nabla \cdot \left(\phi_n \mathbf{v}\right) = \nabla \cdot \left[\Lambda \phi_n \nabla \frac{\delta f}{\delta \phi_n}\right], \\
&\tau_{ns} = \frac{2}{Re_n}\mathbf{D}, \quad \tau_s = \frac{2}{Re_s}\mathbf{D}, \quad g_c = A\phi_n c,
\end{aligned} \tag{3.53}$$

with the dimensionless free energy

$$f = \frac{\Gamma_1}{2}||\nabla\phi_n||^2 + \Gamma_2\left[\chi\phi_n^2\left(\phi_{max.} - \phi_n\right)^2\right] \tag{3.54}$$

3.4 Numerical Methods

A finite difference scheme is used to solve the system of equations with a uniform spatial and time descretization. The space and time steps size is denoted by Δy and Δt respectively. Given information about the volume fraction ϕ_n at the previous time step $n-1$ and the current time step n the volume fraction at the next time step ϕ_n^{n+1} can be found with the Cahn-Hilliard equation (3.5) as follows.

$$\begin{aligned}\frac{\phi_n^{n+1} - \phi_n^n}{\Delta t} + \theta\Lambda\nabla_y \cdot \left[\bar{\phi_n}^{n+\theta}\nabla_y\left(\Gamma_1\nabla_y^2\phi_n^{n+1} - 2\Gamma_2\chi\phi_{max}^2\phi_n^{n+1}\right)\right] \\ = -(1-\theta)\Lambda\nabla_y \cdot \left[\phi_n^n\nabla_y\left(\Gamma_1\nabla_y^2\phi_n^n - 2\Gamma_2\chi\phi_{max}^2\phi_n^n\right)\right] \\ +\Lambda\nabla_y \cdot \left[\bar{\phi_n}^{n+\theta}\Gamma_2\nabla_y h\left(\bar{\phi}_n^{n+\theta}\right)\right]\end{aligned} \tag{3.55}$$

The function $h\left(\phi_n\right) = 4\phi_n^3 - 6\phi_{max}\phi_n^2$ is the non-linear term to come out of the variational derivative of f in the Cahn-Hilliard equation. An extrapolated value for ϕ_n is used in the non-linear terms as well. It is defined as $\bar{\phi}_n^{n+\theta} = (1+\theta)\,\phi_n^n - \theta\phi_n^{n-1}$. The one dimension model does not need a vector differential operator but ∇_y is used in place of $\frac{\partial}{\partial y}$. In the two dimension model the vector differential operator will be used. The time discretization is done with the Crank-Nicholson method by letting $\theta = 0.5$, making the linear part of the equation half implicit and half explicit in time, in the equation (3.55) which gives second order accuracy [37]. Since there is no polymer growth in the model the spatial discretization is done with central differencing to be volume preserving and second order accurate.

The interval I was divided into J sub-intervals with $J+1$ nodes which results in the boundary conditions in equation (3.47) being numerically represented as [25]

$$\phi^n_{n,1} = \phi^n_{n,-1}, \quad \phi^n_{n,2} = \phi^n_{n,-2}, \quad \phi^n_{n,J-1} = \phi^n_{n,J+1}, \quad \phi^n_{n,J-2} = \phi^n_{n,J+2}, \tag{3.56}$$

$$\mathbf{v}^n_0 = \mathbf{0}, \qquad \mathbf{v}^n_J = [10^{-3},\ 0,\ 0] \tag{3.57}$$

3.5 Using $\phi_n^2 (\phi_{max} - \phi_n)^2$ is a Valid Change to the Energy.

Before getting to the numerical results the change that was made to the Flory-Huggins energy when going from equation (3.3) to (3.49) needs to be examined. It was claimed earlier that this was a valid substitution to make. The following results will show that the change to the energy does not change the model enough to raise any concern. The results from using equation (3.49) as the energy will be compared with results from using equation (3.3). Unless otherwise stated $\phi_{max} = 1$ in the following simulations.

In Figure 3.5 the Flory-Huggins energy, equation (3.3), and the modified energy, (3.49), profiles are shown. In this plot the Flory-Huggins energy is plotted using a temperature less than the critical temperature which is defined as $T_c = \frac{\chi_{AB}}{2R}$ where χ_{AB} is the coefficient from equation (3.21) [34].

Given the same starting point similar results would be expected when changing the energy from equation (3.3) to (3.49). The results of a simple simulation can be seen in Figure 3.6. In the simulation the same parameters and initial condition are used but a different $f(\phi_n)$ is used to arrive at two different set of results. While Figure 3.5 doesn't show a large difference between the two profiles there is a large enough of a difference that they do not match exactly. The difference is not in long term behavior but in the speed at which things happen. When using the Flory-Huggins

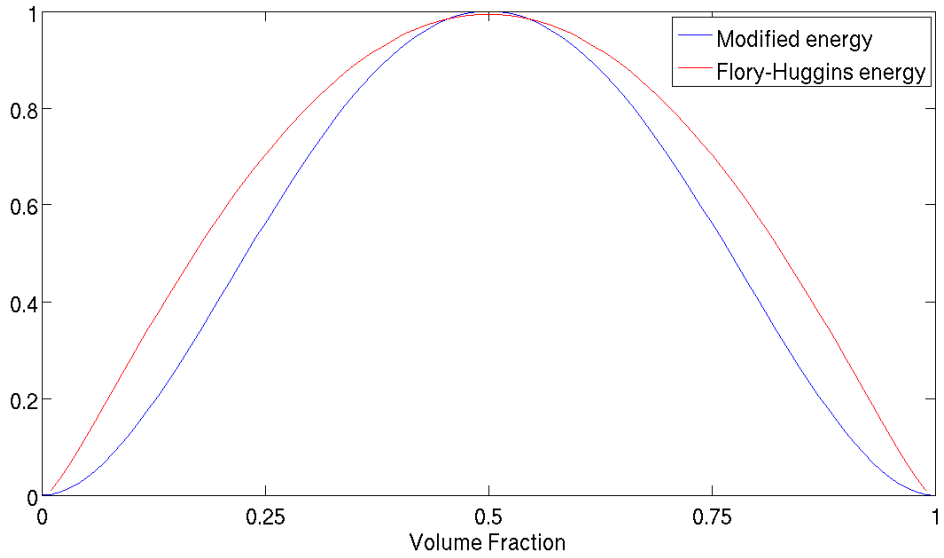

Figure 3.5: (a)A comparison on the two different types of energies. The Flory-Huggins energy from equation (3.3) and the simplified form from equation (3.49) are both shown.

energy in equation (3.3) a much larger time needs to be used to get agreement with the modified energy results from using equation (3.49). Another approach would be to increase the speed at which things happen when using the Flory-Huggins energy. One way to do this is to increase the parameter γ_1 in the Flory-Huggins Energy. Figure 3.6(c) shows what a change to this parameter will do. As can be seen the profiles match much closer when a larger γ_1 is used when equation (3.3) is used for the energy.

3.5.1 Distortional Versus Separation Energies.

As was discussed earlier γ_1 is the parameter that measures the strength of the distortional energy [25]. If γ_1 is small then larger gradients of ϕ_n will be allowed and if γ_1 is large it is more likely that the biofilm will have a flatter profile. The bulk free energy in equation (3.3) is measured by γ_2 [25]. While γ_2 is large the biofilm will favor

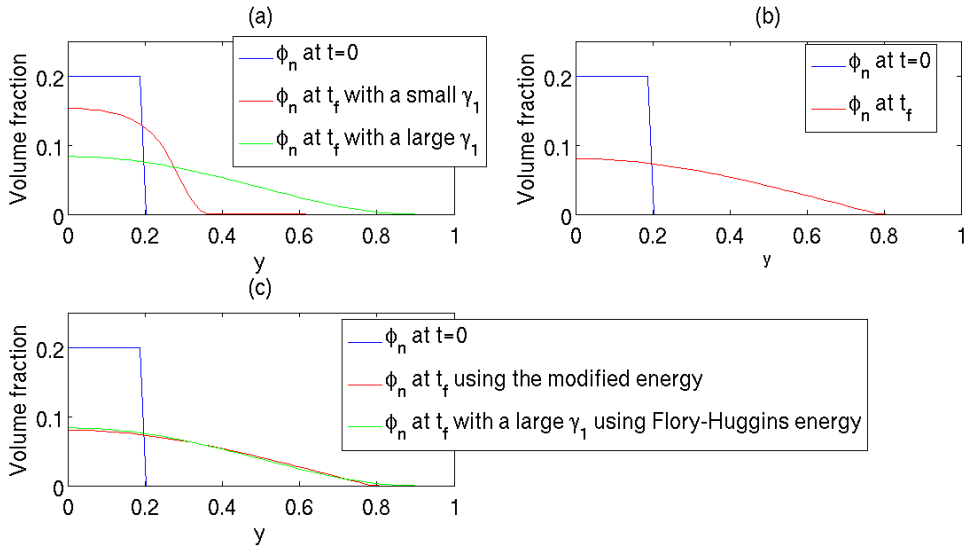

Figure 3.6: (a)The results from using the Flory-Huggins energy from equation (3.3). There are two different γ_1 values used. (b)The results from using the modified energy. (c)The Flory-Huggins energy with a larger γ_1 matches well with the modified energy.

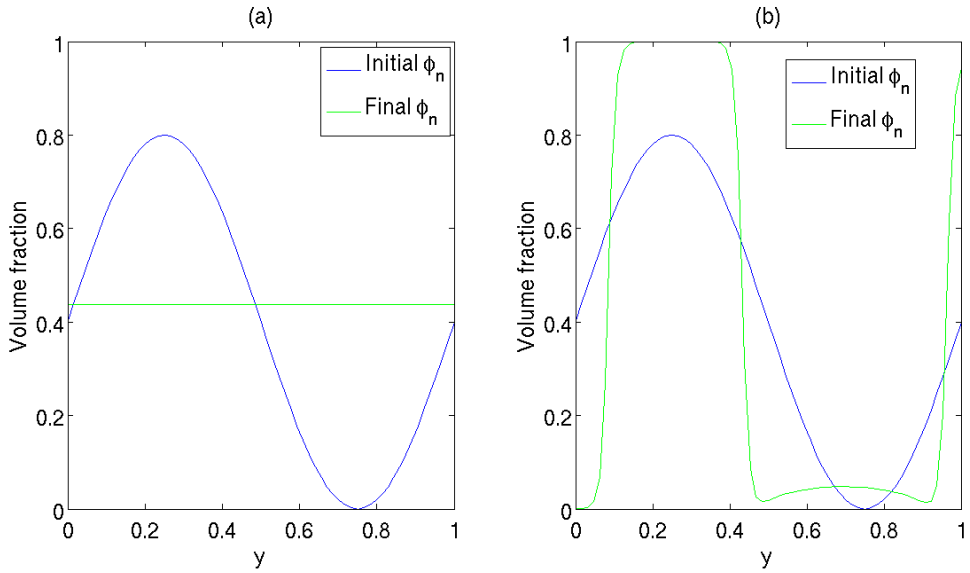

Figure 3.7: (a)The distortion energy is dominant and the biofilm reaches equilibrium when there is a constant volume fraction throughout the domain. (b) The separation energy is dominant and the biofilm nearly separates into pure states, one of pure polymer and one of pure solvent.

volume fractions for ϕ_n that minimize the separation energy which are $\phi_n = 0$ and $\phi_n = 1$, since $\phi_{max} = 1$. If the total energy, $\int f(\phi_n)\, dx$, with f defined by equation (3.49) is minimized the results could be flat like in Figure 3.7(a) or the results could be completely separate states like in Figure 3.7(b) or anywhere in between. As will be seen in the rest of this chapter and the next the results depend on a wide variety of factors; including but not limited to: initial profile, initial volume fraction, and the location of the polymer.

A short example will be given to help understand what is happening in the results. This example will use unrealistically large ϕ_n values to better show the results of each case. The results of this example are meant to show behavior of each part of the energy. There is no attempt to have the distortion and separation energy balance each other. For this example equation (3.49) will be used for the energy functional with $\phi_{max} = 1$ for simplicity and the initial profile for the biofilm is given by $\phi_n(y, 0) = 0.4 \sin(2\pi y) + 0.4$. Starting with the initial condition the distortion energy, $||\nabla \phi_n||^2$, will move the polymer towards as flat a profile as possible. In this case it will be minimized when the $\phi_n = 0.4$ because this is the average value of the initial condition and there is conservation of mass up to numerical errors in this model. The final profile is not exactly 0.4 in Figure 3.7(a) but it does move closer to 0.4 if Δy is made smaller. This points to the error being numerical in nature and not an unexpected growth or instability in the numerics. The separation energy, $\chi \phi_n^2 (1 - \phi_n)^2$, will be minimized when ϕ_n fits a step function with maximum at one and minimum at zero. Figure 3.7 shows the end results when each energy is dominant. The separation energy in Figure 3.7(b) separates the biofilm into almost pure states of polymer and solvent. The results in Figure 3.7(b) show what would minimize the energy for the specific initial profile but any step function with max at one and min at zero that has the same area under the curve as the initial condition would minimize

the energy as well. These two cases are the extreme cases. The following numerical results will have influence from both energies instead of a dominant energy that drives the biofilm to one extreme or the other.

3.6 Results

The results in this section come from using the modified energy in equation (3.49).

Table 3.1: List of parameters values used for the simulations in chapter 3.

Symbol	Parameter	Value	Units
T	Temperature	303	K
γ_1	Distortional energy	1×10^7	$\mathrm{kgm^{-1}s^{-2}}$
γ_2	Separation energy	1×10^{17}	$\mathrm{kgm^{-1}s^{-2}}$
χ	Flory-Huggins parameter	0.55	
λ_{CH}	Mobility parameter	1×10^{-10}	$\mathrm{kg^{-1}}m^3s$
N	Generalized polymerization parameter	1×10^3	
μ	Max production rate	1.4×10^{-4}	$\mathrm{kgm^{-3}}s^{-1}$
A	Max consumption rate	1	$\mathrm{kgm^{-3}}s^{-1}$
D	Diffusion coefficient.	2.3×10^{-9}	$\mathrm{m^2s^{-1}}$
η_n	Dynamic viscosity of the network	4.3×10^2	$\mathrm{kgm^{-1}}s^{-1}$
η_s	Dynamic viscosity of the solvent	1.002×10^{-3}	$\mathrm{kgm^{-1}}s^{-1}$
ρ_n	Network density	1×10^3	$\mathrm{kgm^{-1}}$
ρ_s	Solvent density	1×10^3	$\mathrm{kgm^{-1}}$
t_0	Characteristic time scale.	1×10^3	s
h_0	Characteristic length scale	1×10^{-3}	m
c_0	Characteristic substrate concentration.	1×10^{-3}	$\mathrm{kgm^{-3}}$
M	number of spatial intervals	64	

3.6.1 Results with Varying γ_1 and γ_2 Values

As was seen in the example above if only one energy is used the general result is known before the simulation is run. The results are different and have different possible explanations if both energies are used. The end results depends on a variety of

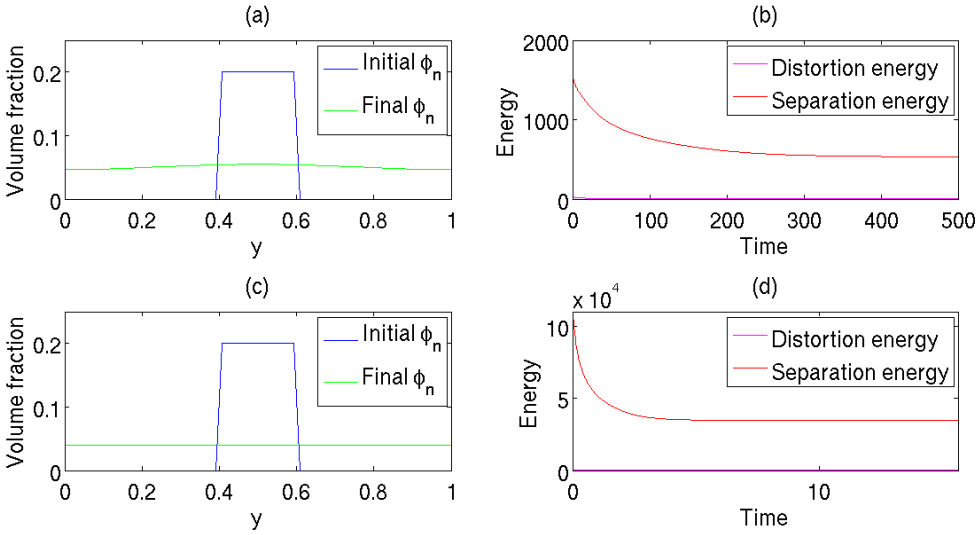

Figure 3.8: (a) The initial profile of a square in the center of the domain is influenced by both the distortion and separation energy to reach the final flat profile. (b) The distortion energy and separation energy for the simulation from part (a). (c) A larger separation energy from a factor of 10 larger γ_2 causes the evolution of the profile to happen faster. (d) The distortion and separation energy for the simulation in part (c). The time to reach equilibrium is much shorter compared to parts (a) and (b).

factors. These factors include but are not limited to the strength of each components relative to the other as determined by the γ_1 and γ_2 coefficients, the total amount of polymer within the domain, the location of the polymer and the volume fraction of the polymer.

The first set of results are from starting with a single piece of polymer away from the boundary. The initial condition can be seen in Figure 3.8(a). The initial profile is a square mass centered in the domain and a volume fraction of 0.2. It can be seen from the final profile that this initial condition flattens out over time. While it may not look like it in Figure 3.8(a) but both energies are used in this simulation. The initial impression might be that with this initial condition and set of parameters the distortion energy was dominant which leads to a flat final profile. The separation

energy is actually the dominant energy in the simulation. This can be seen in Figure 3.8(b). The distortion energy is orders of magnitude smaller than the separation energy. In this case the separation energy is giving preference to $\phi_n = 0$ over $\phi_n = 1$. One explanation is that the profile just described may be a lower total energy but the system may need some outside energy first to reach that state. This would be similar to an activation energy in chemical reactions. Another possible explanation for this are because the overall energy would be higher having places where $\phi_n = 1$ and other places where $\phi_n = 0$ similar to Figure 3.7(b). If all the polymer were to stay in a single location and have a volume fraction of one the width of polymer would be 0.04 units. This would lead to a large distortion energy causing the overall energy to be larger even though the separation energy would be zero. A small increase of γ_2 causes the time evolution of the polymer to happen faster. This can be seen in Figure 3.8(c). The final time in Figure 3.8(c) is smaller than in (a) yet ϕ_n is flatter in (c) than in (a). This is due to what was mentioned above. Similar to Figure 3.8(b) the separation energy in the simulation for Figures 3.8(c) and (d) is the only energy that is impacting the evolution of the biofilm. This means that the polymer will reach equilibrium faster when compared to part (a).

As was mentioned earlier the location of the polymer can play a role in determining the evolution of the biofilm. In Figures 3.9(a) and (b) both have the same amount of polymer but the starting location is different in each case. As can be seen in Figure 3.9(a) the final volume fraction reaches large unrealistic values where as (b) has a final profile similar final profile to Figure (3.8). Since the energy equation does not have a term that is affected by location of the polymer there must be a reason in the two terms present for this difference. The separation energy would be one place to look first since the final profiles are different in the aspects that would be affected by the separation energy. Part (a) has a large volume fraction at the

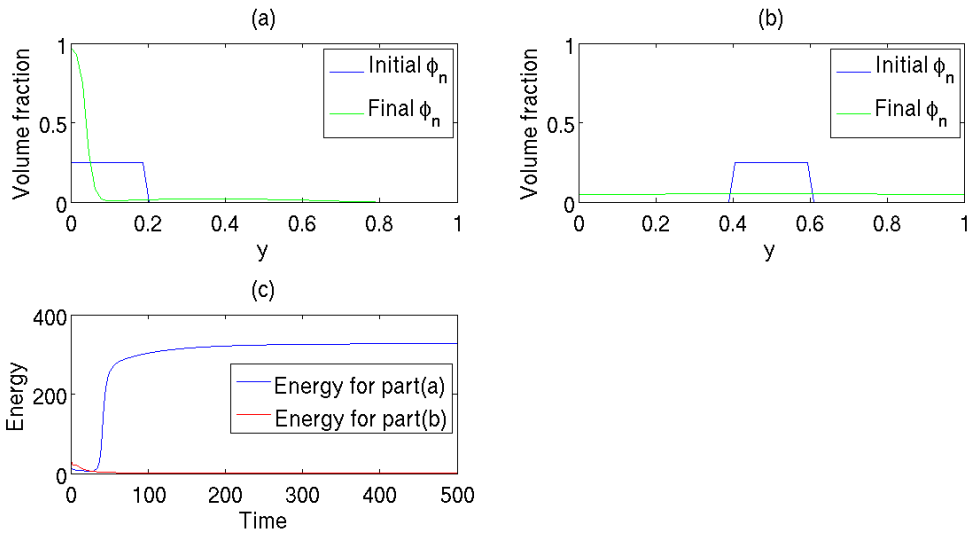

Figure 3.9: (a)The location of the initial mass of polymer plays a roll in determining the final profile. The initial location along the left boundary allows the polymer to increase in volume fraction there. (b) The central location of the polymer at the start causes the minimum energy to occur at a flat profile. (c) The distortion energy for part (a) and (b).

final time in one small location and part (b) has a small volume fraction throughout the entire domain at the final time. The separation energy is determined by how far away ϕ_n is from the ideal values of $\phi_n = 0$ and $\phi_n = 1$. Both of the initial profiles in Figures 3.9(a) and (b) have an initial max volume fraction of 0.25 and a width of 0.2. The only difference is the location of this initial profile. Due to these similarities the separation energy would be initially identical for both of these. This leaves the distortion energy as the cause of the difference. The distortion energy penalizes large gradients. The gradient of both plots is the same except on the left side of the initial profile. Figure 3.9(b) has a non-zero gradient on both the left and the right while part (a) only has a non-zero gradient on the right. Initially part (a) has a distortion energy that is half of part (b). During the evolution of the biofilm the distortion energies go in different directions but the initial difference is enough that part (a) allows the separation energy to cause the polymer to cluster together instead of spread out.

3.7 The Addition of a Movement Energy

The overarching idea that motivated most of this project was that the biofilm should somehow separate into distinct regions. This was the motivating idea behind the changes that were discussed to the velocity driven model in chapter 2 in section 2.5. In this chapter the movement energy is the additional energy that was implemented to achieve this. In some cases it acts as an attachment energy causing the polymer to move to the bottom of the domain and have it attach to the boundary. In other cases it gives a slight preference to different areas in the domain for the polymer to be located in. This term was added as a general function to the energy functional in equation (3.49) to allow easy modification of the type of function used for the

movement energy. With this addition the new energy used in the model is

$$f(\phi_n) = kT\left[\frac{\gamma_1}{2}||\nabla\phi_n||^2 + \gamma_2\left(\chi\phi_n^2\left(\phi_{max}-\phi_n\right)^2\right) + \gamma_3\phi_n g(y)\right]. \tag{3.58}$$

The movement energy function, $g(y)$ only depends on the spatial variable for the domain. It is the part of the energy that gives a location to where the polymer would be at a lower energy. The ϕ_n makes the movement energy dependent on whether or not there is polymer at the location. Without the ϕ_n the total energy would always have a contribution from $g(y)$. For example if there is no polymer within the domain the total energy should be zero but if there is no ϕ_n in the movement energy then the total energy would not be zero.

Numerically the movement energy was implemented using an upwind scheme. Depending on what $g(y)$ was there could be polymer moving to the left or the right. Starting with equation (3.5) and using only the movement energy in the chemical potential as well as using the y component of the velocity being zero results in the equation

$$\frac{\partial\phi_n}{\partial t} = \nabla\cdot\left(\lambda\phi_n\nabla g\right). \tag{3.59}$$

This can be solved using the upwind method with variable velocity where $\frac{\partial g}{\partial y}$ is the term used for the upwinding.

3.8 Results with Movement Energy

The movement energy should have a small influence to the system. It should not be the dominant energy in the system. Unless otherwise noted the movement energy will provide a small contribution to the overall energy relative to the total energy. Due to the movement energy function being arbitrary there really is not a limit as to

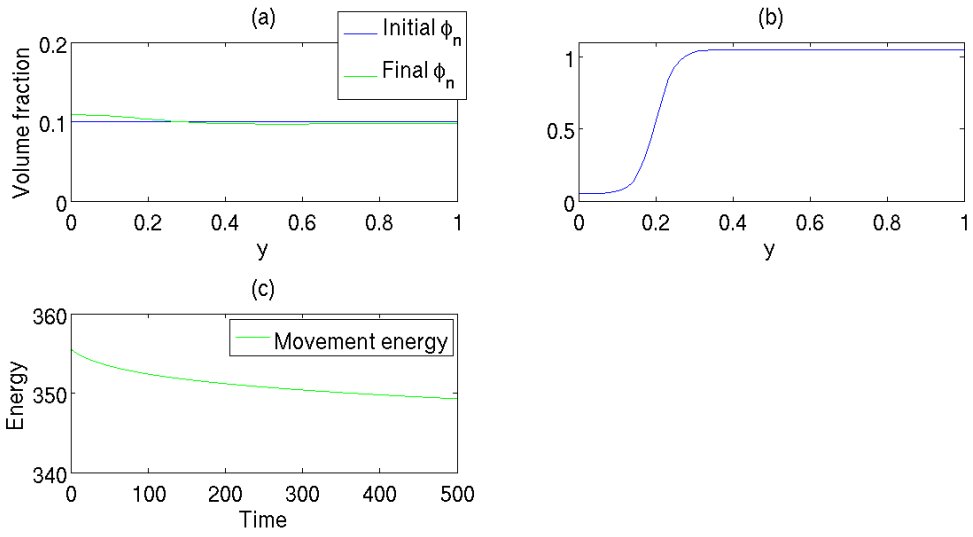

Figure 3.10: (a)The evolution of the polymer over time due to the new movement energy that was added. (b) The function $g(y)$ which adds the movement to the system. (c) The movement energy decreases with time due to the polymer moving to the left of the domain.

what can be used. Reasonable restrictions should be placed on what is allowed due to properties of the biofilm and that this is a model of a real system. A limited few examples chosen because they have a physical basis will be discussed below. The first simulation starts with a flat initial profile for ϕ_n. As can be seen in the plot of the time evolution of ϕ_n in Figure 3.10(a) the final profile is shifted slightly to the left. This is due to the movement energy which is determined in this case by the $\tanh(y)$ function shown in Figure 3.10(b). The difference between the largest and smallest value in the plot of the final ϕ_n is approximately 0.01. As was mentioned about the movement energy was never meant to be a strong contributor to the final profile of ϕ_n it was meant to provide a slight preference to certain locations which was done in this case.

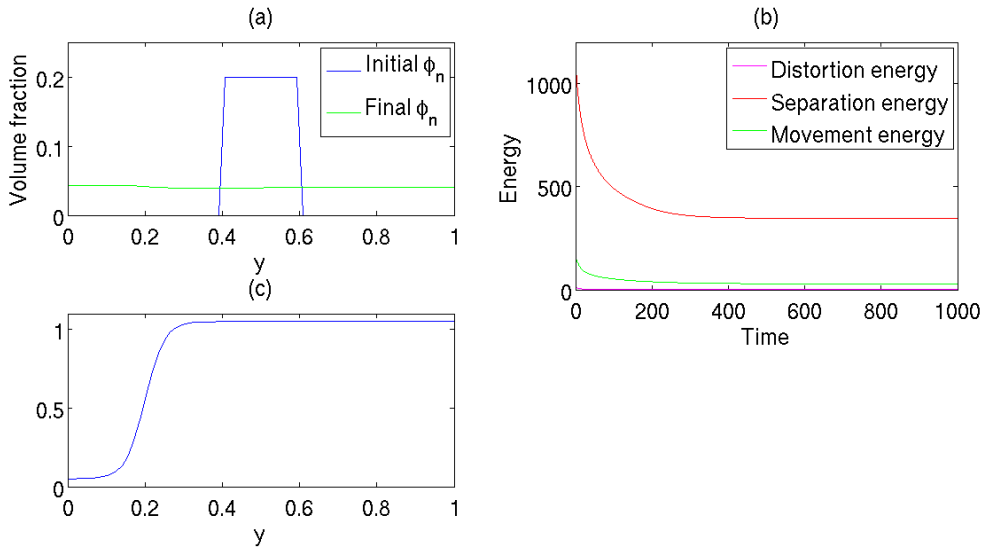

Figure 3.11: (a)The same initial profile as Figure 3.8 with the movement energy added. The movement energy gives a preference to the left boundary which accounts for the difference between Figure 3.8 and the current results. (b) The three energies that determine how the biofilm will evolve over time. (c) The movement energy that was used for this set of results is a hyperbolic tangent function.

Next, the simulation from Figure 3.8 will be revisited with the movement energy added in. In Figure 3.8 the initial mass of polymer in the center of the domain spread throughout the domain and lowered the volume fraction until it reaches a flat final profile. The movement energy function is the same $\tanh(y)$ function shown in Figure 3.10(b). In Figure 3.11(a) the movement energy causes a slight increase along the left boundary in the final profile when compared to Figure 3.8(a). The energies have reached equilibrium which is shown in Figure 3.11(b).

The final result to be looked at will be an initial condition of three peaks that merge into a single mass and then move according to the movement energy. There will be two separate cases investigated with this initial condition. The initial profile in Figure 3.12(a) merges into a single mass quickly due to the the distortion energy causing polymer to move into the regions between the peaks to increase the volume

fraction there which will lower the gradient. The polymer is also spread throughout the domain as has been seen in earlier examples. Even though the movement energy is part of the energy the entire time its influence it not noticeable until the distortion energy has been decreased through the smoothing that was just described. The movement energy's influence can be seen in Figure 3.12(a) in the plot of ϕ_n at the final time t_f. The curve is no longer close to symmetric like it is in the plot of ϕ_n when $t = 50$. On the left side a slight increase can be seen. The energies are different from previous examples as well. In Figure 3.11(b) all three energies are always decreasing and eventually all reach a equilibrium at around the same time. Looking at the graph of those three energies it looks likely that the system has reached equilibrium. The same can not be said for the energies in Figure 3.12(b). In this case the separation energy is closest to equilibrium but the plot shows it increasing. The distortion energy has both increased and decreased throughout the simulation. Finally, the movement energy is decreasing for all time. At the end the only energy that matters is the total energy. As was shown in section (3.1) with equation (3.32) the total energy must always be decreasing, which it is as can be seen in Figure 3.12(b) with the plot of the total energy. The three components of the energy functional only need to add up to a decreasing function not be decreasing individually.

The second case examined is to show that the movement energy works with other movement energy functions, $g(y)$. For the previous examples the $\tanh(y)$ function was used for the movement energy. In this case the function

$$g(y) = \begin{cases} 0.8 & : y \in [0, 0.4] \cup [0.6, 1] \\ \\ 0.1 & : y \in (0.4, 0.6) \end{cases} \tag{3.60}$$

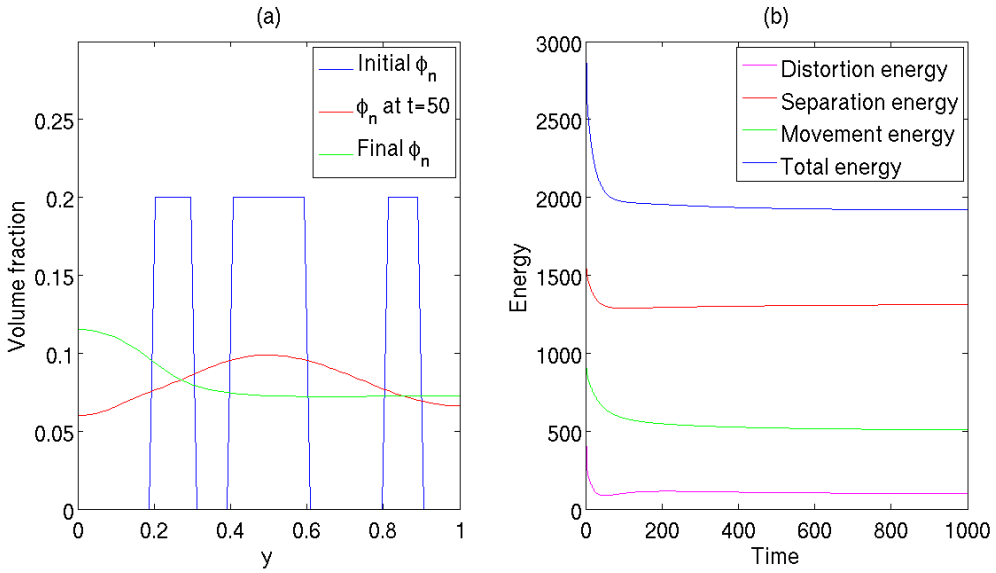

Figure 3.12: (a)The polymer merges together into a single mass and then moves to the left boundary due to the movement energy. (b) The three energies that determine how the biofilm will evolve over time. Most of the change happens before $t = 200$. This shows the system is essentially at equilibrium.

is used in the movement energy. For this movement energy it would be expected that the polymer would tend to group up in the middle of the domain and have less amounts in the outside region. As seen in Figure 3.13(a) this does happen. The same things that have been discussed already still apply to this simulation. Total energy will decrease even if the individual energies do not all decrease, the polymer will have a larger volume fraction where the movement energy function is smaller, and there will not be any large gradients nor will the profile of ϕ_n be flat over the entire domain.

3.9 Conclusion

As can be seen from what has been presented the results of the modified model agree with previous models. The movement energy does a good job of acting as an attachment energy or providing a way to move the polymer around the domain when

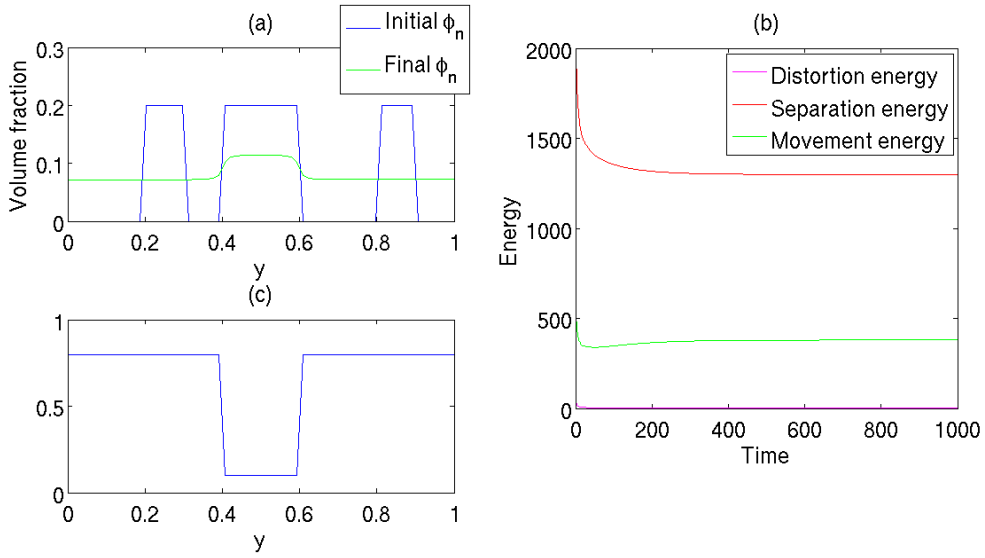

Figure 3.13: (a)The polymer merges together into a single mass and then moves to the center due to the movement energy. (b) The three energies that determine how the biofilm will evolve over time. This shows the system is at equilibrium. (c) The movement energy that was used for this set of results is a hyperbolic tangent function.

needed. While the 1D model is not ideal since some assumptions needed for a 1D model are not realistic it does give a starting point for what to investigate in higher dimensions. Based on what is shown in 1D the model will be expanded into 2D. A select few of the results from the 1D model will be compared to 2D results in the next chapter.

CHAPTER FOUR

THE 2D MODEL

This chapter takes the model that was developed in chapter 3 and expand it to two dimensions. There are some changes in the 2D model. These include some of the numerical methods that are used for convenience and some that are forced due to the nature of the equations. A few of the results from chapter 3 are simulated again in 2D and the results are compared. Some of these have expected behavior based on the 1D simulations but some exhibit different behavior simply due to the simulation being in 2D. A few changes are made to the model in 2D as well. The movement energy is changed due to a problem that arises in this chapter.

4.1 Changing from 1D to 2D.

The biggest difference is the most obvious one. The addition of a second dimension in the model allows for the biofilm to change in two directions now instead of just one. Now the biofilm may have variation in both the vertical direction, as in the previous chapter, and the horizontal direction. A cartoon picture of this is in Figure 4.1. As can be seen in the cartoon the flow of the bulk fluid will now affect the biofilm as the biofilm can now move and change in the same direction as the flow. There were a number of things that changed when going from 1D to 2D mathematically as well. Some of them were simple things to do such as changing from a scalar derivative, $\frac{\partial}{\partial y}$, to a vector derivative, ∇. This results in more difficult equations to solve or at least more time consuming to solve. Since the ∇_y operator was used in chapter 3 the only difference is now gradients and divergences have their

standard definition. The equations are already in chapter 3 so they will not fully appear here.

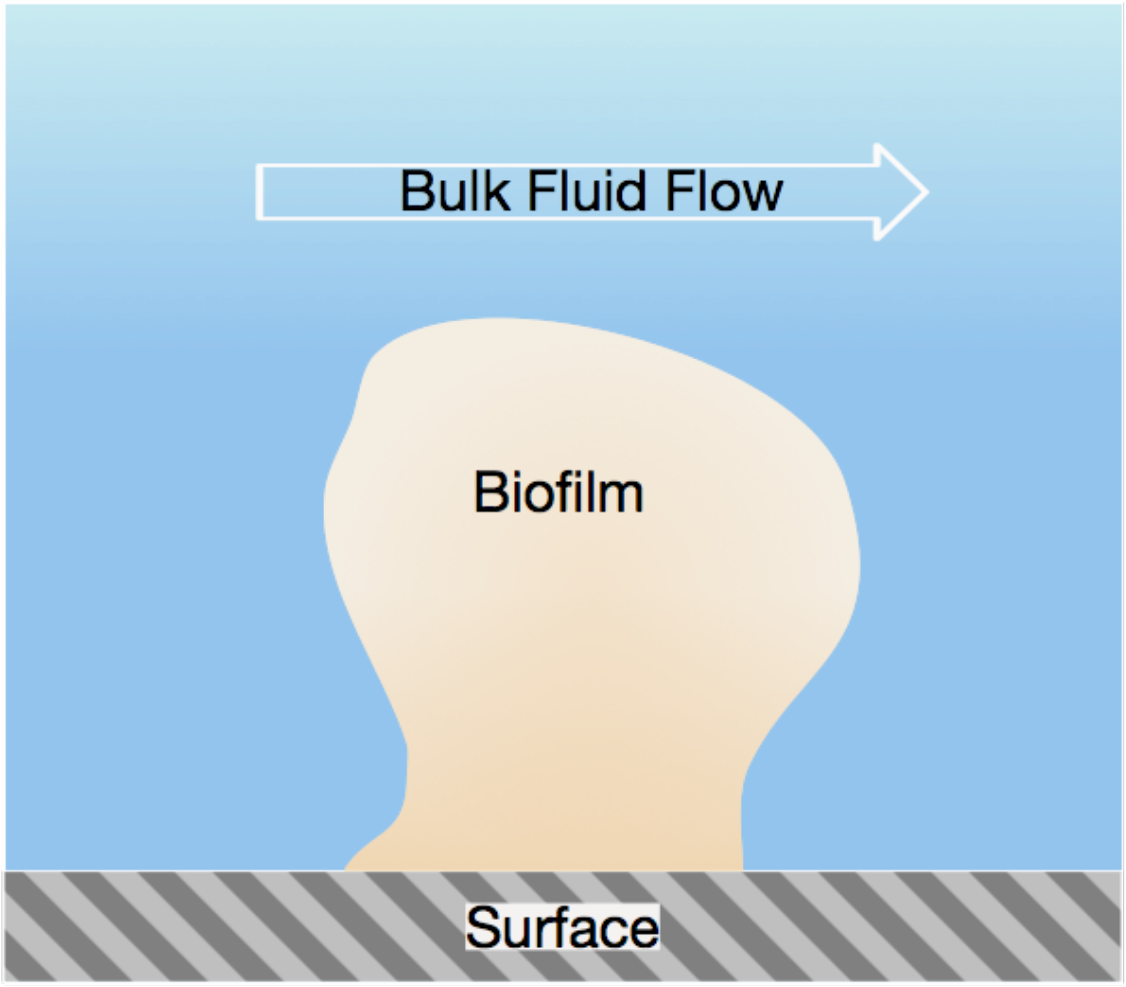

Figure 4.1: The biofilm is now allowed to change in both the horizontal and vertical directions.

Some of the other changes are more difficult to deal with. The upwind method becomes more difficult in 2D when compared to 1D. Instead of implementing the 2D upwind scheme central differences were used in place of it. This still maintains the second order accuracy from the previous methods [37]. The other major change was in solving parts of the system of equations. The momentum and continuity equations

become more difficult to solve numerically in 2D. This is described in more detail in the following section.

4.2 The 2D Numerical Methods.

A difference between the 1D and 2D numerics was how the momentum and continuity equations are solved. In 1D these equations are solved with numerical methods such as Runge-Kutta and an upwind scheme. In 2D these equations are more difficult to solve. Let $\mathbf{v}$ be the average velocity, p is the pressure, and ϕ_n and ϕ_s are the network and solvent volume fractions. The equations to be solved are [32]

$$\nabla \cdot \mathbf{v} = 0 \tag{4.1}$$

$$\rho \frac{d\mathbf{v}}{dt} = \nabla \cdot (\phi_n \tau_n + \phi_s \tau_s) - [\nabla p + \Gamma_1 \nabla \cdot (\nabla \phi_n \nabla \phi_n)] \,. \tag{4.2}$$

where $\rho = \rho_n \phi_n + \rho_s \phi_s$ is the volume fraction averaged density with ρ_n and ρ_s being the network density and solvent density respectively, τ_n and τ_s are the stress tensors for the network and solvent. As previously defined k is the Boltzmann constant, T is the temperature, γ_1 and γ_2 are defined as they were in chapter 3 in section 3.1.

The problem is that the pressure and velocity are coupled within the same equation. The projection method first proposed by Alexandre Chorin in 1967 works equally well for both 3D and 2D [57]. The benefit of this method is that it only requires solving two decoupled equations for pressure and velocity which makes it efficient for numerical simulations [58]. There are three types of projection methods discussed by Guermond et al. [58]: the pressure-correction schemes, velocity-correction schemes, and the consistent splitting schemes [58].

4.2.1 The Projection Method.

The projection method is a way to handle the difficulty that comes from solving a system of equations similar to equations (4.1) and (4.2). The projection method proposed by Chorin is based on Helmholtz's theorem. Helmholtz's theorem states "Let $\mathbf{F}$ be a vector field on a bounded domain $V \subseteq \mathbb{R}^3$, which is twice continuously differentiable, and let S be the surface that encloses the domain V. Then $\mathbf{F}$ can be decomposed into a curl-free component and a divergence-free component." The curl-free and divergence-free components can each be determined by a sum of a volume integral over V and a surface integral over S. This gives the basis for the projection method which will be described generally. Starting with the conclusion of Helmholtz's theorem in formula form

$$\mathbf{u} = \mathbf{u}_{\text{sol}} + \mathbf{u}_{\text{irrot}} = \nabla \times \mathbf{A} + \nabla\psi. \tag{4.3}$$

Taking the divergence of (4.3) results in

$$\nabla \cdot \mathbf{u} = \nabla^2\psi \tag{4.4}$$

which is a Poisson equation that can be solved if $\mathbf{u}$ is known. Now, since $\mathbf{u}^{n+1}$ is known, where the $n+1$ superscript denotes the next time step, and ψ was just found equation (4.3) can be used again to find the divergence free velocity. This gives the following equation

$$\mathbf{u}_{\text{sol}}^{n+1} = \mathbf{u}^{n+1} + \nabla\psi \tag{4.5}$$

This process is the basic idea behind the projection method.

1 While the basic idea is presented above there are a few more details to fill in for the projection method that was used here. The pressure corrected projection

method will be described here because it is what was used. The pressure corrected projection method treats the pressure explicitly or ignores it completely to solve for velocity that is not divergence free. Then the pressure is used to find the divergence free velocity. The main difference between this method and the velocity corrected projection method is the order in which things are done. The velocity corrected method is similar but the order is reversed, pressure is solved for first and then the pressure is corrected by projecting the velocity.

The projection method originally proposed by Chorin in [57] starts with the incompressible Navier-Stokes equation, which, using slightly different notation is

$$\rho\left(\frac{\partial \mathbf{u}}{\partial t} + \mathbf{u}\cdot\nabla\mathbf{u}\right) = -\nabla p + \frac{1}{Re_a}\nabla^2\mathbf{u} + \mathbf{F} \tag{4.6}$$

where $Re_a = \phi_n Re_n + \phi_s Re_s$ is the volume fraction averaged Reynolds number. The projection method involves two sub-steps for each full time step. The first step is to solve for an intermediate velocity, u^*, by ignoring the pressure gradient and solving the following equation.

$$\frac{\mathbf{u}^* - \mathbf{u}^n}{\Delta t} = -\mathbf{u}^n\cdot\nabla\mathbf{u}^n + \frac{1}{\rho Re_a}\nabla^2\mathbf{u} \tag{4.7}$$

where $\mathbf{u}^*$ is the velocity field at the $n+1$ timestep that is no longer divergence free. To correct the velocity and end with a divergence free velocity the following equation is solved [58].

$$\mathbf{u}^{n+1} = \mathbf{u}^* - \frac{\Delta t}{\rho}\nabla p^{n+1} \tag{4.8}$$

This requires knowledge of p^{n+1}. If order to find this updated pressure the divergence can be applied to equation (4.8). Since $\nabla\cdot\mathbf{u}^{n+1} = 0$, due to it being divergence free, the following Poisson equation must be solved with a boundary condition of

$\frac{\partial p^{n+1}}{\partial n}|_{y=0,H} = 0$ [32].

$$\nabla \cdot \mathbf{u}^* = \frac{\Delta t}{\rho} \nabla^2 p^{n+1} \tag{4.9}$$

The next step is to solve for p^{n+1}, the FISHPACK library was used here. Then substitute p^{n+1} into equation (4.8) and solve again to find the divergence free velocity.

The starting point given in equation (4.6) is different from what is given in equation (4.2). This difference can be fixed using the following equations

$$\mathbf{R} = -\nabla \cdot (\Gamma_1 \nabla \phi_n \nabla \phi_n) + \nabla \cdot \left(\phi_n \tau_n + \phi_s \tau_s - \frac{2}{Re_a} \mathbf{D} \right) \tag{4.10}$$

where $\mathbf{D}$ is defined as it was in section 3.1. This allows the momentum transport equation to be rewritten as

$$\rho \left(\frac{\partial \mathbf{v}}{\partial t} + \mathbf{v} \cdot \nabla \mathbf{v} \right) = -\nabla p + \frac{1}{Re_a} \nabla^2 \mathbf{v} + \mathbf{R}. \tag{4.11}$$

Additional detail about the specific application to this equation are found in the work of Zhang, Cogan, and Wang [32].

4.3 Results

The system of equations that are solved are the same as they are in chapter 3 with the only difference now being that the ∇ operator is the vector differential operator instead of a single derivative. The two main dimensionless equations are still the same as in chapter 3

$$\frac{\partial \phi_n}{\partial t} + \nabla \cdot (\phi_n \mathbf{v}) = \nabla \cdot \left[\Lambda \phi_n \nabla \frac{\delta f}{\delta \phi_n} \right], \tag{4.12}$$

$$f(\phi_n) = \frac{\Gamma_1}{2} ||\nabla \phi_n||^2 + \Gamma_2 \left[\chi \phi_n^2 \left(\phi_{max} - \phi_n \right)^2 \right] + \Gamma_3 g(x,y) \phi_n$$

where $\Gamma_3 = \frac{\gamma_3 kT t_0^2}{\rho_0 h^2}$.

Table 4.1: List of parameters values used for the simulations in chapter 4.

Symbol	Parameter	Value	Units
T	Temperature	303	K
γ_1	Distortional energy	1×10^7	$\mathrm{kgm^{-1}s^{-2}}$
γ_2	Separation energy	1×10^{17}	$\mathrm{kgm^{-1}s^{-2}}$
χ	Flory-Huggins parameter	0.58	
λ_{CH}	Mobility parameter	1×10^{-10}	$\mathrm{kg^{-1}}m^3s$
N	Generalized polymerization parameter	1×10^3	
μ	Max production rate	1.4×10^{-4}	$\mathrm{kgm^{-3}}s^{-1}$
A	Max consumption rate	0.1	$\mathrm{kgm^{-3}}s^{-1}$
D	Diffusion coefficient.	2.3×10^{-9}	$\mathrm{m^2s^{-1}}$
η_n	Dynamic viscosity of the network	4.3×10^2	$\mathrm{kgm^{-1}}s^{-1}$
η_s	Dynamic viscosity of the solvent	1.002×10^{-3}	$\mathrm{kgm^{-1}}s^{-1}$
ρ_n	Network density	1×10^3	$\mathrm{kgm^{-1}}$
ρ_s	Solvent density	1×10^3	$\mathrm{kgm^{-1}}$
t_0	Characteristic time scale.	1×10^3	s
h_0	Characteristic length scale	1×10^{-3}	m
c_0	Characteristic substrate concentration.	1×10^{-3}	$\mathrm{kgm^{-3}}$
M	number of spatial intervals	64	

4.3.1 No Movement Energy.

Before moving directly into looking at results with all three energy terms, distortion, separation, and movement, a few examples with no movement energy similar to what was done first in chapter 3 will be examined. The first simulation was meant to mirror the results in Figure 3.8. As can be seen in Figure 4.2(b) the profile does not quite achieve the same end profile as is in Figure 3.8(c) but this is more due to the final time than any differences between the results. Given a larger final time the profile in Figure 4.2(b) would be much closer to what is seen in Figure 3.8(c). Even with this small difference the polymer is spreading throughout the domain as

would be expected after already seeing the results from Figure 3.8(c) The energy results are decreasing as expected.

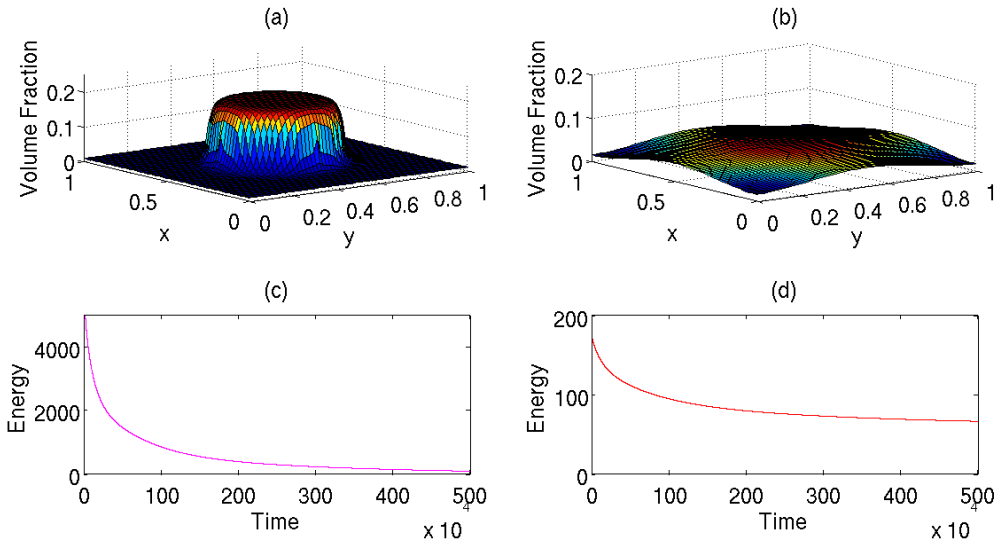

Figure 4.2: (a) The initial polymer is a cylinder at the center of the domain. (b) The final profile of the polymer has flattened out and is nearly constant. (c) The distortion energy is decreasing for all time due to the flattening of the polymer. (d) The separation energy is decreasing for all time since the polymer is getting closer to a volume fraction of zero.

The second set of results was meant to mimic the results found in Figure 3.9(a). The initial profile is a semi-circle centered along the x-axis with an initial volume fraction of 0.25 which is the same as the 1D case. The final results do have some similarities but what is seen in Figure 4.3(b) is quite different from the final results from Figure 3.9(a). Both results have final volume fractions that are near one but that is about the only similarity they have. In Figure 3.9(a) the polymer stays attached to the left boundary the entire simulation. In Figure 4.3 the polymer separates into two separate pieces and then separates from the boundary along the x-axis. The difference in results can be attributed to the difference in dimension. In the 1D simulation the only way for the polymer to separate from the boundary would be to move to the

right which as was discussed earlier would lead to a doubling of the distortion energy. In 2D there is room for the polymer to first separate into the two pieces seen in Figure 4.3(b) first and then separate from the wall. Since the polymer first separated into two pieces there would not be a doubling of the distortion energy when the polymer breaks away from the boundary. It would be a minor increase relative to what had already happened. The distortion energy in Figure 4.3(c) shows this. The polymer is separating into two pieces from the start until near a time of $t = 150$. After this point is where the polymer pulls away from the boundary. The increase in energy is more rapid for $100 \leq t \leq 150$, when the polymer is separating, than from $150 \leq t \leq 200$, when the polymer is pulling away from the wall. Figure 4.3(d) shows why any separation of the polymer happens. While the polymer is separating into two pieces and from the wall there is a large decrease in the separation energy. As before the total energy is what drives the system and the total energy is decreased by the evolution seen here.

These two simulations show that some things in 2D remain the same as they were in 1D. However, the second dimension gives an extra direction for things to change in which leads to the possibility that similar starting points may have different results depending on the number of dimensions. The next set of results to be looked at are ones in which the movement energy is added into the energy functional.

4.3.2 Various Movement Energies

The first initial profile to be examined starts with a constant volume fraction of polymer throughout the entire domain. There are two results that will be investigated. In this simulation the starting point is a constant volume fraction as can be seen in Figure 4.4(a). It evolved over time using a plane for the movement energy in Figure 4.4(d). This results in the profile shown in Figure 4.4(b). The energies are nearly

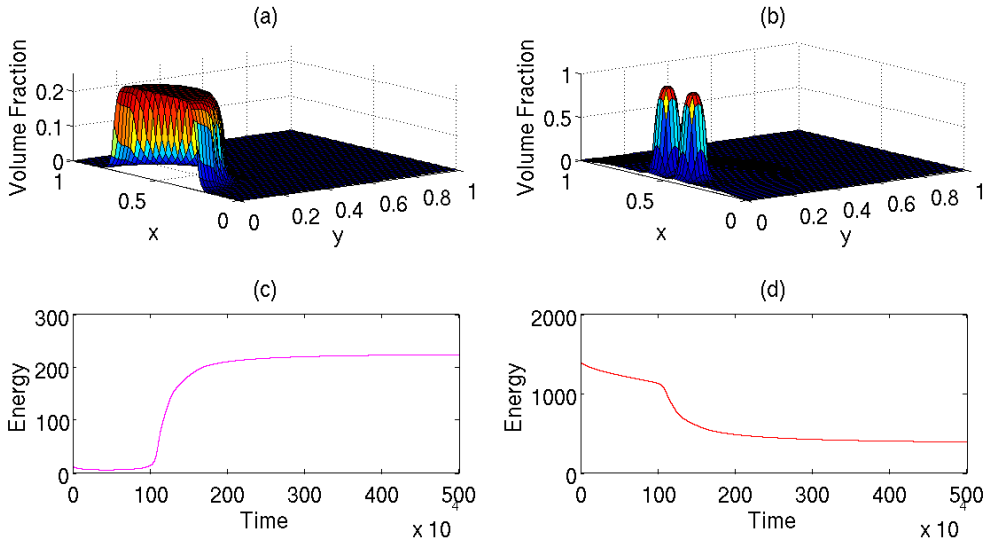

Figure 4.3: (a) The initial condition for the polymer is a semi-circle centered on the x-axis. (b) The final profile shows the polymer forming two separate pieces of polymer with a much smaller radius than part (a) and a volume fraction near one. (c) The distortion energy increases throughout time due to the formation of two separate high volume fraction pieces of polymer. (d) The separation energy decreases over time due to the polymer being concentrated into small regions where the volume fraction is near one and the volume fraction is near zero everywhere else.

constant due to how slowly things change. The movement energy is decreasing, the distortion energy is increasing slightly, and the separation energy is increasing but only a very small amount. There is still conservation of matter in 2D for the same reasons as from before. There is no growth and no flux boundary conditions are used. In order for an area to increase in volume fraction near the x-axis there must be an equal corresponding decrease somewhere else, in this case near the y-axis. The initial profile was already flat which minimizes the distortion energy and was shown in chapter 3 in Figure 3.8 that a flat profile can minimize the separation energy. This leave the movement energy as the only energy that is not minimized at the start. This movement energy is what causes the changes in the final profile.

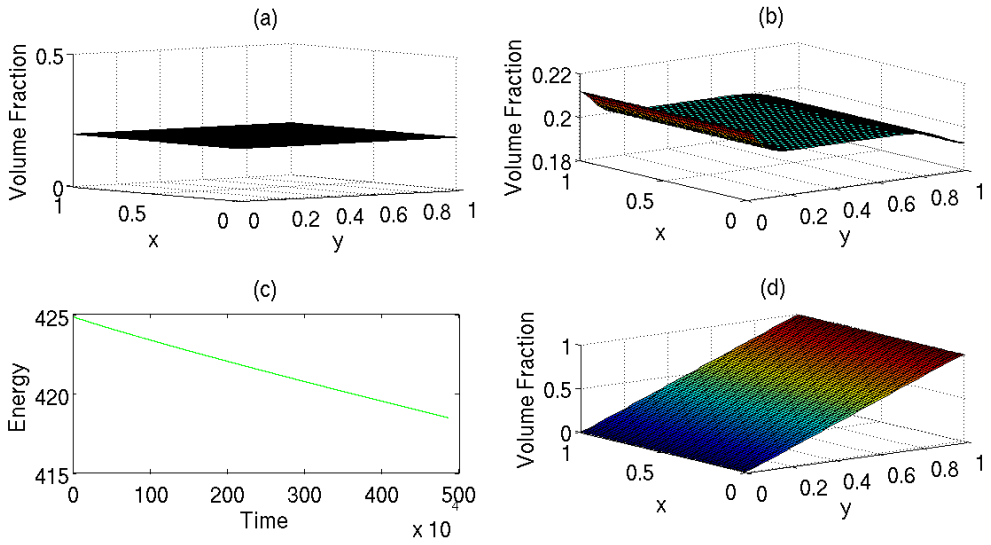

Figure 4.4: (a)The initial polymer volume fraction is constant throughout the domain. (b)The polymer is slowly moving towards the left boundary due to the movement energy. (c) The movement energy is decreasing due to the change in the profile of ϕ_n. (d) The function $g(x, y)$ for the movement energy. In this case the function is constant with respect to x and is defined by $g(x, y) = y$.

The results shown in Figure 4.4(b) come from mainly the movement energy in this case. The movement energy in this case is a plane that has a lower energy when everything is on the x-axis boundary. As was mentioned above the polymer volume fraction is increasing at the x-axis and decreasing closer to $y = 1$. This is due to the function $g(x, y)$. The movement energy is a plane which allows the polymer to flow at a constant rate towards the x-axis. This explains why the decrease occurs near the $y = 1$ boundary. When the volume fraction increases close to the x-axis the material doesn't come from the boundary near $y = 1$; it comes from the nearest neighbors to that place where it increases. When polymer flows from y values near $y = 0.5$ to the smaller x values increasing the volume fraction near the x-axis the same thing is happening with polymer flowing from y values near $y = 1$ to the center near $y = 0.5$ which is why it looks like the center is staying constant and material is

somehow being transported from $y = 1$ to the x-axis. This behavior of constant flow is missing from the next example which will result in quite different results.

The next simulation shown in Figure 4.5 starts with the same initial profile as the previous simulation. The initial condition for this simulation is the same as in Figure 4.4(a). In Figure 4.5(a) the final result for this simulation can be seen. The shape of the polymer profile is due to the $\tanh(y)$ function that is used for the movement energy, which can be seen in Figure 4.5(d). The reason that part (a) takes on the shape it does is because the function $g(x, y)$ in the movement energy is approximately flat for $y \in [0, 0.3] \cup [0.7, 1]$. Due to the Cahn-Hilliard equation the movement of polymer is determined by the gradient of $g(x, y)$. In the regions where $\nabla g(x, y) = \mathbf{0}$ no movement of the polymer due to the movement energy would be expected. The movement will all take place within the region where $\nabla g(x, y) \neq \mathbf{0}$. This movement will be from larger y values to smaller y values. Similar to the previous results conservation of matter requires that if the polymer increases in volume fraction in one location that it must decrease in another location. Unlike the previous simulation the movement energy no longer has a constant gradient throughout the domain. In this simulation everything must occur in the small region where $\nabla g(x, y) \neq \mathbf{0}$. Polymer cannot flow from the boundary where $y = 1$ all the way to the boundary where $y = 0$. The places where $\nabla g(x, y)$ changes from zero to non-zero near $y = 0.3$ and again near $y = 0.7$ act as a mathematical walls preventing the polymer from flowing across this numerical boundary. There was no intent to model a physical boundary at these places but one is being created numerically.

This type of behavior is mathematically correct but it does not match what intuition says should happen. The idea that objects tend towards lower energy states if available is one of the basic ideas of physics and chemistry. It has been mentioned before here as well. There is a lower energy state available near the boundary formed

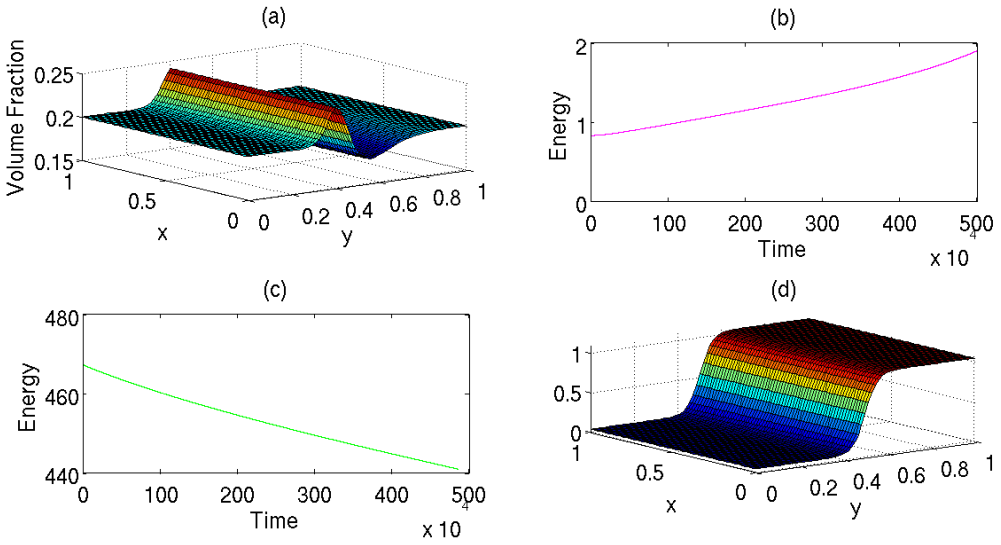

Figure 4.5: (a)The polymer is slowly moving towards the x-axis boundary due to the movement energy. (b) The distortion energy is increasing slightly. (c) The movement energy is decreasing due to the movement towards the region where $g(x, y)$ is smaller. (d) The function $g(x, y)$ for the movement energy. In this case the function is constant with respect to x and is defined by a $\tanh(y)$ function.

by the x-axis. The movement energy is supposed to move any polymer that is at a large movement energy to a location with a lower movement energy. In this case it is allowing polymer to stay in the region where $y \in [0.7, 1]$ in the domain even though the movement energy is high there. It is also preventing the polymer from moving to the left boundary where the movement energy is the lowest by creating an artificial mathematical wall in the middle of the domain. This matter is investigated further in the next simulation.

Instead of starting with polymer throughout the domain an initial profile for the polymer that is completely contained within the region where $\nabla g = \mathbf{0}$ and $g \approx 1$. Another difference is that initial profile was changed to a small cylinder instead of a constant value in Figure 4.6. This was done to allow influence from the distortion and separation energy. It can be seen in the final plot in Figure 4.6(b) that the

polymer never moves out of the region of high movement energy. As above in the previous simulation this is a problem. The polymer volume fraction is close to zero already and other than the small boundary of the cylinder the distortion energy is zero. This means other then possibly reducing the sharpness of the boundary of the cylinder the first thing that should be done is to move the polymer into the region with low movement energy. As was mentioned earlier the Cahn-Hilliard equation has the gradient of the chemical potential; combine this with the form of the movement energy, $\phi_n g(x, y)$, and this results in zero contribution to the evolution of the polymer by the movement energy. Again, the result does match the mathematics but not it is not capturing the desired behavior.

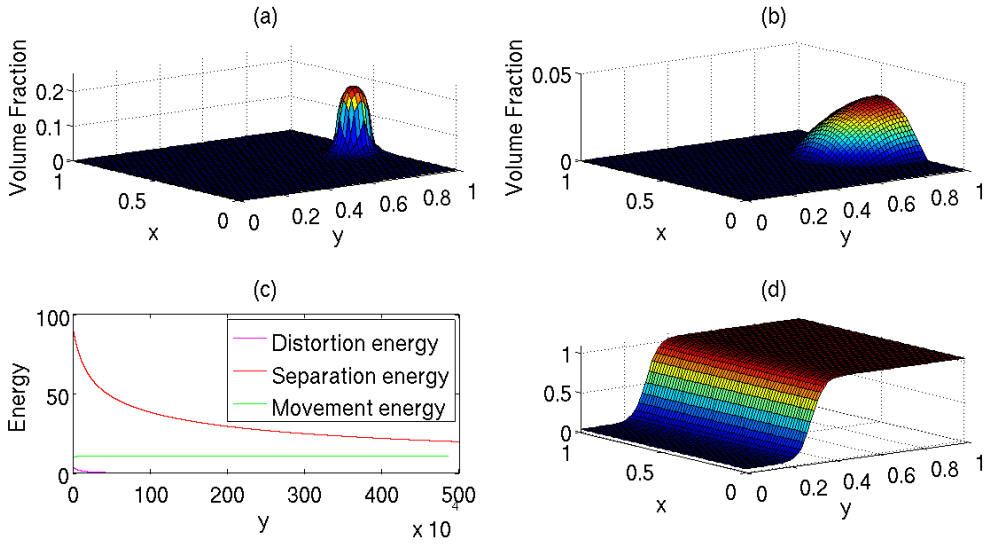

Figure 4.6: (a)The initial amount of polymer is in a region where $\nabla g(x, y) = \mathbf{0}$. (b)Throughout the time evolution the polymer never leaves the region where the movement energy is high. (c) The distortion energy decreases rapidly while the separation energy decreases more slowly. The movement energy is largely stays constant. (d) The function $g(x, y)$ for the movement energy.

This leaves two choices to pursue for the movement energy. Either only allow functions $g(x, y)$ such that $\nabla g(x, y) \neq \mathbf{0}$ or change the movement energy. The former

seems unreasonable. Disallowing a large number of functions that possibly have a reason for being used is not a sound approach to fixing the problem. This leaves the latter as the method that was used. The movement energy was changed to be $0.5\phi_n^2 g(x,y)$. This change makes it so that the movement energy is no longer zero in the Cahn-Hilliard equation (4.12) when $\nabla g(x,y) = \mathbf{0}$. When using this new movement energy in equation (4.12) and ignoring all terms except those that come from the movement energy the chemical potential is $\mu = \phi_n g(x,y)$. Both ϕ_n and $g(x,y)$ depend on both x and y so when $\nabla\mu$ is calculated it is no longer zero even if $g(x,y)$ is flat in regions of the domain.

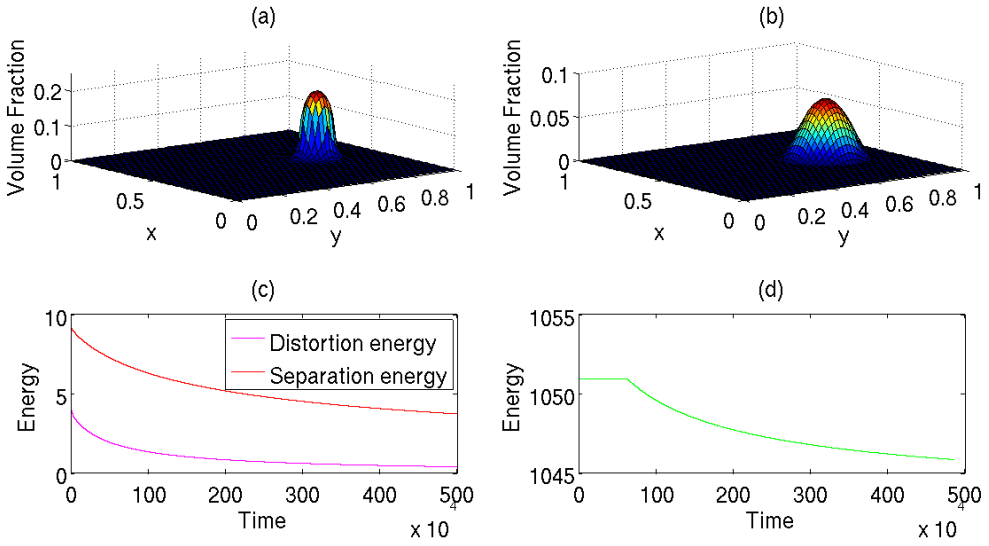

Figure 4.7: The movement energy used is $g\phi_n$(a) The initial profile the polymer. The volume fraction is non zero is a region where $\nabla g = \mathbf{0}$. (b) The final profile of the polymer. The entire amount of the polymer is still completely contained within the region where $\nabla g = \mathbf{0}$. (c) The distortion and separation energies are both decreasing. (d) The movement energy is decreasing but not due to the movement energy itself having an affect of the biofilm.

Changing the movement energy does change the results as can be seen when comparing Figure 4.7(b) with Figure 4.8(b). Both simulations start with the same

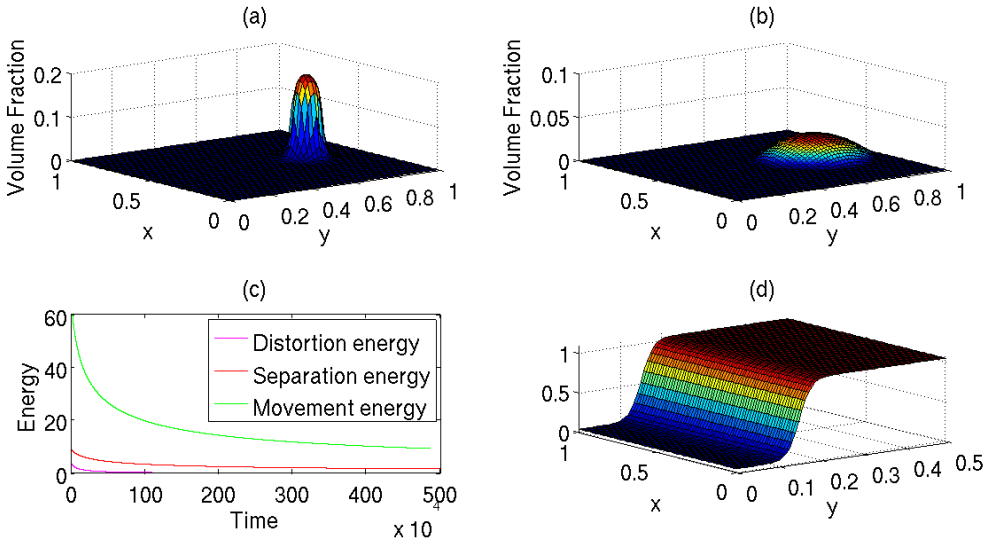

Figure 4.8: The movement energy used is $.5g\phi_n^2$. (a) The initial profile the polymer. The volume fraction is non zero is a region where $\nabla g = \mathbf{0}$. (b) The final profile of the polymer. The entire amount of the polymer is still completely contained within the region where $\nabla g = \mathbf{0}$. (c) The distortion, separation, and movement energies are all decreasing. (d) The movement energy function $g(x, y)$. This is used for both this simulation and the simulation in Figure 4.7.

initial profile in part (a) of both figures. As was discussed above the movement energy used in Figure 4.7(b) does not contribute to the evolution of the biofilm at all which results in the max final volume fraction being larger when compared to Figure 4.8(b) where the movement energy does contribute to the evolution of the biofilm. Another difference can be seen when looking at the energies. In Figure 4.7(c) the distortion and separation energies decrease more slowly than they do in Figure 4.8(c). This difference is due to the last energy. In Figure 4.7(d) the movement energy decreases only because the other two energies work to flatten out the polymer which in turn makes $g\phi_n$ smaller. In Figure 4.8(c) the movement energy re-enforces the other two energies. Even though the movement energy does not have the same affect on the polymer that it had in previous results such as in Figures 4.4-4.5 it is moving the

polymer. Using only the new movement energy in the Cahn-Hilliard equation (4.12) and treating $g(x, y)$ as a constant since where $g(x, y)$ is not constant $\phi_n = 0$ it can be seen that the movement energy does contribute.

$$\begin{aligned}\frac{\partial \phi_n}{\partial t} &= \nabla \cdot \left(\lambda_{ch} \phi_n \nabla \frac{\delta f}{\delta \phi_n} \right) \\ &= \nabla \cdot (\lambda_{ch} \phi_n \nabla g \phi_n) \\ &= \nabla \cdot (\lambda_{ch} \phi_n g \nabla \phi_n) \end{aligned} \tag{4.13}$$

Equation (4.13) shows that the movement energy adds a $\nabla \phi_n$ contribution to the evolution of the biofilm. Since the energy is being minimized it means this new movement energy will re-enforce the smoothing that is done by minimizing the distortion energy. This is the reason the maximum final volume fraction is lower in Figure 4.8(b) than it is in Figure 4.7(b). This can also be seen in Figure 4.9. While the polymer is not completely moving to the region where the movement energy is lower it is moving in a way that is lowering the overall energy which is all that the model can guarantee.

4.3.3 Modeling Treated Surfaces

There are a few things left to investigate with the movement energy. The first of which is whether or not the movement energy will allow the polymer to flow around a location where the biofilm is unable to attach or cause it to become attached. As can be seen in Figure 4.10(b) with a small total amount of polymer the polymer slowly spreads out into a parabaloid shape and flows around the obstruction. Figure 4.10(b) is a contour plot to make the flow around the obstruction easier to see. For this simulation $\gamma_3 = 1 \times 10^{17}$ was used to increase the speed at which the polymer moved

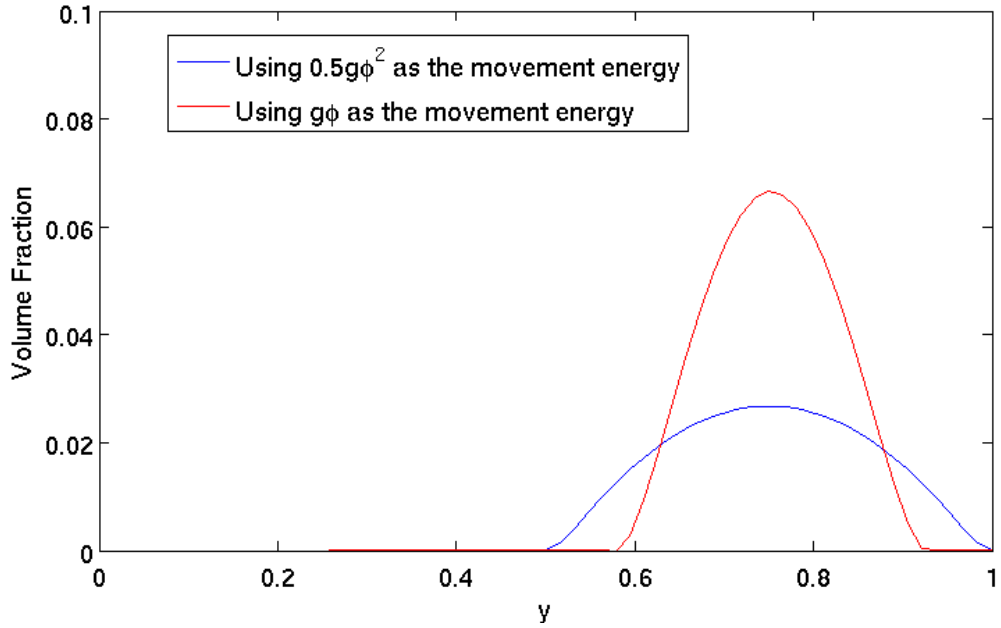

Figure 4.9: The $t_f = 500$ 1D results of the simulations from Figures 4.7 and 4.8. These are the traces of the polymer profiles and the plane $x = 0.5$.

towards the x-axis. This is the reason the movement energy is the largest energy in Figure 4.10(c). All three energies are decreasing.

The simulation in Figure 4.11 starts with a higher total amount of polymer within the domain as well as a much larger maximum volume fraction in the cylinder at the center in Figure 4.11(a). This leads to the distortion energy having a larger affect on the polymer and spreading it throughout the domain faster. The intermediate state where the polymer is flowing around the obstruction can be seen in Figure 4.11(b). This is similar to the result in Figure 4.10(b) as would be expected. The larger volume fraction also causes the movement energy to affect the evolution of the polymer faster. This simulation is essentially at equilibrium at a time of $t = 2000$ as seen in Figure 4.11(d). This also happens to be the final time of the simulation for Figure 4.10 which is not at equilibrium yet. The equilibrium result in this simulation

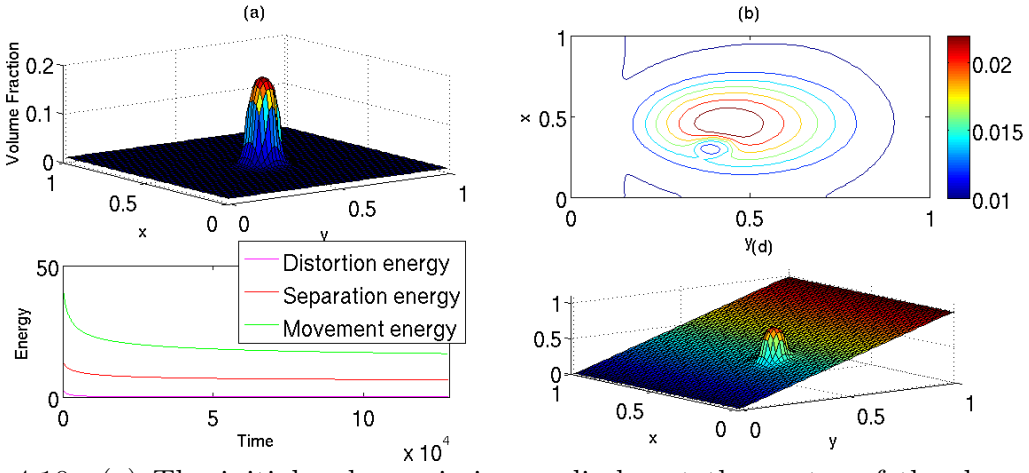

Figure 4.10: (a) The initial polymer is in a cylinder at the center of the domain. There is a small amount of polymer throughout the entire domain. (b) A contour plot of the polymer flowing around the location where it cannot attach within the domain. (c) The three energies for the evolution of the biofilm. The movement energy is highest to increase the rate at which the polymer flowed towards the x-axis. (d) The movement energy with a cylinder acting as the location where the biofilm cannot attach within the domain. The movement energy favors the polymer being closer to x-axis.

is seen in Figure 4.11(c). The polymer is evenly distributed in the x direction for each y value, except where the obstruction is at. The polymer has also grouped up along the x-axis as much as is allowed by the distortion energy. Whether or not the polymer would break apart into separate pieces given an energy where it was preferable was also investigated. The results came from a copy and paste into the wrong movement energy in the C++ code. One explanation for the results would be that the biofilm has attached to something in the middle of the domain and another force has caused the polymer to break away. The initial polymer is located in the center with movement energy seen in Figure 4.12(d). It can be clearly seen in the contour plot in Figure 4.12(b) combined with the surface plot in Figure 4.12(c) that the polymer splits into two separate pieces. One moves towards the x-axis where the $\tanh y$ function is smaller and the other moves into the cylinder shaped region where

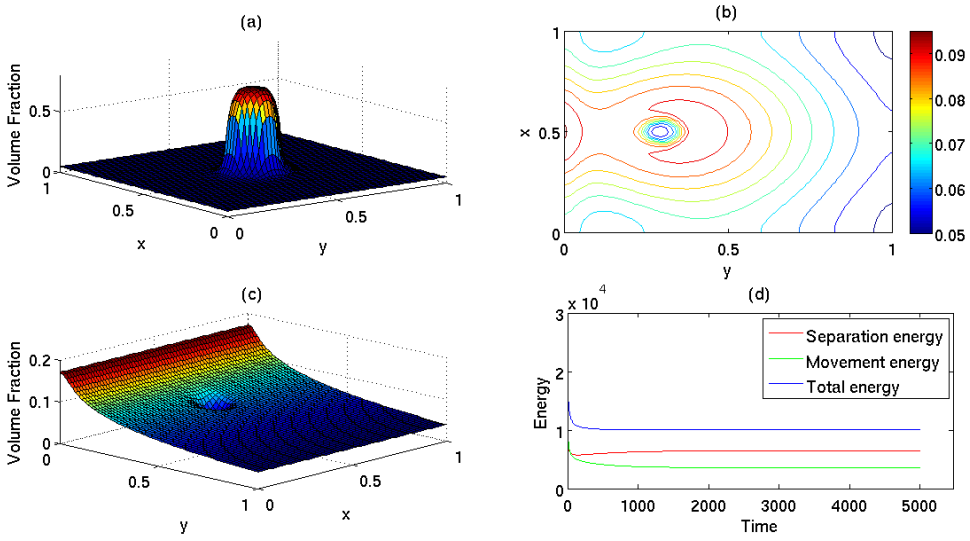

Figure 4.11: (a) The initial polymer is in a cylinder at the center of the domain. There is a slightly larger amount of polymer throughout the entire domain compared to Figure 4.10. (b) A contour plot of the polymer flowing around the central obstruction within the domain. (c) The polymer has reached equilibrium. (d) The separation and movement energies with the total energy of the system. The total energy is at a minimum which means the system is at equilibrium.

the movement energy is lower. This is the first simulation that shows the polymer separating. All other simulations have either started with a single piece of polymer or have combined the polymer from an initially separated state as in Figures 3.12 and 3.13.

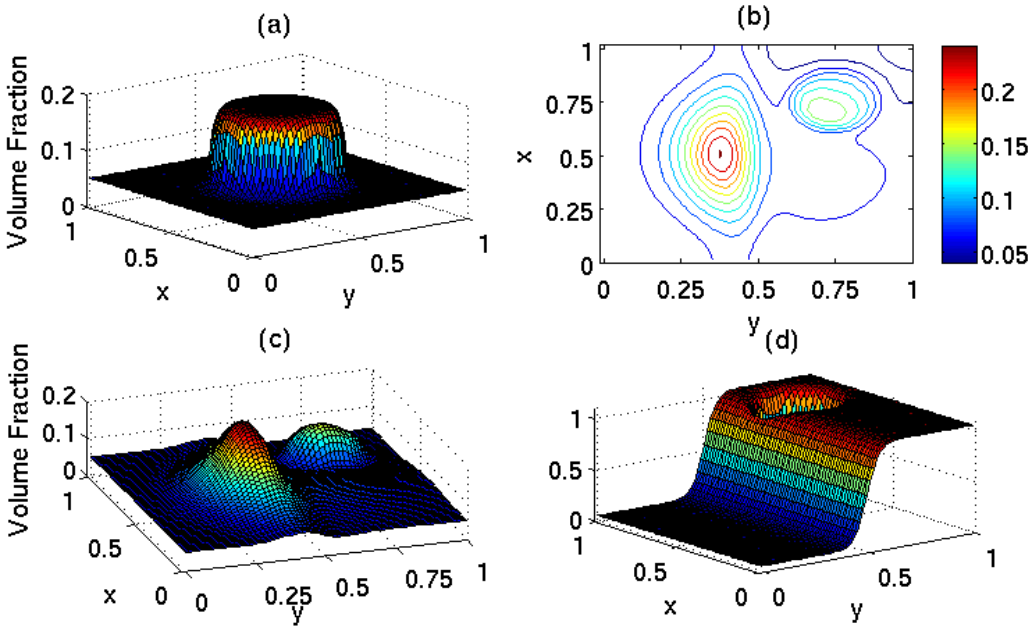

Figure 4.12: (a) The initial polymer is in a cylinder at the center of the domain. There is a small amount of polymer throughout the entire domain. (b) A contour plot showing that the polymer has separated into two separate places. One contained within the cylinder of the movement energy and the other moving towards the x-axis. (c) Another view of the polymer breaking into two pieces. (d) The movement energy with a cylinder of low energy in the region of high energy from the $\tanh y$ function.

CHAPTER FIVE

CONCLUSION

Biofilms are ubiquitous in nature and man made settings. Wherever there is water, nutrient, and a surface a biofilm can be found. This can be good, as in bioremediation, or bad, as in food processing, but regardless of whether a person wants the biofilms there or not knowledge about them is always a good thing. Advances in technology allow for a better and deeper understanding of biofilms through experiments. Mathematics does still play an important roll in helping to understand what may happen within systems where biofilms are prevalent. Math models give a cheap and quick way to predict what could happen in an experiment. Models also provide insight into what should and should not be done in an expensive and time consuming laboratory experiment. In this dissertation we investigated the idea of polymers moving around within the biofilm in two different ways. The first model used basic 1D mass balance and advection equations to gain an understanding of this idea. The second model used well established ideas and laws of physics and chemistry to study this idea.

5.1 The Velocity Driven Model

The velocity driven model tried to capture the movement of polymers within the biofilm using expansion and erosion terms. Concentrations of each component did change in the simulations. There are results that show the concentration increasing and decreasing. This was not the problem with the initial system of equations. The problem was that everything within the biofilm moved in the same direction. The stated goal was to try and get the polymers to separate, maybe not into pure states

but at least so that one polymer had a higher concentration in a region. If everything is moving in the same direction this is not possible. Another issue with the original model was how the height grew. The way the original model was written the height would grow unbounded if there was growth within the biofilm.

These problems were "fixed" in the sense that the model no longer had these problems. The height problem was correctly fixed by implementing a change to the height differential equation that made the erosion proportional to the height squared which caused the height to converge to an equilibrium point instead of diverge to infinity. The change made to the three components of the biofilm did allow each component to move towards equilibrium. The problem is that they all were able to converge to their exact ideal concentration function that was arbitrarily chosen before the start of the simulation. This means that all the forces acting within a biofilm were ignored. The two polymers are able to move around the biofilm as if a separate simulation is run for each one and the results combined at the end.

The second set of results is better over all. The problem with the separation or movement of the EPS not being realistic was still present. There was also the problem of the number of arbitrary choices that can be made in this model. Where the equation says the lower energy is for the polymer is an important choice but here it is completely arbitrary. There are enough models available that describe the energy in polymer physics, such as the Flory-Huggins theory and Flory-Krigbaum theory [43, 52], that we do not need to rely completely on arbitrary choices. There were two options for how to proceed from this point; either more changes to the model are implemented or a different model needs to be investigated. We chose the latter option and moved on to an energy based model.

5.2 The Energy Based Model

The second model investigated is an energy based model. This model uses ideas and laws from physics and chemistry in order to derive the equations. The main two equations discussed in this dissertation are the Cahn-Hilliard equation and the Flory-Huggins free energy density. These equations have been used to study a wide range of topics that involve the separation of two fluids. While our work focuses purely on the biofilm applications of these two equations there are uses in geology, polymer physics, and other areas of fluid dynamics.

In the 1D model we showed that the results from previous papers agreed with results from the slightly modified equation used here. From there the movement energy, $\gamma_3\phi_n g(y)$, was added to the model. The choice of $g(y)$ in the model is an arbitrary choice but the interaction of the movement energy with the other parts of the Flory-Huggins energy keeps it from moving all the polymer exactly where it prescribes as in the previous model. These results show that the model can be modified in a way to give the polymer a preference to where it should be located in order to minimize the energy.

In the 2D model the results shown again agree with previous publications and the results from the 1D model. While there is one unexpected result the difference can be explained due to the addition of the second dimension to the model. The movement energy was shown to have a flaw in its current form. If $\nabla g(\mathbf{x}) = \mathbf{0}$ there was a problem with the movement energy not actually doing anything to change the biofilm in order to minimize the biofilm's energy. This is fixed by changing the movement energy to $\frac{\gamma_3}{2}\phi_n^2 g(\mathbf{x})$. This change made it so that even if $\nabla g(\mathbf{x}) = \mathbf{0}$ the movement energy would still contribute to changing the biofilm as it normally would.

There are a few places to expand on the work presented here. Going back to the model presented in chapter 2 and investigate in more depth the problems that led us to abandon that model. If there are workable solutions then implement them. In the energy model a second polymer has not yet been added to the system. This would be a place that work still needs to be done. Looking further into how both external and internal effects change a biofilm may help identify more functions that would be valid to use as part of the movement energy.

REFERENCES CITED

[1] W. B. Whitman, D. C. Coleman, and W. J. Wiebe, "Prokaryotes: the unseen majority," *Proceedings of the National Academy of Sciences*, vol. 95, no. 12, pp. 6578–6583, 1998.

[2] D. P. MacEachran, G. A. OToole, S. Kjelleberg, and M. Givskov, "Do not fear commitment: the initial transition to a surface lifestyle by pseudomonads," *The Biofilm Mode of Life: Mechanisms and Adaptations*, pp. 23–36, 2007.

[3] M. E. Davey and G. A. O'Toole, "Microbial biofilms: from ecology to molecular genetics," *Microbiology and molecular biology reviews*, vol. 64, no. 4, pp. 847–867, 2000.

[4] M. Vert, K.-H. Hellwich, M. Hess, P. Hodge, P. Kubisa, M. Rinaudo, F. Schué, *et al.*, "Terminology for biorelated polymers and applications (iupac recommendations 2012)," *Pure and Applied Chemistry*, vol. 84, no. 2, pp. 377–410, 2012.

[5] H.-C. Flemming, "The perfect slime," *Colloids and Surfaces B: Biointerfaces*, vol. 86, no. 2, pp. 251–259, 2011.

[6] B. Szomolay, I. Klapper, J. Dockery, and P. S. Stewart, "Adaptive responses to antimicrobial agents in biofilms," *Environmental Microbiology*, vol. 7, no. 8, pp. 1186–1191, 2005.

[7] P. E. De Lancey, "Bacterial biofilms: a review of current research.," *Nephrologie*, vol. 22, no. 8, pp. 439–441, 2000.

[8] A. W. Decho, T. Kawaguchi, M. A. Allison, E. M. Louchard, R. P. Reid, F. C. Stephens, K. J. Voss, R. A. Wheatcroft, and B. B. Taylor, "Sediment properties influencing upwelling spectral reflectance signatures: The" biofilm gel effect"," *Limnology and Oceanography*, vol. 48, no. 1; NUMB 2, pp. 431–443, 2003.

[9] J. Wingender, T. R. Neu, and H.-C. Flemming, "What are bacterial extracellular polymeric substances?," in *Microbial extracellular polymeric substances*, pp. 1–19, Springer, 1999.

[10] M. Stanczak, "Biofouling: its not just barnacles any more," *Dostep on-line*, vol. 10, p. 2013, 2004.

[11] R. M. Donlan, "Biofilms and device-associated infections.," *Emerging infectious diseases*, vol. 7, no. 2, p. 277, 2001.

[12] C. G. Kumar and S. Anand, "Significance of microbial biofilms in food industry: a review," *International journal of food microbiology*, vol. 42, no. 1, pp. 9–27, 1998.

[13] B. Costerton, "Medical biofilm microbiology: The role of microbial biofilms in disease," *Chronic Infections, and Medical Device Failure, CD-ROM, Montana State University*, 2003.

[14] H. H. Tabak, P. Lens, E. D. van Hullebusch, and W. Dejonghe, "Developments in bioremediation of soils and sediments polluted with metals and radionuclides–1. microbial processes and mechanisms affecting bioremediation of metal contamination and influencing metal toxicity and transport," *Reviews in Environmental Science and Bio/Technology*, vol. 4, no. 3, pp. 115–156, 2005.

[15] A. J. Phillips, R. Gerlach, E. Lauchnor, A. C. Mitchell, A. B. Cunningham, and L. Spangler, "Engineered applications of ureolytic biomineralization: a review," *Biofouling*, vol. 29, no. 6, pp. 715–733, 2013.

[16] R. Späth, H.-C. Flemming, and S. Wuertz, "Sorption properties of biofilms," *Water Science and Technology*, vol. 37, no. 4-5, pp. 207–210, 1998.

[17] C. Picioreanu, M. C. Van Loosdrecht, J. J. Heijnen, *et al.*, "Mathematical modeling of biofilm structure with a hybrid differential-discrete cellular automaton approach," *Biotechnology and bioengineering*, vol. 58, no. 1, pp. 101–116, 1998.

[18] C. Picioreanu, M. van Loosdrecht, and J. Heijnen, *Multidimensional modeling of biofilm structure*. Delft University of Technology, Faculty of Applied Sciences, 1999.

[19] C. Picioreanu, J.-U. Kreft, and M. C. van Loosdrecht, "Particle-based multidimensional multispecies biofilm model," *Applied and environmental microbiology*, vol. 70, no. 5, pp. 3024–3040, 2004.

[20] C. Picioreanu, J. Xavier, and M. C. van Loosdrecht, "Advances in mathematical modeling of biofilm structure," *Biofilms*, vol. 1, no. 04, pp. 337–349, 2004.

[21] C. Picioreanu, "Modelling biofilms with cellular automata," *Final report to European Environmental Research Organisation*, 1996.

[22] E. Alpkvist and I. Klapper, "A multidimensional multispecies continuum model for heterogeneous biofilm development," *Bulletin of mathematical biology*, vol. 69, no. 2, pp. 765–789, 2007.

[23] C. Picioreanu, M. C. van Loosdrecht, J. J. Heijnen, *et al.*, "A new combined differential-discrete cellular automaton approach for biofilm modeling: application for growth in gel beads," *Biotechnology and bioengineering*, vol. 57, no. 6, pp. 718–731, 1998.

[24] N. Cogan and J. P. Keener, "Channel formation in gels," *SIAM Journal on Applied Mathematics*, vol. 65, no. 6, pp. 1839–1854, 2005.

[25] T. Zhang, N. G. Cogan, and Q. Wang, "Phase field models for biofilms. i. theory and one-dimensional simulations," *SIAM Journal on Applied Mathematics*, vol. 69, no. 3, pp. 641–669, 2008.

[26] I. Klapper, C. Rupp, R. Cargo, B. Purvedorj, and P. Stoodley, "Viscoelastic fluid description of bacterial biofilm material properties," *Biotechnology and Bioengineering*, vol. 80, no. 3, pp. 289–296, 2002.

[27] O. Wanner and W. Gujer, "A multispecies biofilm model," *Biotechnology and bioengineering*, vol. 28, no. 3, pp. 314–328, 1986.

[28] A. Nostro, L. Cellini, M. Di Giulio, M. D'Arrigo, A. Marino, A. R. Blanco, A. Favaloro, G. Cutroneo, and G. Bisignano, "Effect of alkaline ph on staphylococcal biofilm formation," *Apmis*, vol. 120, no. 9, pp. 733–742, 2012.

[29] L. Pavlovsky, R. A. Sturtevant, J. G. Younger, and M. J. Solomon, "Effects of temperature on the morphological, polymeric, and mechanical properties of staphylococcus epidermidis bacterial biofilms," *Langmuir*, vol. 31, no. 6, pp. 2036–2042, 2015.

[30] P. Stoodley, R. Cargo, C. Rupp, S. Wilson, and I. Klapper, "Biofilm material properties as related to shear-induced deformation and detachment phenomena," *Journal of Industrial Microbiology and Biotechnology*, vol. 29, no. 6, pp. 361–367, 2002.

[31] T. Zhang, B. Pabst, I. Klapper, and P. S. Stewart, "General theory for integrated analysis of growth, gene, and protein expression in biofilms," *PloS one*, vol. 8, no. 12, p. e83626, 2013.

[32] T. Zhang, N. Cogan, and Q. Wang, "Phase field models for biofilms. ii. 2-d numerical simulations of biofilm-flow interaction," *Commun. Comput. Phys*, vol. 4, no. 1, pp. 72–101, 2008.

[33] J. Cahn and J. Hilliard, "Free energy of a nonuniform system. iii: Nucleation in a two component incompressible fluid," *The Journal of Chemical Physics*, vol. 31, pp. 688–699, Sept. 1959.

[34] D. Lee, J.-Y. Huh, D. Jeong, J. Shin, A. Yun, and J. Kim, "Physical, mathematical, and numerical derivations of the cahn–hilliard equation," *Computational Materials Science*, vol. 81, pp. 216–225, 2014.

[35] E. Kuhl and D. W. Schmid, "Computational modeling of mineral unmixing and growth," *Computational Mechanics*, vol. 39, no. 4, pp. 439–451, 2007.

[36] J. Rogawski, *Calculus: Early Transcendentals (Paper)*. Macmillan, 2011.

[37] K. W. Morton and D. F. Mayers, *Numerical solution of partial differential equations: an introduction*. Cambridge university press, 2005.

[38] G. H. Golub and C. F. Van Loan, *Matrix computations*, vol. 3. JHU Press, 2012.

[39] R. W. Farebrother, *Linear least squares computations*. Marcel Dekker, Inc., 1988.

[40] B. D. Jackson, *Transport of dissolved and particulate material in biofilm-lined tubes and channels*. MONTANA STATE UNIVERSITY, 2015.

[41] C. Mayer, R. Moritz, C. Kirschner, W. Borchard, R. Maibaum, J. Wingender, and H.-C. Flemming, "The role of intermolecular interactions: studies on model systems for bacterial biofilms," *International journal of biological macromolecules*, vol. 26, no. 1, pp. 3–16, 1999.

[42] M. Wloka, H. Rehage, H.-C. Flemming, and J. Wingender, "Rheological properties of viscoelastic biofilm extracellular polymeric substances and comparison to the behavior of calcium alginate gels," *Colloid and Polymer Science*, vol. 282, no. 10, pp. 1067–1076, 2004.

[43] P. J. Flory, *Principles of polymer chemistry*. Cornell University Press, 1953.

[44] T. Tadros, *Encyclopedia of Colloid and Interface Science*. Springer, 2013.

[45] J. Cahn and J. Hilliard, "Free energy of a nonuniform system. i: Interfacial free energy," *The Journal of Chemical Physics*, vol. 28, pp. 258–267, Feb. 1958.

[46] R. B. Bird, R. C. Armstrong, and O. Hassager, "Dynamics of polymeric liquids. vol. 1 & 2," 1987.

[47] K. A. Dill and S. Bromberg, "Molecular driving forces: Statistical thermodynamics in chemistry and biology (garland science, new york)," 2003.

[48] I. M. Gelfand, R. A. Silverman, *et al.*, *Calculus of variations*. Courier Corporation, 2000.

[49] L. C. Evans, "Partial differential equations and monge-kantorovich mass transfer," *Current developments in mathematics*, pp. 65–126, 1997.

[50] R. G. Parr and W. Yang, "Density–functional theory of atoms and molecules, international series of monographs on chemistry, vol. 16," *Breslow, R*, pp. 160–180, 1989.

[51] N. Media, "Press release: The 1974 nobel prize in chemistry," 1974. [Online; accessed 21-June-2016].

[52] P. Flory and W. Krigbaum, "Statistical mechanics of dilute polymer solutions. ii," *The Journal of Chemical Physics*, vol. 18, no. 8, pp. 1086–1094, 1950.

[53] S. T. Milner, "Dynamical theory of concentration fluctuations in polymer solutions under shear," *Physical Review E*, vol. 48, no. 5, p. 3674, 1993.

[54] H. Tanaka, "Viscoelastic model of phase separation," *Physical Review E*, vol. 56, no. 4, p. 4451, 1997.

[55] T. Zhang and Q. Wang, "Cahn-hilliard vs singular cahn-hilliard equations in phase field modeling," *Communications in Computational Physics*, vol. 7, no. 2, p. 362, 2010.

[56] M. Reiner, "The deborah number," *Physics today*, vol. 17, no. 1, p. 62, 1964.

[57] A. J. Chorin, "A numerical method for solving incompressible viscous flow problems," *Journal of computational physics*, vol. 2, no. 1, pp. 12–26, 1967.

[58] J. Guermond, P. Minev, and J. Shen, "An overview of projection methods for incompressible flows," *Computer methods in applied mechanics and engineering*, vol. 195, no. 44, pp. 6011–6045, 2006.